Single Molecule Studies of Conformatitional Switching and Nucleotide Binding in a AAA+ Protease ClpXP

By

Harris Walpole Manning

Dissertation

Submitted to the Faculty of the

Graduate School of Vanderbilt University

in partial fulfillment of the requirements

for the degree of

DOCTOR OF PHILOSOPHY

in

Chemical and Biomolecular Engineering

January 31, 2020

Nashville, Tennessee

Approved:

Matthew J. Lang, Ph.D.

Jamey D. Young, Ph.D.

Rizia Bardhan, Ph.D.

Carl H. Johnson, Ph.D.

To my dear parents, Harris and Donna Manning, for their sacrifices and encouragement and to my darling fiancée, Shundra, for her love and friendship.

ACKNOWLEDGMENTS

Earning my Ph.D. has been an enlightening, challenging and enriching process. I have grown tremendously as a scientist and a person because I have been surrounded by a group of kind and supportive colleagues and friends. None of this work could have been possible without their help.

First, I would like to thank my advisor, Matt Lang, for being an exceptional mentor. Matt is not only an excellent scientist but a wonderful person as well. He gave me the opportunity to work on exciting projects and encouraged me to find creative solutions to difficult problems. He was always patient and gave me the space to grow into an independent researcher. I appreciate the example he set with his work ethic, how he treated people and how he always put his family first. Most importantly, Matt genuinely cared about my development as a scientist and my personal well-being and was always there to lend a helping hand. I would not be the scientist I am today if I did not have such a great advisor as Matt.

Thank you to the other members of my Ph.D. committee: Jamey Young, Rizia Bardhan, and Carl Johnson. I am grateful for your helpful advice and steadfast encouragement. I am also indebted to my unofficial advisors: Puck Ohi, Marija Zanic, and Adrian Olivares. Thank you for taking the time to offer insightful suggestions to strengthen my work.

I thank my collaborators Bob Sauer, Tania Baker, Ben Stinson, Tristan Bell, Reuben Saunders, and Drew Nager. I am grateful I had the opportunity to work with such a talented group of biologists.

I am fortunate to have worked with some of the most brilliant, hard-working and nicest people I have ever met. I thank Yongdae for training me in the world of single-molecule fluorescence. I thank JC for teaching me how to do optical trapping experiments. Thank you to James, Sonia, Andy, Nikki, Mark, Dev, Hannah, Maddie, and Debasis for being great friends, helping me brainstorm, and always making my time in lab enjoyable. Thank

you to my undergaduate/summer mentees Zane, Victoria, Sergio, Yokari, Cash, and Aaron. It was a pleasure working with all of you.

Thank you to the Ohi, Zanic and Olivares lab members for being warm and welcoming colleagues. Getting an outside perspective from your questions and comments has helped me sharpen my research.

Thank you to every administrator and staff member who has gone above and beyond to help me at Vanderbilt. In particular, thank you to Don Brunson, Ruth Schemmer, Stacey Satchell, Sheri Kimble, and Amanda King. You have made Vanderbilt feel like home. I cannot thank the former and current ChBE staff enough. Mary Gilleran, Rae Uson, Julie James, Angie Pernell, Mark Holmes, Felisha Baquera, Dee Inmon, and Jenni Powell: you are the heart of our department and the reason for our success.

I am lucky to have made many lifelong friends at Vanderbilt. In particular, thank you to Amin, Faizan, Dushyant, and Mariana for being such wonderful people. I have met too many amazing people to list them all here, but I will forever cherish the close-knit community I was a part of in the ChBE department.

None of this could have been possible without the love of my family and friends. Thank you to my parents for their unwavering support and countless sacrifices. Mom and Dad, you have always believed in me and cheered me on and any success I experience in life is because of you. Thank you to my siblings Stacilee, Tricia, Marchelene, and Andrew for always being there for me. I am blessed to have the most caring and supportive sisters and brother in the world. Thank you to my friends from home and college for checking in on me and always being willing to listen to me talk about my research. Thank you to my amazing fiancée Shundra. You are the love of my life and best friend. Thank you for your love and support. Your focus and determination has been an inspiration to me and I look forward to a lifetime of us achieving our dreams together.

TABLE OF CONTENTS

LIST OF FIGURES

Chapter 1

INTRODUCTION

1.1 AAA+ Machines

Molecular motors are vital proteins that power muscle contraction, orchestrate cell division and transport synaptic vesicles across axons in the brain [1]. AAA+ (ATPases Associated with various cellular Activities) motors are an ancient family of molecular motors that use the energy of ATP hydrolysis to remodel macromolecules. Although AAA+ motors are generally ring-shaped oligomers with similar structural elements, these enzymes have diverse roles such as membrane fusion, DNA unwinding and protein degradation [2]. Despite their disparate functions, AAA+ motors share a conserved AAA+ domain that binds ATP [3]. Although the exact roles of some AAA+ motors are still unknown, AAA+ enzymes typically use ATP-fueled conformational motions to perform mechanical work on substrate molecules. The work presented in this dissertation details the molecular mechanisms of ClpX from Escherichia coli, a protein unfolding enzyme and model AAA+ motor.

1.2 AAA+ Diseases

Since AAA+ machines are essential for a multitude of cellular processes, mutations in a single AAA+ motor can cause a range of debilitating diseases. For example, PEX1 and PEX6 are AAA+ motors involved with peroxisome biogenesis. Mutations in the genes that encode these proteins cause the Zellweger's syndrome spectrum [4]. This disease is characterized by liver problems, vision loss, hearing loss and developmental delay. One condition, hereditary spastic paraplegia (HSP), will develop if either paraplegin or spastin, two AAA+ proteins, are defective. Spinal axons deteriorate over time in this disorder, which causes rigid, weak muscles in the lower half of the body. Spastin participates in microtubule severing and paraplegin is responsible for quality control in mitochondria. Although these

proteins have different functions, they both lead to the same effect downstream. A better understanding of AAA+ motors, in general, will lead to the development of better therapies for these congenital disorders.

1.3 Intracellular Proteolysis

Proteins are the workhorses of the cell. They catalyze biochemical reactions, facilitate complex signaling cascades and maintain the structural integrity of cells. Therefore, protein quality control is essential to ensuring cellular homeostasis in the crowded cytosol. When proteins are no longer needed or are inactive due to being misfolded, they are degraded through intracellular proteolysis [5]. Intracellular degradation must be specific so that off-target proteins are not degraded unintentionally. Three methods have evolved in cells for targeted proteolysis: encapsulation in lysosomes, specific proteases and AAA+ proteases.

The lysosome is a membrane-bound organelle that contains an assortment of enzymes that degrade biomolecules, including proteins. Any peptides trapped within the lumen of the lysosome are susceptible to degradation by proteolytic enzymes. Lysosomal proteases are only destructive in the acidic environment ($\sim$pH 5) of the lysosome, preventing degradation of proteins in the neutral cytosol [6].

Proteolysis in the cytosol is regulated by specific proteases and AAA+ proteases. Specific proteases will only sever a peptide bond after first recognizing a distinct amino-acid sequence. For example, the TEV protease recognizes the sequence ENLYFQS in the polyprotein of the tobacco etch virus and cleaves it between the glutamine and serine residues to produce smaller, useful proteins [7]. Biochemists have utilized the TEV protease's high specificity to cleave fusion proteins [8]. Specific proteases help regulate protein activity and signaling pathways, but general cytosolic protein degradation would be inefficient if every protein had an associated protease. General degradation of proteins tagged for degradation is accomplished by AAA+ proteases.

1.4 AAA+ Proteases

AAA+ proteases are found in all branches of life [9]. AAA+ proteases consist of a gate-keeping AAA+ unfoldase that recognizes unique peptide sequences and uses ATP binding and hydrolysis to unfold and threads its substrate through its axial pore and a degradation chamber that destroys the incoming polypeptide (Fig. 1.1) [10]. Once sequestered in the barrel-shaped peptidase, the polypeptide is shredded into short amino-acid segments and released into the cytosol to be recycled [5]. Different AAA+ proteases vary in their ability to degrade substrates of different stabilities. For instance, ClpAP consists of two-stacked hexameric unfoldases that can degrade substrates faster than the single ring of ClpXP [11]. Single-molecule measurements showed that this increase in rate is due to ClpAP's faster rate of unfolding [12]. Biologists have identified numerous AAA+ proteases such as the 26S proteasome found in the cytosol and nucleus of eukaryotes; ClpXP, ClpAP, ClpCP FtsH, HsIUV and Lon are present in eubacteria and eukaryotic mitochondria and chloroplasts; and PAN-20 can be found in archaea [13].

The AAA+ ring of the 26S proteasome is a heterohexamer with 6 unique polypeptide subunits. ClpA and ClpC are composed of double hexamers while FtsH and Lon family proteases have a fused AAA+ and peptidase ring. ClpX is a homohexamer with a single AAA+ module per subunit. Since ClpX is less complex than some of its counterparts but has the fundamental building blocks that all of them share, it is an ideal candidate to serve as a model AAA+ protease. Indeed, it is one of the best characterized AAA+ proteases to date [14].

1.5 Protein Unfolding by AAA+ Proteases

The process of protein degradation by AAA+ proteases has been revealed for ClpXP and ClpAP through optical tweezer nanometry [15, 12, 16, 17, 18, 19, 20]. Pore loops in ClpXP first bind the ssrA (sequence: AANDENYALAA) degradation tag, or degron

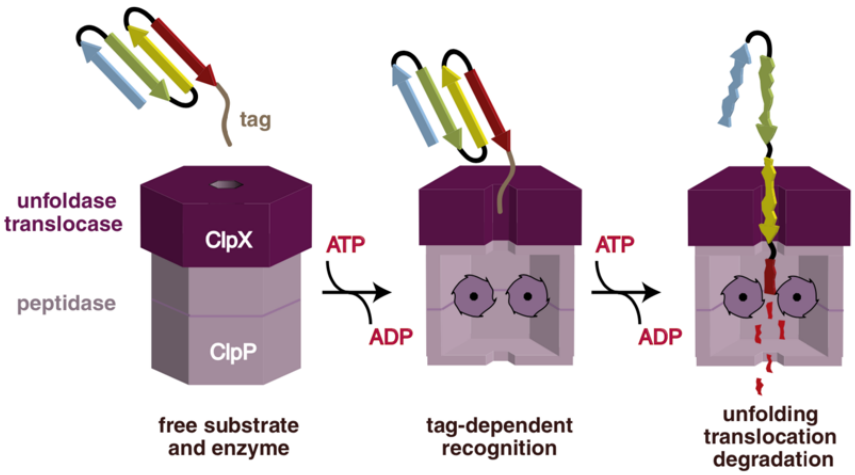

Figure 1.1: **Protein Degradation Cycle by AAA+ Protease** This schematic shows the reaction cycle for degradation of a substrate protein by a protease like ClpXP. First, the degradation tag, or degron, binds to the axial pore of ClpX. ClpX uses ATP-fueled conformational motions to repeatedly pulls on the degron until the protein unfolds. Then ClpX translocates the polypeptide chain to the interior of the ClpP barrel for degradation. Figure taken from Baker et al[5].

appended to the substrate protein. The ssrA tag is appended to the C-terminus of proteins being translated by the ribosome in eubacteria when translation stalls [5]. ClpXP then uses several rounds of ATP binding and hydrolysis to power mechanical pulling on the ssrA tag until the protein unravels cooperatively in a single step. Afterward, ClpX processively spools the polypeptide through the axial pore of ClpP for degradation. ClpX has many other degrons such as the C-terminal MuA and N-terminal λO and σ^S [5].

1.6 Structure of AAA+ Machines

A subunit of ClpX consists of a large and small domain connected by a hinge region and an auxiliary N-domain (Fig. 1.2) [10]. The N-domain acts as a docking site for adapter proteins like SspB which bind protein substrates to increase their effective concentration and promote ClpX recognition. Previous studies have shown that the N-domain is not required for robust machine function [21]. AAA+ proteases perform mechanical work on substrates through ATP powered conformational motions in their subunits. Confor-

mational changes can be inferred from crystal structures, but it is unknown whether the conformational states seen in these structures are functionally relevant [22, 23]. Crystal structures for ClpX show two distinct types of subunit conformations: nucleotide-loadable (L) and nucleotide-unloadable (U) arranged in an L/U/L/L/U/L pattern [22]. Stinson et al. saw a similar pattern in their ClpX crystals regardless of nucleotide identity or mutations present. However, one of their wild-type ClpX crystals exhibited an L/L/L/L/L/L or 6L pattern [23]. Recent cryo-EM structures of ClpXP engaged with substrate contained 6L subunits [24]. Although these structural studies help us understand the range of movements accessible to ClpX subunits, single-molecule experiments are necessary to monitor conformational dynamics in real-time. How do we know that ClpX maintains its ring structure

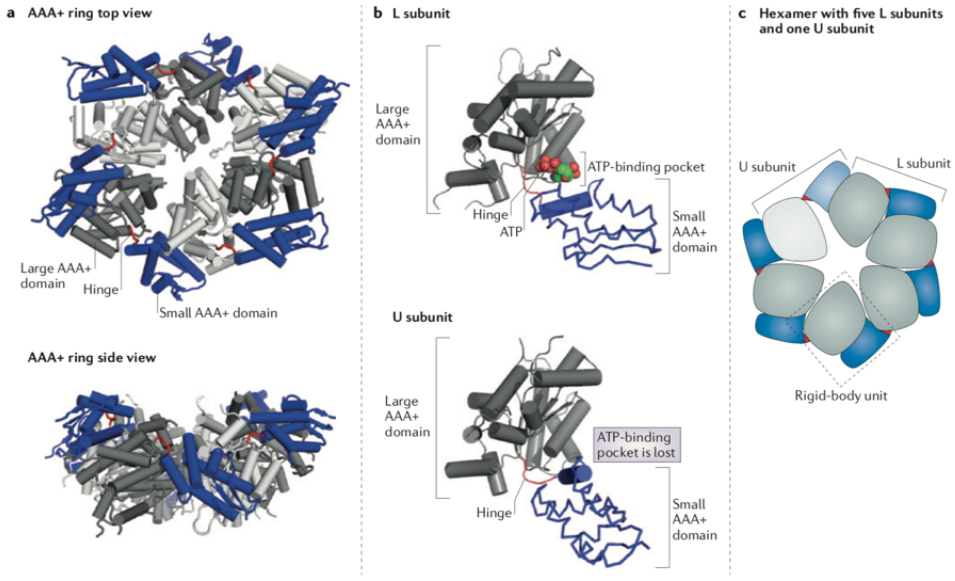

Figure 1.2: **Structure of ClpX Hexamer** (A) Top and side view of a ClpX crystal structure (PDB code: 3WHS). Large domains are dark and light gray, small domains are blue and the hinge region is colored red. (B) Nucleotide loadable (L) and unloadable (U) conformations observed in the 3HWS crystal structure. A nucleotide binding pocket forms in L subunits between the large and small domain. An 80° rotation of the small domain relative to the large domain in U subunits occludes this binding pocket. (C) Schematic showing ClpX subunits arranged in a possible 5L:1U pattern. Figure taken from Olivares et al.[14]

during substrate degradation or where motions in subunits occur? Biochemical experiments demonstrated that disulfide bonding at the rigid-body interface between subunits does not

affect substrate degradation, but stitching residues near the hinge region severely inhibits degradation activity [25]. This result suggests that ClpX rings remain topologically closed during substrate processing and conformational motions arise from rotations at the hinge. Ensemble measurements also prove that conformational motions are necessary for robust machine function. ClpX hexamers with a subunit locked into either an L or U conformation have a reduced substrate degradation rate [23, 26]. Interestingly, hexamers with an L-locked subunit have an increased ATP hydrolysis rate. These results suggest that not only do ClpX subunits require conformational interconversion, structural motions also appear to be required for coupling ATP hydrolysis to useful work.

1.7 Nucleotide Interactions

Many researchers have investigated how ClpX interacts with different nucleotides and how that interaction affects ClpX's function. ClpX interacts binds to ClpP and ssrA-tagged substrates in the presence of ATP and ATPγS but not with the non-hydrolyzable nucleotide ADP [27, 28, 29, 30]. Isothermal titration calorimetry experiments show that 3-4 ATP molecules bind to a hydrolytically defective ClpX (E185Q ClpX6) hexamer at any given time [31]. However, throughout these measurements, most of the ATP molecules will have hydrolyzed to ADP in solution. Nevertheless, this result provides good evidence that ClpX binds multiple nucleotides at a time. Additionally, this study showed that the ATP-dependence of ssrA-tagged protein binding has strong positive cooperativity, indicating that multiple ATP molecules must bind to support substrate binding. Hersch et al. used either a radioactive or fluorescent ATP analog with E185Q ClpX6 to measure dissociation kinetics. They found that nucleotide dissociation was biphasic for both assays indicating that some ClpX subunits have different affinities for nucleotides [31]. Chapter 2 of this dissertation explores the kinetics and stoichiometry of nucleotide binding in a functional ClpX motor at the single-molecule level.

1.8 Subunit Coordination of Molecular Motors

Three models have been proposed for how AAA+ motors coordinate conformational motions and nucleotide hydrolysis between subunits: concerted, sequential and probabilistic. In the concerted model, all subunits bind, hydrolyze and release ATP at the same time (Fig. 1.3). Thus, their conformational motions are also synchronized. This mechanism has been proposed for the SV40 helicase based on crystal structures showing all subunits of the motor in the same nucleotide state [32]. A sequential mechanism requires subunits to successively adopt nucleotide states and conformations in order around the ring. Subunits cannot be skipped. Enermark et al. posited this model for the E1 helicase based on crystal structures of the motor bound to its DNA substrate with E1 subunits making contacts with the DNA in a spiral staircase arrangement [33]. Although these data are compelling, X-ray crystallography only provides a static picture of an enzyme and should be supplemented with rigorous ensemble solution and single-molecule measurements to confirm a given mechanism. Martin et al. proposed a probabilistic model for ClpX based on biochemical measurements on mutated psuedohexamers [21]. They covalently linked different arrangements of hexamers with either parental or mutated ClpX subunits. They found that a ClpX hexamer with only a single hydrolytically active subunit could still degrade ssrA-tagged substrate, albeit at a much lower rate than wild-type ClpX. This result rules out concerted and sequential mechanisms, which would lead to non-functional hexamers with these defects. Chapters 2 and 3 delve into different aspects of ClpX subunit coordination and overall mechanism.

1.9 Single-Molecule Techniques

Single-molecule techniques allow researchers to characterize distinct populations and states of biomolecules obscured by ensemble averaging [34]. The force (piconewton) and displacement (nanometer) resolutions of single-molecule techniques overlap with the force

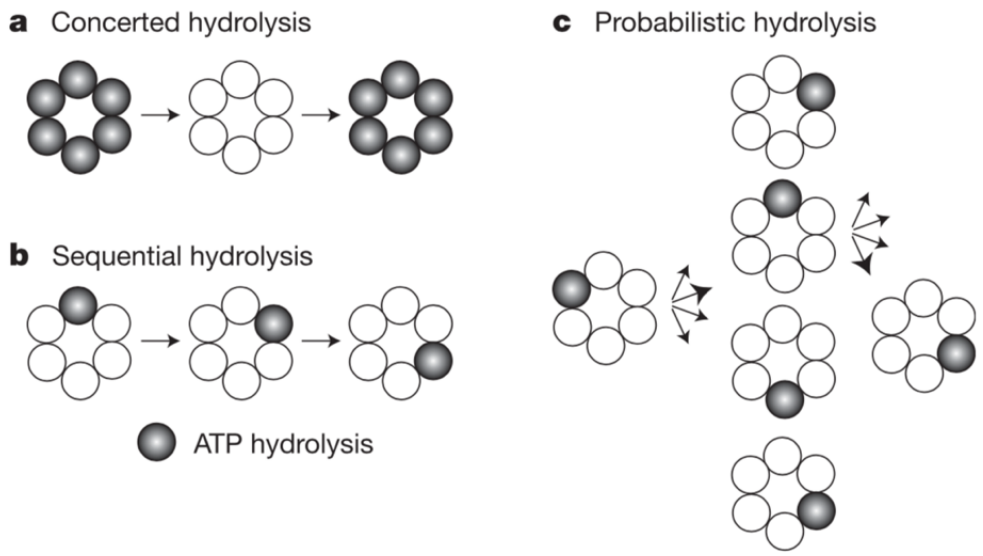

Figure 1.3: **Potential Mechanisms for AAA+ motors** (A) In a concerted model, all subunits in the ring go through their mechanochemical steps simultaneously. (B) For a sequential model, each subunit fires in a precise order around the ring. (C) In a probabilistic model, each subunit has a probability of firing based on its current state and the state of other subunits in the ring. The order of events is not strictly ordered. Figure taken from Martin et al[21].

and displacement resolution of biological events. Optical tweezer nanometry and single-molecule fluorescence are two of the most popular single-molecule techniques. Optical tweezers have allowed scientists to characterize the biophysical properties of motor proteins like kinesin and myosin. Single-molecule fluorescence has been employed to understand the stepping mechanism of kinesin and myosin [35, 36], observe the mechanochemical cycle of the rotary molecular motor F1 ATPase [37] and visualize biological tissue with nanometer resolution by extending it with superresolution methods [38].

1.10 Single-Molecule Fluorescence

1.10.1 Fluorescence

Fluorescence is a phenomenon where certain molecules emit light after absorbing light of a shorter wavelength (Fig. 1.4) [39]. When the fluorescent molecule, or fluorophore,

absorbs a photon of light, one of its electrons gets promoted from its ground state to an excited state. Because electronic energy levels in molecules are discrete, only photons with energies that match the difference between these levels can be absorbed. The excited electron quickly undergoes vibrational relaxation to the lowest vibrational level ($\sim$ps) before emitting the rest of its energy as a photon ($\sim$ns). This discrepancy between the energies of absorbed and emitted photons is called the Stokes shift and leads to the emission spectra of fluorophores being red-shifted from their absorption spectra [40].

1.10.2 TIRF

There are two main strategies for imaging fluorescent molecules one at a time. One can use confocal microscopy to limit the number of molecules in an excitation volume or immobilize the fluorophores to a surface and image them using total internal reflection fluorescence (TIRF) microscopy [41]. For total internal reflection to occur, light must be directed obliquely towards an interface with media of different indices of refraction above a critical angle. At this critical angle, the light ray does not refract through to the other medium because it undergoes total internal reflection. However, an evanescent wave of light emerges from the interface and decays exponentially into the second medium. The typical penetration depth for this evanescent wave is 200 nm, so for TIRF microscopy, only surface-immobilized fluorescent molecules get illuminated [42].

1.10.3 Triplet State and Photobleaching

Fluorescence emission is not the only pathway for excited electrons. Excited electrons sometimes experience a process called intersystem crossing where they are converted from the singlet state to the triplet state. Triplet state electrons can emit photons and relax back to the ground state, but this process is very slow and the triplet state can persist for up to 100 seconds. Oxygen is a natural triplet state quencher but oxygen radicals also cause irreversible photobleaching of fluorophores [44]. Single-molecule biophysicists have

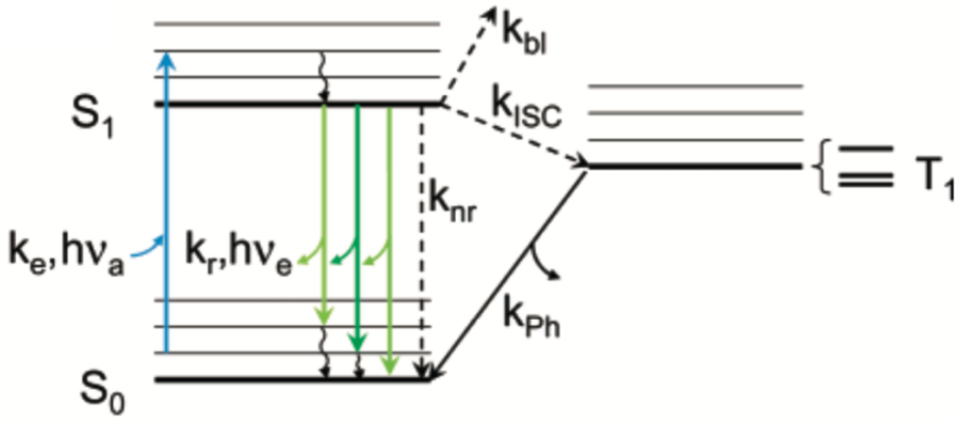

Figure 1.4: **Fluorescence** This Jablonski diagram shows the process of excitation and emission of photons by a fluorophore. An electron in the fluorophore first absorbs a photon and gets excited to a higher energy level, S1 (blue arrow). The electron then quickly relaxes to the lowest vibrational energy level in the excited state (upper black arrow). Then, the electron releases the rest of its energy as a photon and relaxes back down to the ground state S0 (green arrows). This entire process occurs on the order of nanoseconds. Occasionally, intersystem crossing occurs (kISC) and the excited electron transitions to a long-lived triplet state, T1. Relaxation to the ground state from the triplet state is known as phosphorescence and can take much longer than fluorescence, leading to persistent dark states of the fluorophore. The use of triplet-state quenchers reduces occupancy in the triplet state. Figure taken from Michalet et al.[43]

addressed both problems by using oxygen scavengers like the glucose oxidase-catalase (gloxy) system and triplet state quenchers such as Trolox. The use of these additives leads to stable, long-lasting fluorophores that serve as good molecular beacons.

1.10.4 FRET

Förster resonance energy transfer (FRET) is a short-range non-radiative energy transfer between two fluorophores (Fig. 1.5) [42]. The energy transfer is mediated through dipole-dipole coupling and FRET pairs typically have a Förster radius (distance for 50% FRET efficiency) of $\sim$ 5nm [41]. During FRET, an excited donor molecule transfers its energy to an acceptor before relaxing back to the ground state and the acceptor then releases a photon as it relaxes to its ground state. This technique is the gold standard in single-molecule fluorescence for measuring intramolecular conformation motions and in-

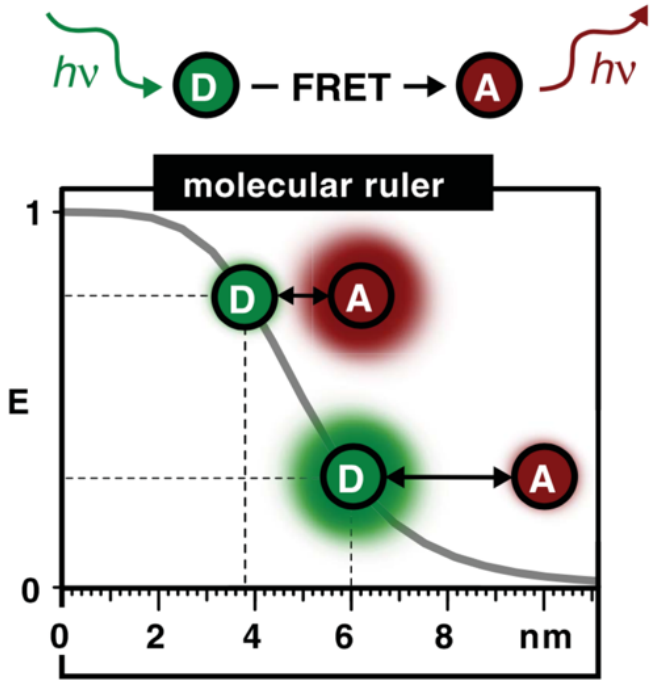

Figure 1.5: **FRET** Förster resonance energy transfer (FRET) is the non-radiative exchange of energy from a donor fluorophore to an acceptor fluorophore whose emission and absorption spectra, respectively, overlap. The lower curve shows that the fraction of energy transferred to the acceptor, or FRET efficiency, depends on the proximity of the probes. Figure taken from Lerner et al.[41]

termolecular biomolecular interactions [45]. The FRET efficiency, E, can be calculated from the following equation:

$$E = \frac{1}{1 + (\frac{R}{R_0})^6}$$

Where R is the distance between the donor and acceptor and R_0 is the Förster radius for the FRET pair. FRET efficiency can be determined experimentally using this equation:

$$E = \frac{I_A}{I_A + \gamma I_D}$$

where I_A is the intensity of the acceptor, I_D is the intensity of the donor and γ is a correction factor that accounts for the quantum efficiency of the probes and detection efficiency for

their respective channels. is given by

$$\gamma = \frac{\Delta I_A}{\Delta I_D}$$

Where ΔI_A and ΔID are the change in average acceptor and donor intensity upon acceptor photobleaching, respectively.

1.10.5 Fluorescence Quenching

Despite its popularity, FRET is insensitive to distance changes 1 nm greater or less than the Förster radius. Dark quenchers have emerged as a viable alternative to traditional FRET acceptors. Dark quenchers absorb photons like conventional FRET acceptors, but instead of fluorescing, these chromophores relax to the ground state through non-radiative pathways [46]. Additionally, dark quenchers have a much shorter lifetime than traditional FRET acceptors making them less susceptible to complex photophysics like intersystem crossing and photobleaching [47]. Quenching efficiency for a dark quencher-fluorophore pair can be monitored through this equation

$$QE = \frac{I_D}{I_{(D,Uq)}}$$

where I_D is the intensity of the donor in the presence of the dark quencher and $I_{D,Uq}$ is the average intensity of the donor in the absence of the quencher.

1.11 Optical Trapping

Optical trapping is a technique used to manipulate micron-sized dielectric particles with a highly-focused laser beam (Fig. 1.6). Optical trapping was first observed by Arthur Ashkin at Bell Labs in 1970 and has evolved into a powerful tool for biophysics [48]. For a bead to be optically trapped, light rays from a focused laser beam must pass through

the transparent particle. As the beam is deflected, there is a transfer of momentum to the

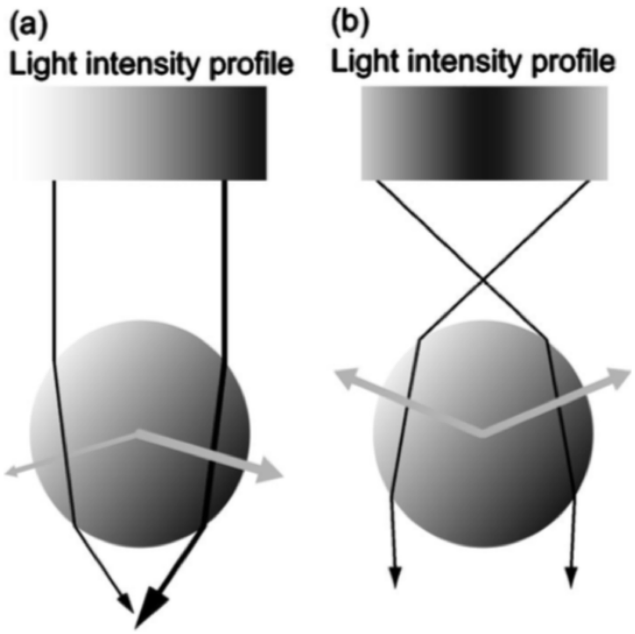

Figure 1.6: **Optical Trapping** Optical trapping is a technique used to manipulate microscopic dielectric particles with a highly-focused laser beam with a gaussian profile. (A) When a bead is just outside the center of the trap to the left, the light intensity is strongest on the right. As light rays coming from the right get deflected to the left, there is an equal and opposite force pushing the bead to the right. Because there are more light rays on the right than on the left, the bead feels a greater push to the right and returns to the center of the trap. (B) When the bead is in the center of the trap, the light rays on the left and right of the bead are equal in intensity and the bead feels a net 0 force. Figure taken from Neuman et al.[49]

beads. The balance of forces from light scattering and the gradient force that emerges from the refraction of light rays from a gaussian laser beam produce an energy well with zero force at the center of the laser beam. If the bead gets deflected outside of the trap center, a net force pulls it back to its equilibrium position [49]. The resultant force on the bead is linearly dependent on distance for distances less than $\sim$200 nm and can be modeled as a Hookean spring with the following equation:

$$F = -k_{trap}x$$

Where k is the trap stiffness and x is the bead's displacement from the center of the

trap. Optical trapping has been used extensively to characterize molecular motors such as kinesin, RNA polymerase and ClpXP. Infrared lasers are typically used for optical traps because light absorption by water and proteins is low between the wavelengths of 750 – 1200 nm [50]. This strategy reduces sample heating, phototoxicity and frees the visible range for combining this technique with fluorescence imaging.

Lang *et al.* was the first to demonstrate simultaneous, coincident optical trapping and single molecule fluorescence [51]. Researchers in our lab further extended this technique by rapidly alternating the trapping and excitation lasers (50 kHz) to protect the photostability of the fluorophore of interest [52]. This technique is called interlaced optical force-fluorescence and was used in chapter 4 to simultaneously observe mechanical events in ClpXP mediated protein degradation and conformational switching in a single subunit of ClpX.

1.12 Bibliography

[1] Manfred Schliwa & Gunther Woehlke. Molecular motors. *Nature*, 422(April):759–765, 2003.

[2] T Ogura and a J Wilkinson. AAA+ superfamily ATPases: common structure–diverse function. *Genes to cells : devoted to molecular & cellular mechanisms*, 6(7):575–97, jul 2001.

[3] Petra Wendler, Susanne Ciniawsky, Malte Kock, and Sebastian Kube. Structure and function of the AAA+ nucleotide binding pocket. *Biochimica et Biophysica Acta - Molecular Cell Research*, 1823(1):2–14, 2012.

[4] Susan Roehl White and Brett Lauring. AAA+ ATPases: achieving diversity of function with conserved machinery. *Traffic (Copenhagen, Denmark)*, 8(12):1657–67, dec 2007.

[5] Tania a Baker and Robert T Sauer. ClpXP, an ATP-powered unfolding and protein-degradation machine. *Biochimica et biophysica acta*, 1823(1):15–28, jan 2012.

[6] Ira Mellman, Renate Fuchs and Ari Helenius. ACIDIFICATION OF THE ENDOCYTIC AND EXOCYTIC PATHWAYS. *New England Journal of Medicine*, 55:663–700, 1986.

[7] Rachel B. Kapust, József Tözsér, Jeffrey D. Fox, D. Eric Anderson, Scott Cherry, Terry D. Copeland, and David S. Waugh. Tobacco etch virus protease: Mechanism of autolysis and rational design of stable mutants with wild-type catalytic proficiency. *Protein Engineering*, 14(12):993–1000, 2001.

[8] T. Dawn Parks, Kerstin K. Leuther, Eric D. Howard, Stephen A. Johnston, and William G. Dougherty. Release of proteins and peptides from fusion proteins using a recombinant plant virus proteinase, 1994.

[9] Andrew F. Neuwald, L. Aravind, John L. Spouge, and Eugene V. Koonin. AAA+: A class of chaperone-like ATPases associated with the assembly, operation, and disassembly of protein complexes. *Genome Research*, 9(1):27–43, 1999.

[10] Robert T Sauer and Tania a Baker. AAA+ proteases: ATP-fueled machines of protein destruction. *Annual review of biochemistry*, 80:587–612, jun 2011.

[11] Susan Gottesman, Eric Roche, Yan Ning Zhou, and Robert T. Sauer. The ClpXP and ClpAP proteases degrade proteins with carboxy-terminal peptide tails added by the SsrA-tagging system. *Genes and Development*, 12(9):1338–1347, 1998.

[12] Adrian O Olivares, Andrew R Nager, Ohad Iosefson, Robert T Sauer, and Tania A Baker. Mechanochemical basis of protein degradation by a double-ring AAA+ machine. *Nature Structural & Molecular Biology*, 21(10):871–875, 2014.

[13] Adrian O. Olivares, Tania A. Baker, and Robert T. Sauer. Mechanistic insights into bacterial AAA+ proteases and protein-remodelling machines. *Nature Reviews Microbiology*, 14(1):33–44, 2015.

[14] Adrian O Olivares, Tania A Baker, and Robert T Sauer. Mechanical Protein Unfolding and Degradation. *Annual Review of Physiology*, 80(1):413–429, 2018.

[15] Marie-Eve Aubin-Tam, Adrian O Olivares, Robert T Sauer, Tania a Baker, and Matthew J Lang. Single-molecule protein unfolding and translocation by an ATP-fueled proteolytic machine. *Cell*, 145(2):257–67, apr 2011.

[16] Adrian O. Olivares, Hema Chandra Kotamarthi, Benjamin J. Stein, Robert T. Sauer, and Tania A. Baker. Effect of directional pulling on mechanical protein degradation by ATP-dependent proteolytic machines. *Proceedings of the National Academy of Sciences*, page 201707794, 2017.

[17] Juan Carlos Cordova, Adrian O Olivares, Yongdae Shin, Benjamin M Stinson, Stephane Calmat, Karl R Schmitz, Marie-Eve Aubin-Tam, Tania a Baker, Matthew J Lang, and Robert T Sauer. Stochastic but Highly Coordinated Protein Unfolding and Translocation by the ClpXP Proteolytic Machine. *Cell*, 158(3):647–658, jul 2014.

[18] Rodrigo a Maillard, Gheorghe Chistol, Maya Sen, Maurizio Righini, Jiongyi Tan, Christian M Kaiser, Courtney Hodges, Andreas Martin, and Carlos Bustamante. ClpX(P) generates mechanical force to unfold and translocate its protein substrates. *Cell*, 145(3):459–69, apr 2011.

[19] Maya Sen, Rodrigo A. Maillard, Kristofor Nyquist, Piere Rodriguez-Aliaga, Steve Pressé, Andreas Martin, and Carlos Bustamante. The ClpXP Protease Unfolds Substrates Using a Constant Rate of Pulling but Different Gears. *Cell*, 155(3):636–646, oct 2013.

[20] Piere Rodriguez-Aliaga, Luis Ramirez, Frank Kim, Carlos Bustamante, and Andreas Martin. Substrate-translocating loops regulate mechanochemical coupling and power production in AAA+ protease ClpXP. *Nature Structural and Molecular Biology*, 23(11):974–981, 2016.

[21] Andreas Martin, Tania a Baker, and Robert T Sauer. Rebuilt AAA + motors reveal operating principles for ATP-fuelled machines. *Nature*, 437(7062):1115–20, oct 2005.

[22] Steven E Glynn, Andreas Martin, Andrew R Nager, Tania a Baker, and Robert T Sauer. Structures of asymmetric ClpX hexamers reveal nucleotide-dependent motions in a AAA+ protein-unfolding machine. *Cell*, 139(4):744–56, nov 2009.

[23] Benjamin M. Stinson, Andrew R. Nager, Steven E. Glynn, Karl R. Schmitz, Tania A. Baker, and Robert T. Sauer. Nucleotide Binding and Conformational Switching in the Hexameric Ring of a AAA+ Machine. *Cell*, 153(3):628–639, apr 2013.

[24] Xue Fei, Tristan A Bell, Simon Jenni, Benjamin M Stinson, Tania A Baker, Stephen C Harrison, and Robert T Sauer. Structures of the ATP-fueled ClpXP proteolytic machine bound to protein substrate. *bioRxiv*, page 704999, 2019.

[25] Steven E Glynn, Andrew R Nager, Tania a Baker, and Robert T Sauer. Dynamic and static components power unfolding in topologically closed rings of a AAA+ proteolytic machine. *Nature structural & molecular biology*, 19(6), may 2012.

[26] Benjamin M Stinson, Vladimir Baytshtok, Karl R Schmitz, Tania A Baker, and Robert T Sauer. Subunit asymmetry and roles of conformational switching in the hexameric AAA+ ring of ClpX. *Nature Structural & Molecular Biology*, 22(5):411–416, 2015.

[27] David A. Wah, Igor Levchenko, Tania A. Baker, and Robert T. Sauer. Characterization of a specificity factor for an AAA+ ATPase: Assembly of SspB dimers with ssrA-tagged proteins and the ClpX hexamer. *Chemistry and Biology*, 9(11):1237–1245, 2002.

[28] Daniel N Bolon, Robert A Grant, Tania A Baker, and Robert T Sauer. Nucleotide-Dependent Substrate Handoff from the SspB Adaptor to the AAA ClpXP Protease Flynn et al., 2001). ClpXP degrades any ssrA-tagged protein, but K M for degradation is lowered markedly by the SspB adaptor, which mediates formation of a sub. *Molecular Cell*, 16:343–350, 2004.

[29] Shilpa a Joshi, Greg L Hersch, Tania a Baker, and Robert T Sauer. Communication between ClpX and ClpP during substrate processing and degradation. *Nature structural & molecular biology*, 11(5):404–411, 2004.

[30] Mary E. Lee, Tania A. Baker, and Robert T. Sauer. Control of substrate gating and translocation into ClpP by channel residues and ClpX binding. *Journal of Molecular Biology*, 399(5):707–718, 2010.

[31] Greg L Hersch, Randall E Burton, Daniel N Bolon, Tania a Baker, and Robert T Sauer. Asymmetric interactions of ATP with the AAA+ ClpX6 unfoldase: allosteric control of a protein machine. *Cell*, 121(7):1017–27, jul 2005.

[32] Dahai Gai, Rui Zhao, Dawei Li, Carla V. Finkielstein, and Xiaojiang S. Chen. Mechanisms of conformational change for a replicative hexameric helicase of SV40 large tumor antigen. *Cell*, 119(1):47–60, 2004.

[33] Eric J. Enemark and Leemor Joshua-Tor. Mechanism of DNA translocation in a replicative hexameric helicase. *Nature*, 442(7100):270–275, 2006.

[34] S. Weiss. Fluorescence Spectroscopy of Single Biomolecules. *Science*, 283(5408):1676–1683, mar 1999.

[35] Erdal Toprak and Paul R Selvin. New fluorescent tools for watching nanometer-scale conformational changes of single molecules. *Annual review of biophysics and biomolecular structure*, 36:349–69, jan 2007.

[36] Erdal Toprak and Ahmet Yildiz. Why kinesin is so processive. *Proceedings of the* . . . , 106(31):12717–12722, 2009.

[37] Kengo Adachi, Kazuhiro Oiwa, Takayuki Nishizaka, Shou Furuike, Hiroyuki Noji, Hiroyasu Itoh, Masasuke Yoshida, and Kazuhiko Kinosita. Coupling of Rotation and Catalysis in F1-ATPase Revealed by Single-Molecule Imaging and Manipulation. *Cell*, 130(2):309–321, 2007.

[38] George Patterson, Michael Davidson, Suliana Manley, and Jennifer Lippincott-Schwartz. Superresolution imaging using single-molecule localization. *Annual review of physical chemistry*, 61:345–67, jan 2010.

[39] Joseph R. Lakowicz. *Principles of Fluorescence Spectroscopy*. Third edition, 2006.

[40] Jörg Enderlein Markus Sauer, Johan Hofkens. *Handbook of Fluorescence Spectroscopy and Imaging*. 2011.

[41] Eitan Lerner, Thorben Cordes, Antonino Ingargiola, Yazan Alhadid, Sang Yoon Chung, Xavier Michalet, and Shimon Weiss. Toward dynamic structural biology: Two decades of single-molecule förster resonance energy transfer. *Science*, 359(6373), 2018.

[42] Rahul Roy, Sungchul Hohng, and Taekjip Ha. REVIEW A practical guide to single-molecule FRET. *Nature Methods*, 5(6):507–516, 2008.

[43] Xavier Michalet, Shimon Weiss, and Marcus Jäger. Single-molecule fluorescence studies of protein folding and conformational dynamics. *Chemical Reviews*, 106(5):1785–1813, 2006.

[44] Ivan Rasnik, SA McKinney, and Taekjip Ha. Nonblinking and long-lasting single-molecule fluorescence imaging. *Nature Methods*, 3(11):891–893, 2006.

[45] Chirlmin Joo, Hamza Balci, Yuji Ishitsuka, Chittanon Buranachai, and Taekjip Ha. Advances in single-molecule fluorescence methods for molecular biology. *Annual review of biochemistry*, 77:51–76, jan 2008.

[46] Ludovic Le Reste, Johannes Hohlbein, Kristofer Gryte, and Achillefs N Kapanidis. Characterization of dark quencher chromophores as nonfluorescent acceptors for single-molecule FRET. *Biophysical journal*, 102(11):2658–68, jun 2012.

[47] Phil Holzmeister, Bettina Wünsch, Andreas Gietl, and Philip Tinnefeld. Single-molecule photophysics of dark quenchers as non-fluorescent FRET acceptors. *Photochemical & photobiological sciences : Official journal of the European Photochemistry Association and the European Society for Photobiology*, 13(6):853–8, 2014.

[48] A. Ashkin. Acceleration and Trapping of Particles by Radiation Pressure. *Physical Review Letters*, 24(4):156–159, 1970.

[49] Keir C Neuman and Steven M Block. Optical trapping. *The Review of scientific instruments*, 75(9):2787–809, sep 2004.

[50] K Svoboda and S M Block. Biological applications of optical forces. *Annual review of biophysics and biomolecular structure*, 23:247–85, jan 1994.

[51] MJ Lang, PM Fordyce, AM Engh, and KC Neuman. Simultaneous, coincident optical trapping and single-molecule fluorescence. *Nature methods*, 1(2):1–7, 2004.

[52] Ricardo R Brau, Peter B Tarsa, Jorge M Ferrer, Peter Lee, and Matthew J Lang. Interlaced optical force-fluorescence measurements for single molecule biophysics. *Biophysical journal*, 91(3):1069–77, aug 2006.

Chapter 2

SINGLE-MOLECULE FLUORESCENCE QUENCHING REVEALS CONFORMATIONAL STATE AND DYNAMICS OF ClpX SUBUNITS

2.1 Summary

ATP-fueled conformational motions in the AAA+ motor ClpX power the unfolding of proteins tagged for degradation and the spooling of the denatured polypeptide into ClpP for proteolysis. Crystal and cryo-EM structures of ClpX and ClpXP, respectively, have revealed distinct conformational states and biochemical studies have shown that restricting the movements of ClpX subunits decouples ATP hydrolysis from protein degradation. Yet, the conformational states and dynamics of a working motor have not been characterized. We have developed a single-molecule fluorescence quenching assay that quantitatively reports the distance between the large and small AAA+ domains of a single ClpX subunit in real-time. We observe three subunit classes, with dynamic inter-state transitions in the most abundant class. Additionally, numerous short-lived intermediate states are observed, which are not present in crystal or cryo-EM structures of ClpX or ClpXP. The proportions of different classes and the switching kinetics within classes are altered by the presence of different nucleotides, ClpP, and protein substrates.

2.2 Introduction

AAA+ motors are essential enzymes that perform mechanical work necessary to drive numerous cellular processes, including proteolysis and macromolecular remodeling [1, 2]. These motors harness the energy from cycles of ATP binding and hydrolysis to change both their own structures and those of bound target molecules. Characterizing dynamic structural changes within active AAA+ motors is an important step toward understanding these machines at a deeper mechanistic level.

Escherichia coli ClpX is a AAA+ protein-unfolding machine that functions as a ring hexamer, often in collaboration with ClpP in the ClpXP protease [3]. Peptide degrons (e.g., the ssrA tag) attached to specific proteins bind in the axial pore of the ClpX ring and ATP-fueled conformational changes then power substrate unfolding and threading of the denatured polypeptide into ClpP for degradation [4]. Each ClpX subunit consists of an N-terminal domain and large and small AAA+ domains, although ClpXΔN variants support robust degradation of ssrA-tagged proteins by ClpP [5]. In most crystal structures of ClpXΔN hexamers, four loadable (L) subunits bind ATP/ADP, whereas two unloadable (U) subunits do not, as a consequence of substantial rotations around a hinge between the small and large AAA+ domains [6, 7]. Cryo-EM structures of ClpXP contain only L subunits [**?** 8, 9] with ATP or ADP bound to each subunit. The functional relevance of U subunits is uncertain. In solution studies, crosslinking one subunit of a ClpX hexamer into an L or U conformation dramatically inhibits degradation [7, 10], which suggests either that that conformational switching is important for activity or that the covalent crosslinks interfere with function by another mechanism.

Single-molecule fluorescence assays are ideal for monitoring intramolecular structural changes [11]. Förster Resonance Energy Transfer (FRET) can report conformational motions but is insensitive if the fluorophores are too close in space. Dark fluorescence quenching is an alternative to conventional FRET that can report distance changes on shorter nm-length scales [12, 13]. Dark-quencher photophysics exhibit a very short excited state lifetime, decreasing their susceptibility to triplet states and photobleaching. As a result, the effective observation window is extended relative to conventional FRET. Because only the donor probe emits photons, a single-channel is sufficient for acquisition. Thus, quenchers are attractive as short-distance probes with advantageous spectral and photobleaching properties.

We have developed a single-molecule total internal reflection fluorescence (smTIRF) assay that uses fluorescence quenching to monitor rotation between the large and small

AAA+ domains of a single subunit in a ClpXN hexamer. Using this assay, we observe three subunit classes, with dynamic inter-state transitions in the most abundant class. Additionally, numerous short-lived intermediate states between L and U conformations are observed, which are not present in crystal or cryo-EM structures of ClpX or ClpXP. The proportions of different classes and the switching kinetics within classes are altered by the presence of different nucleotides, ClpP, and protein substrates. Our results show that working ClpX hexamers do not contain dedicated or permanent unloadable subunits. Additionally, subunits do not appear to cycle through sequentially laddered conformations. Unloadable conformational states of the type observed in ClpX crystal structures are rare and the majority of dynamic conformational switching occurs between loadable subunits and subunits with intermediate conformations that do not correspond to those found in static structures.

2.3 Results

2.3.1 Modification of ClpX to report conformation through fluorescence quenching

We engineered single-chain ClpXN hexamers with an ATTO 550 fluorophore attached to a specific cysteine in one large AAA+ domain and a DABCYL Plus dark quencher attached to a specific cysteine in the large AAA+ domain of the clockwise subunit (Fig. 2.1c). This arrangement is sensitive to the conformation of the fluorescent subunit because neighboring large and small AAA+ domains form rigid-body units (Fig. 2.1a). Thus, domain rotations about the hinge of the fluorescent subunit will alter the relative fluorophore and quencher separation. We constructed one single-chain trimer with two parental C169S ClpXN subunits (P) and one C169S ClpXN subunit with an additional Q167C substitution (Q) in the order PPQ. A second trimer contained a parental subunit with an additional K213C substitution (K) and two parental subunits in the order KPP. In ClpX hexamer structures, the distance between the Cβ carbons of the Q and K sites in adjacent subunits ranged

between 0.55 and 1.8 nm for L subunits and between 2.9 and 3.7 nm for U subunits. PPQ trimers were labeled with ATTO 550 maleimide, and KPP trimers were labeled with DAB-CYL Plus maleimide. KPP trimers were also biotinylated at the C-terminus to facilitate attachment to a streptavidin-coated surface for smTIRF imaging. The labeled PPQ and KPP trimers were fused by sortase ligation to produce a covalently linked PPQKPP hexamer that we call QA5B.

To address whether the modifications in QA5B disrupt activity and determine if fluorescence is responsive to the motor state, we performed ensemble measurements. In the presence of saturating ATP, QA5B supported ClpP degradation of a GFP-ssrA substrate at a rate comparable to the parental ClpXN enzyme (Fig. 2.1e). QA5B and the parental enzyme also hydrolyzed ATP at similar rates (Fig. 2.6). These results indicate that the probes do not inhibit function. QA5B fluorescence at 580 nm was quenched substantially in the presence of saturating ATP compared to a no-nucleotide control or a control in which QA5B was degraded with elastase (Fig. 2.1f). Titrating increasing concentrations of ATP resulted in a gradual decrease in QA5B fluorescence, providing further evidence for systematic ring changes and nucleotide-dependent quenching (Fig. 2.7). These bulk experiments show that QA5B is a functional ClpX variant that exhibits nucleotide-dependent quenching.

2.3.2 Quenching distance calibrated through single-molecule DNA annealing

To calibrate fluorescence quenching magnitude as a function of inter-probe distances, we employed a DNA-based fluorescence quenching system. One strand of a 15-base pair DNA oligonucleotide was labeled with ATTO 550 and different batches of the complementary strand were labeled with Dabcyl Plus at varying locations (Fig. 2.2a). The ATTO 550 strand (BA5) was functionalized with a biotin moiety to bind the DNA to a streptavidin coated PEG-coverslip. The fluorescence signal level of surface-attached BA5 was imaged for 60 s before flowing in the complementary strand labeled with the Dabcyl-Plus quencher (Fig. 2.2b). After flow-in, the majority of single-molecule spots showed a rapid decrease

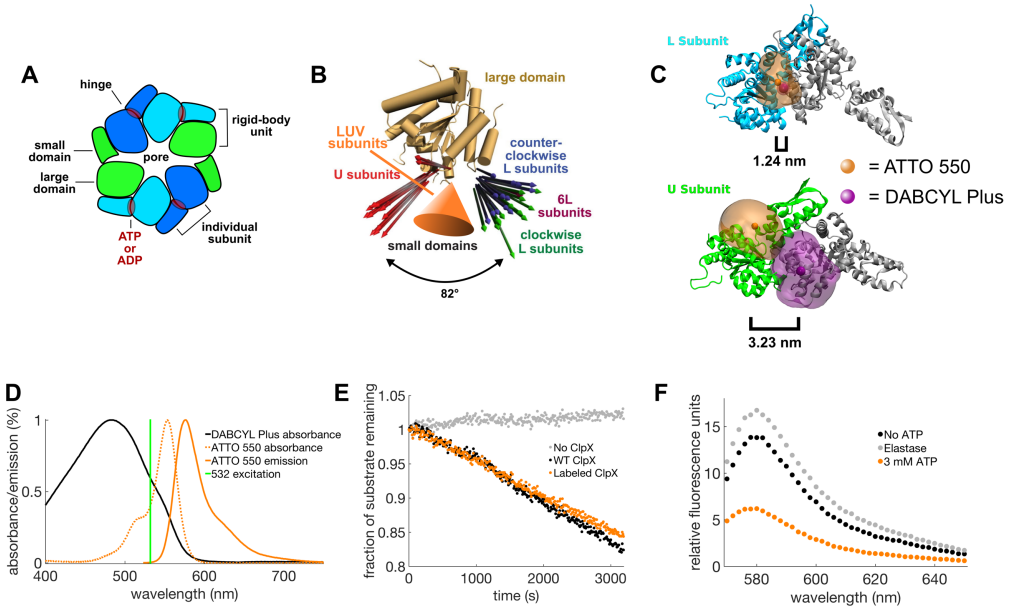

Figure 2.1: **ClpX construct for monitoring conformational motions.** (A) A schematic of the ClpX hexamer. (B) The large domains of eight E. coli ClpX hexamers crystal structures were aligned (PDB codes 3HTE, 3HWS, 4I81, 4I4L, 4I34, 4I5O, 4I63, and 4I9K) and an arrow was used to represent an alpha helix in each the small domain (residues 332–343). (Stinson. Cell 2013) The orange cone represents the hypothetical positions of intermediate states seen in the single-molecule data presented here. (C) Location of fluorophore and quencher. The fluorophore, ATTO 550, was placed in the large domain of the subunit of interest. The quencher, Dabcyl Plus, was inserted into the large domain of the clockwise neighboring subunit which forms a rigid body with the small domain of the subunit of interest. Distances shown are that between the mean positions of accessible volume clouds of ATTO 550 and Dabcyl Plus. (D) Absorption and emission spectra for probes. Because of the overlap of the absorption spectra of DABCYL Plus (black) with the emissions spectra of ATTO 550 (solid orange), fluorescence quenching through a FRET mechanism is likely to occur in addition to contact quenching. (E) Protein substrate degradation assay for labeled ClpX construct. ClpX labeled with ATTO 550 and DABCYL Plus in the presence of ClpP, ATP and an ssra-tagged protein substrate, degrades the substrate at a rate similar to wild-type ClpXP. (F) Ensemble fluorescence quenching of labeled ClpX construct. Labeled ClpX in the presence of 3 mM ATP shows more pronounced fluorescence quenching than labeled ClpX in the absence of nucleotide. Labeled ClpX digested by elastase shows greater unquencing than ClpX in the apo state.

in fluorescence to a new intensity level (Fig. 2.2c). As expected, the degree of quenching depended strongly on the proximity of the fluorophore and quencher (Fig. 2D).

Fluorescence quenching in QA5B can be correlated to distance only if the position of the covalently-linked dyes and their distance from one another are known accurately. We used the FRET Positioning and Screening (FPS) software to estimate the position of the dyes linked to our DNA by generating accessible volumes (AVs) for the dye-linker pairs based on their dimensions [14] (Fig. 2.8). FPS has been used extensively for single molecule FRET studies [**?**]. Recently, FPS was used to establish the distance between a FRET pair for standards used in a multi-laboratory benchmark study on the precision and accuracy of single-molecule FRET measurements [15]. We found the mean position for each AV and measured the distance between those coordinates for ATTO 550 and Dabycl Plus to determine the inter-dye distances for the four duplexes tested. The plot of quenching efficiency versus inter-dye distance shows a similar trend to a graph of the Förster equation (Fig. 2.2e). A fit of the data to the Förster equation results in a Förster radius (distance for 50% quenching) of 2.96 nm. This value is close to the theoretical Förster radius for ATTO 550 and Dabcyl Plus of 3.09 nm (Fig. 2.9) calculated from their emission and absorption spectra, respectively. We made AVs for ATTO 550 and Dabcyl Plus attached to their labeling sites in ClpX and calculated inter-dye distances to ascertain the distance ranges for L and U conformations. Inter-probe distances for L and U subunits are plotted along with our calibration as blue and red shaded regions, respectively (Fig. 2.2e). The most extended L subunit corresponds to an intensity of 0.1 and the most compact U subunit corresponds to and intensity of 0.79. Thus, this quenching pair as constructed straddles the extremes of compact L to extended U conformations and is highly sensitive to conformational changes in a single ClpX subunit.

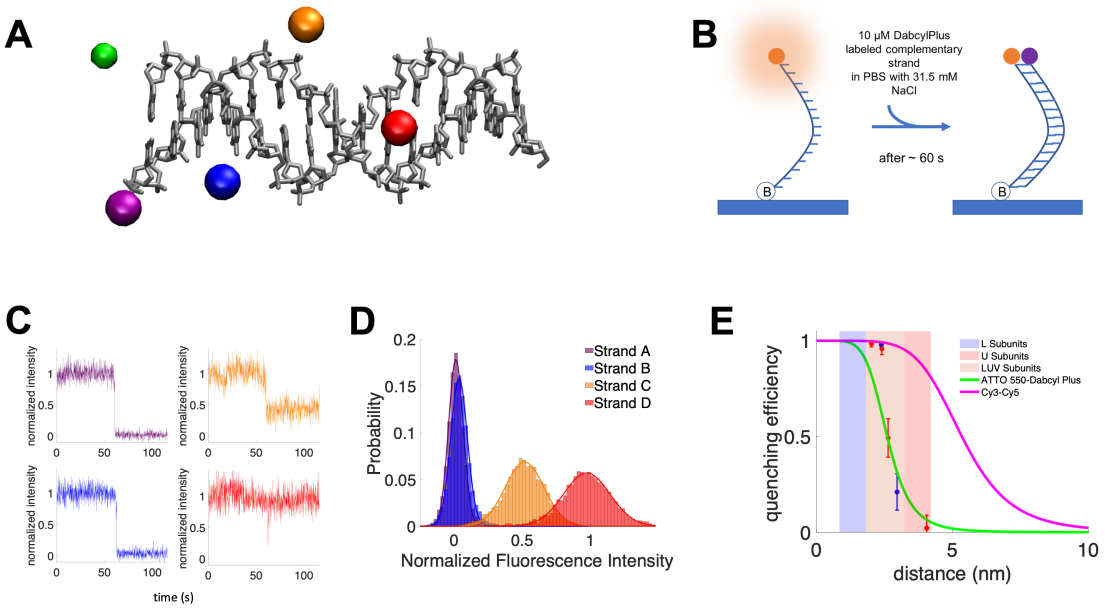

Figure 2.2: **DNA system for calibrating fluorescence quenching of ATTO 550 by Dabcyl Plus.** (A) 15-base pair DNA oligo used for single molecule fluorescence quenching calibration experiments. ATTO 550 (green bead) was attached to the 3' end of one strand and Dabcyl Plus (purple, blue, orange and red) was attached to nucleotides on the complementary strand at varying distances. (B) To observe quenching of ATTO 550 in real-time, complementary strands of our DNA system were annealed in situ. First, the ATTO 550 labeled strand was tethered to a streptavidin-coated coverslip via a biotin moiety on the 5' end. Approximately 60 seconds after the start of acquisition, the Dabcyl Plus labeled complementary strand was flowed-in with 31.5 mM NaCl to promote rapid annealing. (C) Example traces of single-molecule annealing experiments of DNA quenching system. Quenching decreases as the distance between the probes increases. (D) Normalized intensity histograms of single-molecule annealing experiments. Each distribution was fit by a single gaussian function. The mean intensity of each distribution increases as the distance between the probes increases. (E) Quenching efficiency curve for single-molecule annealing experiments. The quenching efficiency (1 – normalized intensity) s.d. was plotted against the inter-probe distances measured through accessible volume simulations of ATTO 550 and Dabcyl Plus. These data were fit to the inverse sixth power law Förster equation. The Förster distance for this fit is 2.9 nm.

2.3.3 ClpX conformational switching signals are normalized by flowing in denaturing surfactant

In objective-side TIRF studies, the emission intensity for an individual spot depends not only on the conformation of the motor but also on the excitation flux, which is highest in the center and lower in the periphery. To normalize the quenching of individual spots, we sought a method to determine the unquenched fluorescence of the ATTO 550 dye in QA5B. To do so, we employed a surfactant, sodium dodecyl sulfate (SDS), that denatures many proteins [16]. QA5B ClpXN was attached to the surface of a PEGylated coverslip via streptavidin and imaged on an smTIRF microscope (Fig. 2.3a) [17]. After acquiring data for 1-2 min, buffer containing 1% (w/v) SDS was introduced resulting in a stable increase in fluorescence before single-step photobleaching (Fig. 2.3c, upper panel). This concentration of SDS appears to unfold QA5B, separating the dye and quencher, but does not disrupt streptavidin tethering to the coverslip. As a control, we showed that the fluorescence of A5B, a ClpX variant that lacked a Dabcyl Plus quencher but was otherwise identical to QA5B, did not change substantially after flowing in SDS and trajectories remained stable until photobleaching (Fig. 2.3c, lower panel). Therefore, SDS can be used to determine the unquenched fluorescence of the ATTO 550 dye and to normalize observed changes in fluorescence. To ensure that single QA5B molecules were being analyzed, we required spots to exhibit stable fluorescence after SDS flow-in and to undergo single-step photobleaching.

2.3.4 Trajectory classes based on intensity and dwell-time analyses

Fluorescence traces for all conditions tested exhibited a variety of intensity states and dwell times (Fig. 2.4a). We employed our ATTO 550/Dabcyl Plus calibration curve and inter-dye distances measured from AVs for ClpX crystal structures to identify conformational states and choose thresholds for analyzing key transitions. We used the ebFRET hidden Markov modeling (HMM) algorithm to identify the conformational states present

in every trace [18]. HMM provides a standardized, statistically robust method for identifying the underlying states masked by the white noise of single-molecule fluorescence data [19, 20, 21, 18]. After finding the idealized states from HMM fits, we chose thresholds for the expected L (0.12) and U (0.77) states. These values were conservatively estimated being 0.02 larger or smaller than the most extended L and compact U subunits, respectively. Interestingly, most traces for all conditions show transient occupancy of intermediate conformations between L and U states. Though short lived, their observation highlights the ability of single-molecule methods to tease out states occluded by ensemble averaging. To simplify our analysis, we sorted traces into three classes: quenched static, quenched dynamic and unquenched. Quenched static traces are those where the intensity remains below the threshold for L subunits. Quenched dynamic traces exhibit at least one transition across the L subunit threshold. Unquenched traces are those where the intensity values remain above the L subunit threshold for the entire duration of the trace. Because true U states (above 0.77 intensity) are rare, transitions between intermediate states and true U states are ignored and transitions between L and U are grouped with transitions between L and the intermediate states. Dwell times from quenched dynamic traces in particular were extracted for kinetic analysis. For dwell time analysis, all conformational states above our L threshold were categorized as intermediate, or I states. These heterogenous trace categories show that not only do ClpX subunits dynamically switch conformations, different subunits exhibit a variety of conformational modes.

2.3.5 Verifying colocalization of ClpX and ClpP

Because ClpX subunits might have different dynamic properties depending upon ClpP binding, we designed a series of colocalization and photobleaching experiments to distinguish ClpX-only spots from ClpXP spots (Fig. 2.3e) [22]. S187CClpP or N193ClpP was fluorescently labeled with Alexa Fluor 647, and labeling of up to seven subunits was confirmed by photobleaching experiments (Fig. 2.10). To verify colocalization, we imaged

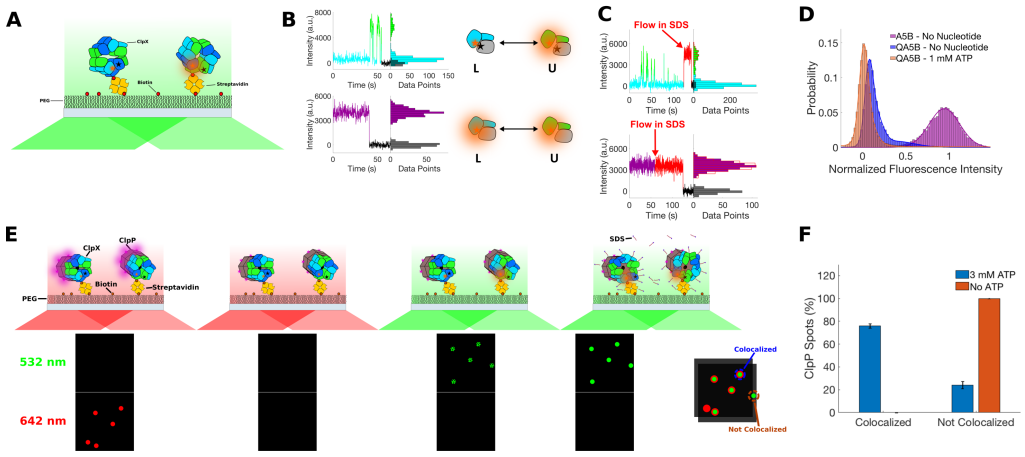

Figure 2.3: **Single-molecule assay shows conformational switching in real time.** (A) Surface-based single-molecule TIRF assay. A biotinylated ClpX construct labeled with ATTO 550 and DABCYL Plus was attached to a PEG treated coverslip surface via streptavidin. (B) Individual trajectories for single molecule data. Upper panel: The construct with both a fluorophore and quencher show quenching and unquenching before photobleaching. Lower panel: A control construct lacking DABCYL Plus shows no quenching before photobleaching in a single step. (C) 1% SDS is used to unquench all molecule simultaneously. Upper panel: Fluorescence quenching abruptly ends at the time point indicated by the red arrow. This technique allows for the recovery of the unquenched fluorescence intensity of ATTO 550 and, thus, the normalization of the different fluorescence states. Lower panel: SDS solution flowed in at the time point indicated by the red arrow does not show a noticeable change in fluorescence intensity. (D) Intensity histograms of QA5B and A5B. The presence of ATP increases quenching in QA5B. (E) Colocalization/conformational switching assay. Surface-bound ClpX molecules (QA5B) were incubated with ClpP labeled with Alexa Fluor 647. Unbound ClpP is washed out and bound ClpP is imaged using 642 nm excitation (first panel). Second panel: ClpX-bound ClpP is photobleached to prevent FRET between ATTO 550 and Alexa Fluor 647. Third panel: Fluorescene quenching is observed in ClpX by exciting ATTO 550 with a 532 nm laser. After 60 seconds of observing quenching dynamics, 1% SDS is flowed into the flow cell to partially unfold ClpX and unquench ATTO 550 from Dabycl Plus. The 532 and 642 nm channels are overlapped and only colocalized ClpX are chosen for further analysis. (F) Bar graph showing the ATP dependence of ClpX-ClpP colocalization.

fluorescent ClpP with a 647 nm excitation laser, and then allowed spots to photobleach (to prevent FRET between ATTO 550 and Alexa Fluor 647) in the absence of an oxygen scavenger or triplet-state quencher, which were subsequently introduced. We then assayed quenching in ClpX subunits, followed by SDS flow-in. The movies for the ClpX and ClpP fluorescence channels were merged and overlapping spots representing ClpXP complexes were chosen for further analysis. Control experiments with A5B showed that ClpX binding to ClpP required ATP or ATPS, as expected (Fig. 2.3f. This set of experiments provides a functional assay of conformational switching of ClpX subunits in ClpXP.

2.3.6 ClpXP is less dynamic when degrading protein substrates

We assayed dynamics in the absence of protein substrate (ClpXP only) and in the presence of native titinI27-ssrA (titin) or a variant unfolded by carboxymethylation of cysteine residues (CMtitin)[4, 7]. The ClpXP-only intensity histogram exhibited a significantly larger shoulder at higher intensities than histograms from experiments with either substrate (Fig. 2.4b, suggesting that substrate binding and processing results in more constrained or tightly organized ClpXP conformations, whereas ClpXP alone has more conformational mobility. Addition of substrate increased the fraction of traces in the quenched-dynamic class and decreased the fractions of the quenched-static and unquenched categories (Fig. 2.4c, suggesting that ClpX subunits become more dynamic when engaging and degrading protein substrates. The presence of substrate also affected dwell-time histograms. L dwells for ClpXP and CMtitin (L = 1.83 s) or titin (L = 1.94 s) were 6-fold longer than for ClpXP only (L = 0.27 s), whereas I dwells were 2-fold longer for ClpXP only (0.4 s) than for ClpXP with CMtitin (0.28 s) or titin (0.2 s). Interestingly, the partitioning of trace types and dwell-time kinetics in the presence of the native and unfolded titin substrates were similar, suggesting that LI transitions are not slowed significantly by unfolding. These results show that an increase in the number of conformational switching subunits may play a role in ClpXP-mediated protein degradation. The unquenched trajec-

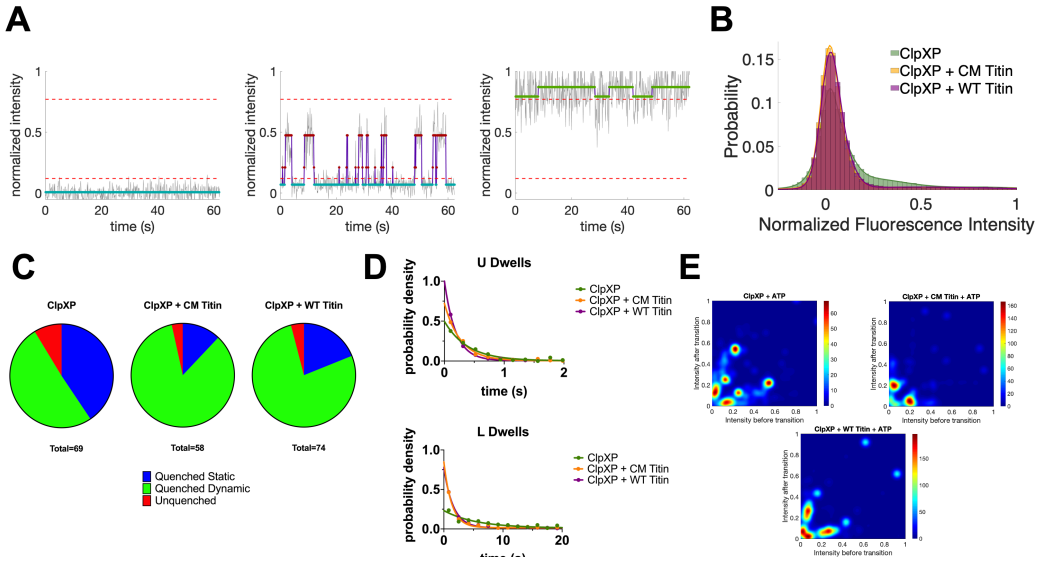

Figure 2.4: **Conformational switching in ClpX combined with colocalization of ClpP binding.** (A) Characteristic traces for single-molecule fluorescence quenching experiments. Left: Quenched static traces have a fluorescence intensity that stays below the threshold for an L conformation (0.12). Middle: Quenched dynamic traces showcase transitions that cross the L conformation threshold. Right: Unquenched traces do not show intensities below the L conformation threshold. (B) Normalized intensity histogram for experiments of ClpXP, ClpXP with ssrA-CM Titin and ClpXP with ssrA-WT Titin. (C) Pie charts showing the fraction of trajectories that fall into the three categories of traces for different substrate conditions. (D) Dwell time histograms for ClpXP trajectories at different substrate conditions. The traces were fit using hidden markov-modeling (HMM) and dwells were extracted based on whether their intensities were above or below the L conformation threshold (0.12). (E) Transition density plots (TDPs) for ClpXP trajectories at different substrate conditions.

tory fraction of traces for ClpXP-only (9%) is triple the percentage for CM Titin (3%) and more than double the percentage for WT Titin (4%).

2.3.7 Multiple distinct Intermediate states are observed which can be revisited in subsequent events

A closer look at the I states in quenched dynamic and unquenched trajectories revealed a distribution of signal intensities. In some cases, ClpX subunits sampled multiple distinct I states during the observation window (Fig. 2.13). In other cases, subunits hopped between

only two states for the entire trajectory (Fig. 2.13). Transition Density Plots (TDPs), heat maps of the initial versus final state during a conformational change, show that that the majority of changes are between states close in intensities (ΔI ¡0.3) (Fig. 2.4e and 2.5e). Additionally, the symmetry of these TDPs highlight that these conformational changes are reversible because there are no forbidden (missing) transitions.

To investigate whether the conformational changes of ClpX subunits follow a sequential or probabilistic mechanism, we measured the change in intensity between dwells one, two or three steps before or after any given dwell (Fig. 2.11 and 2.12). For a strictly sequential model, the difference between a subsequent dwell (In+1) and the current dwell (In) should be positive (In+1 – In = +In+1) except for the last step which would restart the cycles. Therefore, a distribution of these differences should be positive with a much smaller negative population for the resetting step. The opposite trend should occur for previous dwells (In-1 – In = -In-1). Moreover, two successive dwells (In+2) should yield a positive distribution at larger intensity values (In+2 -In = +In+2 2xIn+1). Our data displays a much different pattern. Differences between one state before (In-1) and one state after (In+1) both show positive and negative distributions with similar amplitudes. This means that ClpX subunits generally have an equal probability to increase or decrease in intensity. For two states before (In-2) and after (In+2), a large peak at 0 emerged revealing that the majority of traces revisit a given state after a single excursion to a different state. Half of these states are likely attributed to a transition from a baseline, up and then back to the baseline. Yet a significant additional fraction (25%) of the 0 peak means that excited levels are revisited. Three steps forward and backward showcase distributions that appear to be a mixture of one and two steps. Taken together, the TDPs and intensity difference histograms supports a probabilistic model with reversible transitions rather than a strictly sequential model.

2.3.8 Nucleotide dependence of conformational states in ClpX subunits

What is the relationship between nucleotide binding/hydrolysis and conformational switching in ClpX subunits? We addressed this question by performing QA5B fluorescence quenching experiments in the presence of saturating ATP, ADP, or ATPS or in the absence of nucleotide. The mean intensity of the quenched peaks for ATP (0.01) and ATPS (0.01) histograms were identical and the value for ADP (0.04) was slightly higher (Fig. 2.5a). Interestingly, the mean intensity for the quenched peaks for all three nucleotides were lower than the no nucleotide peak which was centered the highest at (0.08), suggesting that ClpX subunits generally adopt a more compact conformation in the presence of nucleotide. Moreover, the no-nucleotide histogram contains a shoulder on the right indicating that nucleotide-free ClpX subunits adopt more extended conformations. Notably, the ATPS histogram exhibits a broad second population with intensities greater than 0.5, representing extension generally not found in other conditions. ATPS is hydrolyzed at a much slower rate than ATP and increases pausing during translocation [23, 24]. An increase in U-like subunits may be due to more frequent ring resetting caused by this unnatural fuel (see Discussion). Thus, nucleotide binding increases the populations of L subunits, in agreement with structural studies.

Pie charts for the four nucleotide conditions show striking differences (Fig. 2.5b). No quenched static traces appear in the no nucleotide condition, further reinforcing that fewer L subunits are present at this condition. Saturating ADP had the highest percentage of quenched static traces (30%), followed by ATPS (18%) and ATP (11%). ADP cannot be hydrolyzed by ClpX, ATPS is hydrolyzed slowly, and ATP is hydrolyzed 10-fold faster than ATPS. Therefore, the increase in quenched static subunits correlates with the rate of hydrolysis for each nucleotide type. This observation suggests the quenched static state is a nucleotide-bound state. Lastly, ATPS had a higher percentage of unquenched traces than other nucleotides (9%), which was similar to the proportion of unquenched traces for the no nucleotide condition (10%). This result supports a model in which ATPS induces

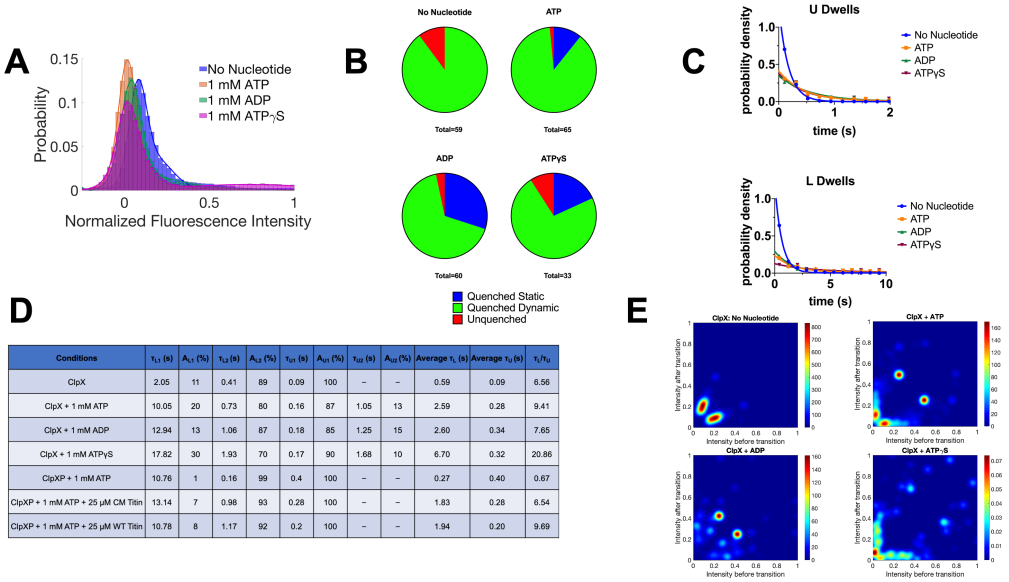

Conditions	τ_{L1} (s)	A_{L1} (%)	τ_{L2} (s)	A_{L2} (%)	τ_{U1} (s)	A_{U1} (%)	τ_{U2} (s)	A_{U2} (%)	Average τ_L (s)	Average τ_U (s)	τ_L/τ_U
ClpX	2.05	11	0.41	89	0.09	100	–	–	0.59	0.09	6.56
ClpX + 1 mM ATP	10.05	20	0.73	80	0.16	87	1.05	13	2.59	0.28	9.41
ClpX + 1 mM ADP	12.94	13	1.06	87	0.18	85	1.25	15	2.60	0.34	7.65
ClpX + 1 mM ATPγS	17.82	30	1.93	70	0.17	90	1.68	10	6.70	0.32	20.86
ClpXP + 1 mM ATP	10.76	1	0.16	99	0.4	100	–	–	0.27	0.40	0.67
ClpXP + 1 mM ATP + 25 μM CM Titin	13.14	7	0.98	93	0.28	100	–	–	1.83	0.28	6.54
ClpXP + 1 mM ATP + 25 μM WT Titin	10.78	8	1.17	92	0.2	100	–	–	1.94	0.20	9.69

Figure 2.5: **Nucleotide type affects subunit class and switching kinetics.** (A) Normalized intensity histograms for different nucleotide conditions. Normalized intensity histograms for quenched dynamic QA5B in the presence of saturating ATP, ADP, ATPS and no nucleotide. (C) Pie charts of percentages of traces that fall into different categories for various nucleotide conditions. (D) Dwell time kinetics. The histogram on top is for extended (U state and intermediate states) dwell times and the one on the right is for the L dwell times. Extended and L dwell times histograms were fitted to single exponential functions. (E) Transition density plots (TDPs) for ClpX trajectories at different nucleotide conditions.

more dramatic conformations or ring resetting events and, as a result, fewer subunits are nucleotide bound than with ATP or ADP. The variation of subunit partitioning into three classes further validates the conclusions that nucleotide binding increases L subunits and ATPS increases non-L-like subunits. Additionally, ADP causes more static subunits.

We extracted the dwell times and binned them into histograms for all four nucleotide conditions. Surprisingly, the no-nucleotide condition had the shortest I (U* = 0.09 s) and L (L = 0.59 s) dwells (Fig. 2.5c). This result indicates that the fastest rate of transition between L and U* states occurs in the absence of nucleotide and is thermally driven. The differences between the three nucleotide conditions were markedly smaller. ATPS had the longest L dwells (L = 6.7 s), possibly due to its slow hydrolysis rate. The L dwells for ATP (L = 2.6 s) and ADP (L = 2.6 s) were identical. All three nucleotides had very similar I dwells (ATP: U* = 0.28 s; ADP: U* = 0.34 s; ATPS: U* = 0.32 s). This similarity implies that the rate of I L transitions represents the nucleotide binding step. This kinetic analysis does not account for dwells in quenched static and unquenched traces because these traces do not cross the transition threshold (0.12), so the bulk of changes in overall hydrolysis rates may be due to changing proportions of these classes. Generally, nucleotide interaction slows down conformational switching and the length of L dwells depend on the rate of hydrolysis.

2.4 Discussion

2.4.1 A new ClpX conformational state is observed and the U state is rare under normal conditions

This study provides direct observation of conformational switching in a single subunit of ClpXP and ClpX in real-time. Both the ensemble and single molecule results shown here demonstrate that conformational asymmetry of ClpX hexamers occurs in solution as seen in ClpX crystal structures [6]. For all conditions tested here, the majority of subunits occupied

L states. This agrees with biochemical data from previous studies, which typically show the majority of ClpX subunits in an L conformation [7]. Conformational switching is necessary for normal ClpX function [7, 10]. ClpXP with single subunits locked into either an L or U conformation have lower degradation rates than wild-type ClpXP even though they have an increased hydrolysis rate. Restricting the movements in two L subunits intensifies these effects while two U-locked subunits decrease the hydrolysis rate while also inhibiting substrate degradation. These studies paired with ours suggest that a working ClpX hexamer adopts a configuration dominated by L-like character (6L) where subunits can frequently visit intermediate extended states (I) but not true U states in contrast to the 4L:2U hexamer seen in crystal structures.

2.4.2 A working ClpX motor requires static L subunits

Our results show that in addition to having unique conformational states, subunits can occupy distinct kinetic classes for conformational switching. Interestingly, one class of subunits, quenched static, persists in the L conformation and does not switch to an intermediate or U state during the minute timescale observation window. For ClpXP, approximately 12% of CM Titin and 19% WT titin are in this category meaning one of six subunits is static through complete cycles of unfolding and translocation. While even more (2-3) subunits appear to be in an off state in the absence of substrate (41%). For ClpX-only approximately 11% of ClpX subunits in saturating ATP and 30% in saturating ADP are in a static state. The existence of a static class indicates that some subunits must remain in a compact conformation while cycles of ATP binding, hydrolysis and conformational change occurs in other subunits. The need for static states when binding and hydrolysis occurs is supported by the fact that no traces fall into a static category in the absence of nucleotide. While static traces could represent inactive motors, binding of ClpP and the increase in percentage of dynamic subunits in the absence of nucleotide suggest these are competent subunits. Moreover, ADP has the highest percentage of subunits in a static category. The

static class appears to represent subunits with nucleotides bound but are not undergoing hydrolysis.

Comparing ClpX-only to when ClpX binds ClpP in the absence of substrate, the percentage of subunits in the quenched static class increases by 30% and the unquenched class by 8%. Previous biochemical measurements have shown the ClpP binding suppresses ATP hydrolysis [23]. Our results show, switching between the L and I state is regulated by nucleotide binding and hydrolysis, so greater proportions of quenched static traces along with slower switching kinetics are expected. Additionally, when comparing ClpXP in the presence of folded substrate to unfolded substrate, there are 8% fewer quenched dynamic and 7% more quenched static traces suggesting translocation increases the activity of subunits and unfolding favors static subunits. Ensemble measurements established that translocation of unfolded substrates enhances ATP hydrolysis rates, but the degradation of folded substrates decreases this turnover rate [4]. This provides further evidence that transitions between L and I are linked to nucleotide binding and hydrolysis.

The second class of subunits present are the quenched dynamic subunits which hop between the L and I states. Quenched dynamic traces appeared in all conditions. ClpXP increases its proportion of subunits that move when substrate is present with the most movement observed with unfolded titin. For ClpX only, about 90% of no nucleotide traces and 89% of saturating ATP traces are dynamic. Similar motions seen in the absence of nucleotide suggest that conformational switching can be thermally driven because neither binding nor hydrolysis is needed for it to occur. However, nucleotide binding and hydrolysis affect both the percentage of quenched dynamic subunits and the rates of switching. With nucleotide, conformational switching is much slower and larger movements are more accessible (Fig. (Fig. 2.5e). Perhaps the nucleotide binding and hydrolysis enhance thermally driven processes. Interestingly, the L and I dwells for ATP and ADP are very similar, but ATPS has a much longer L dwell. This difference suggests that hydrolysis of ATPS may be a rate limiting step for the L I transition. Thus, the observed ring conformations are both

consistent with thermally driven changes and influenced by binding and hydrolysis.

Is ClpXP shifting gears between translocation and unfolding tasks? TDPs for ClpXP show different profiles for unfolding (WT Titin) and translocation states (CM Titin). For ClpXP in the presence of unfolded CM Titin where translocation is occurring we see a single peak representing L to I transitions suggesting translocation has a dominant gear where larger motions occur. For WT titin we expect to observe states corresponding to both unfolding and translocation tasks. Here we see transitions that include: 1) very deep L like transitions 2) a broader peak with L to I states similar to that found in CM Titin and 3) some minor population of true U states. The ClpXP WT Titin plots suggest a few gears can be accessed: a low gear with small L constrained motions and a higher gear with motions spanning L and I positions that likely encompasses translocation.

How are these motions linked to the ATP hydrolysis cycle? TDPs for ClpX only (Fig. 2.5e) help tie the chemical cycle of ATP binding hydrolysis and release of ADP with conformational motions. From observations here and crystal and cryoEM structures the ATP bound state and ATPgS appears to be an L conformation. Movement deep in the L state seems to correspond to nucleotide hydrolysis. While ADP states show significant populations of static L states, the ADP transition density plots populates a I state which is also seen in ClpX with ATP. The no-nucleotide state appears to show a band of I states suggesting subunits breath more. If we assume the major motor conformational change is tied to a I to L transition then these observations suggest it is ATP binding that drives the working stroke and that ADP release is associated with the recovery stroke (L to I).

2.4.3 Sequential versus stochastic models

How do ClpX subunits coordinate their conformational motion? Two models often proposed for AAA+ hexameric rings are the sequential and stochastic model [5]. If ClpX follows a sequential model, we would expect to see patterns of this model in ClpX's conformational motions. Here we observe a class of static quenched subunits are present for

all conditions except no nucleotide. These subunits persist in the L conformation and have no major movements during the observation window. For these subunits to appear in a sequential process, subunits must be skipped often as movements cycle around the ring. Additionally, conformational motions in sequential models progress in one direction until the cycle resets. Our analysis of TDPs and intensity differences between dwells various steps apart show that conformational switching in ClpX subunits is symmetric and thus overwhelmingly reversible (Fig.(Fig. 2.4e and 2.5e). Therefore, rather than moving in one direction as expected with a sequential model, most subunits revisit previous conformations repeatedly. Lastly, subunits generally hop between states close in intensity but can skip states and make large jumps (Fig. 2.13, 2.4e and 2.5e). The trajectories reveal no compelling pattern or sequence of regular ordinary motion. Rather, multiple schemes are observed for active transitioning states for periods of great activity followed by periods of rest (supplemental page 7-8). These observations favor a stochastic model where ClpX subunits have the freedom to explore a wide range of conformations. Bulk measurements have suggested that ClpX's mechanochemical cycle most closely resembles a probabilistic model and does not agree with a sequential model. Our single-molecule analysis further supports this conclusion.

Our observations put further constraints on motion and lead to some potential models for motor function. We observe trajectories with long periods where our labeled subunit doesn't transition much followed by bursts of activity. L dwells are long relative to the times associated with translocation, suggesting most subunits are not undergoing large motions and only a few are actively exhibiting large motions. If L to I and I to L transitions are linked to the translocation motility cycle perhaps the working stroke is associated with transitioning between one subunit or a small subset repeatedly undergoing working stroke motions and recovery. The ring would be in a nominal 6L state where one or more of the subunits would repeatedly adopt a I state and return to L. These particularly mobile subunits can randomly switch to other subunits in the ring on a timescale longer than the

motility cycle time.

Is a single site acting independently and not coupled to its neighbors? We know that rings with hobbled hydrolysis at subunits still support translocation of similar step size distribution but at slower rates and longer pauses [25]. If a single site was acting independently and uncoupled to its neighbors, then translocation trajectories of hobbled motors should show step dwells with similar velocities to WT [25] (Fig. 2.5c). Furthermore, rings with hobbled subunits are not able to work against high loads (26 pN WT vs 10 pN RW-ERWE). We know that ClpXP can take translocation steps of 3 or 4nm against a 26 pN load. The energy associated with this is 78-104 pN*nm which is at or more than the total energy available from hydrolysis of a single ATP molecule. Slower unfolding rates in hobbled motors suggest ATP hydrolysis energy from multiple sites is coupled to translocation. Our observations favor a model where motion of a subunit is energetically coupled to ATP hydrolysis in neighboring sites.

ClpXP is processive which means it holds on tightly to its substrate. Somehow during the translocation process sites need to be able to cycle through cycles of grabbing and release at different locations along the polypeptide backbone. A model where multiple L state pore loops are holding on collectively helps maintain processivity. Perhaps hydrolysis cycles within L like states permits the pore loops to release the polypeptide and re-grip. The small degree of conformational change in these subunits is not consistent with the observed step magnitude. If a single subunit is able to grab and undergo much larger motion of a pore loop the other L like subunits can re-set their position anchoring the additionally translocated polypeptide allowing the actively moving subunit to reach up and reel in more polypeptide rope. If this process can occur out of phase or such that some subunits are holding on during multiple cycles then processivity is increased. Perhaps pore loop grabbing and release dynamics are different among static L, dynamic L and L to I states leads to observed processivity.

Our novel assay utilizes fluorescence quenching to observe conformational motions in

a single subunit of ClpX. The use of a dark quencher instead of a traditional FRET acceptor allowed for dynamic measurements in the critical 1-3nm distance range of small motions within a single ClpX subunit. Through calibration of this quencher-fluorophore pair with a DNA-based spectroscopic ruler, we were able to convert this assay into a ratiometric measure of inter-probe distance similar to FRET. The strategy increased the fluorescence observation time due to the use of a robust fluorophore and a photobleaching-resistant dark quencher. Moreover, only the conventional donor channel was required for imaging ATTO 550 which made the conventional acceptor channel available for colocalization measurements of ClpP labeled with Alexa Fluor 647. This additional experimental layer provided an additional observable for verifying that ClpX is bound to ClpP. Finally, the fidelity of the measurement was improved by employing a simple microfluidic arrangement and sequenced stages of imaging, buffer exchange, photobleaching and SDS unquenching signal levels. Here we visualized a state that hadn't been seen in available crystal or cryoEM structures showing the power of single molecule measurements at native conditions on active systems. These motions are likely important in ClpXP stages of degradation and translocation. Our assay presents a straightforward method to interrogate conformational changes in biomolecules that are shorter than the range of most FRET pairs and a work flow that would be beneficial for visualizing the active state of other complex dynamic biological machines.

2.5 Supplemental Figures

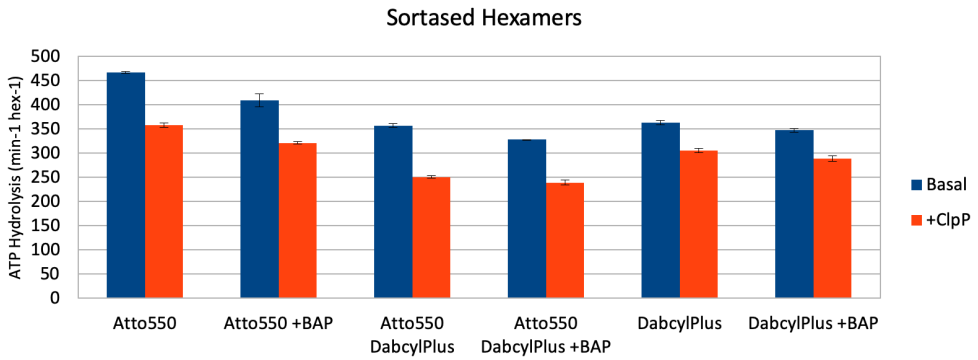

Figure 2.6:

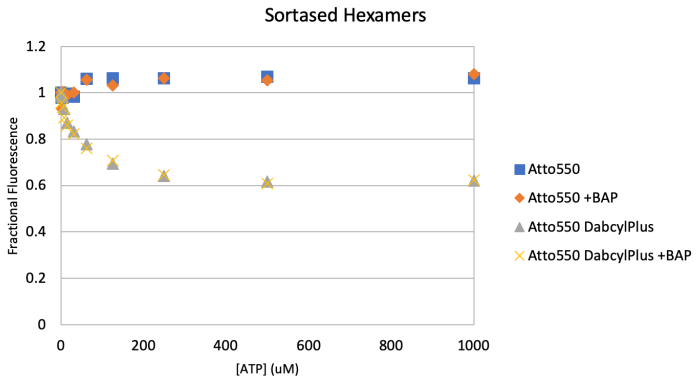

Figure 2.7:

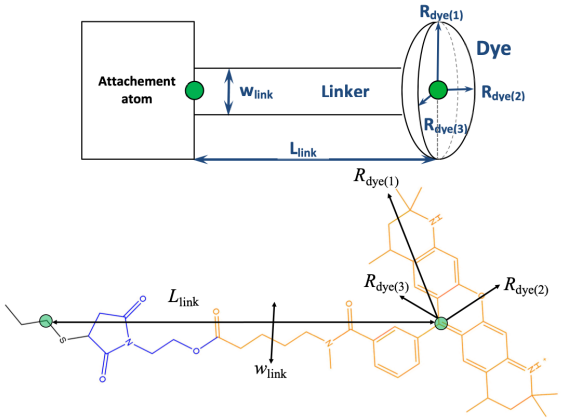

Dye parameters for fluorophores attached to DNA

Dye	Dye Parameters					
	# of linker atoms	L_{link} [Å]	w_{link} [Å]	$R_{dye(1)}$ [Å]	$R_{dye(2)}$ [Å]	$R_{dye(3)}$ [Å]
3′ ATTO 550 Maleimide	18	24.2	4.5	7.9	4.2	1.5
5′ Dabcyl Plus SE	8	14.6	4.5	6.2	2.8	1.5
Internal Dabcyl Plus SE	12	19.8	4.5	6.2	2.8	1.5

Dye parameters for fluorophores attached to cysteine residues in ClpX

Dye	Dye Parameters					
	# of linker atoms	L_{link} [Å]	w_{link} [Å]	$R_{dye(1)}$ [Å]	$R_{dye(2)}$ [Å]	$R_{dye(3)}$ [Å]
ATTO 550 Maleimide		14.5	4.5	7.9	4.2	1.5
Dabcyl Plus Maleimide		15.8	4.5	6.2	2.8	1.5

Figure 2.8:

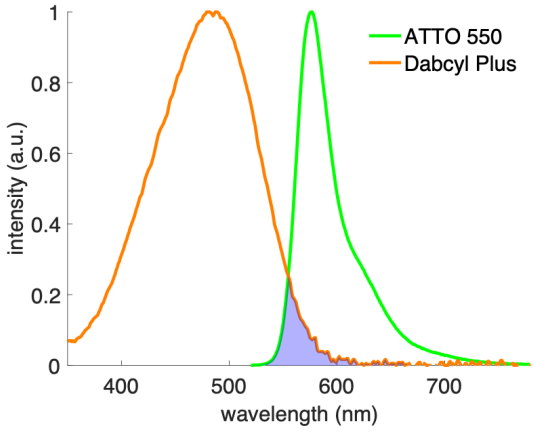

$$R^0 = 0.211(\kappa^2 n^{-4} Q_D J(\lambda))^{1/6} \text{ (Å)}$$

$$J(\lambda) = \frac{\int_0^\infty F_D(\lambda)\varepsilon_A(\lambda)\lambda^4 d\lambda}{\int_0^\infty F_D(\lambda)\, d\lambda}$$

$$\kappa = \frac{2}{3} \qquad n = 1.4 \qquad Q_D = 0.8$$

$$J = 9.89 \times 10^{13}\ nm^4/M \cdot cm$$

$$R^0 = 30.5 \text{ Å}$$

Figure 2.9:

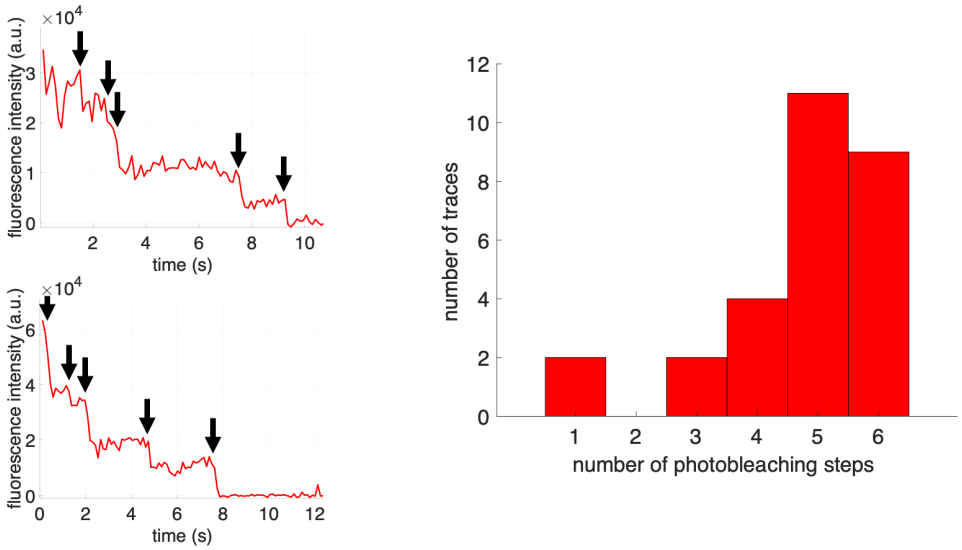
×10^4
fluorescence intensity (a.u.)
time (s)
×10^4
fluorescence intensity (a.u.)
time (s)
number of traces
number of photobleaching steps

Figure 2.10:

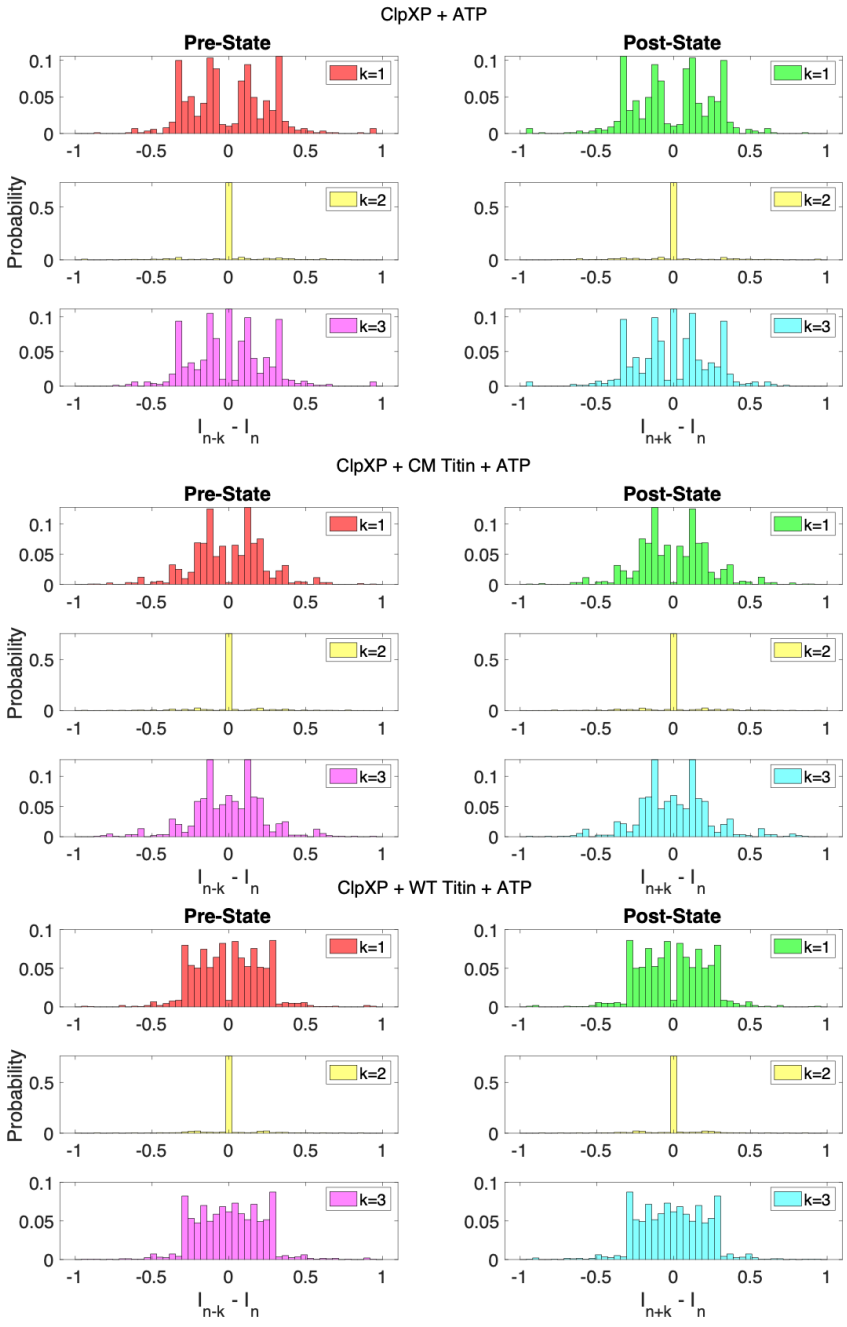
ClpXP + ATP
Pre-State
Post-State
k=1
k=2
k=3
Probability
$l_{n-k} - l_n$
$l_{n+k} - l_n$
ClpXP + CM Titin + ATP
Pre-State
Post-State
k=1
k=2
k=3
Probability
$l_{n-k} - l_n$
$l_{n+k} - l_n$
ClpXP + WT Titin + ATP
Pre-State
Post-State
k=1
k=2
k=3
Probability
$l_{n-k} - l_n$
$l_{n+k} - l_n$

Figure 2.11:

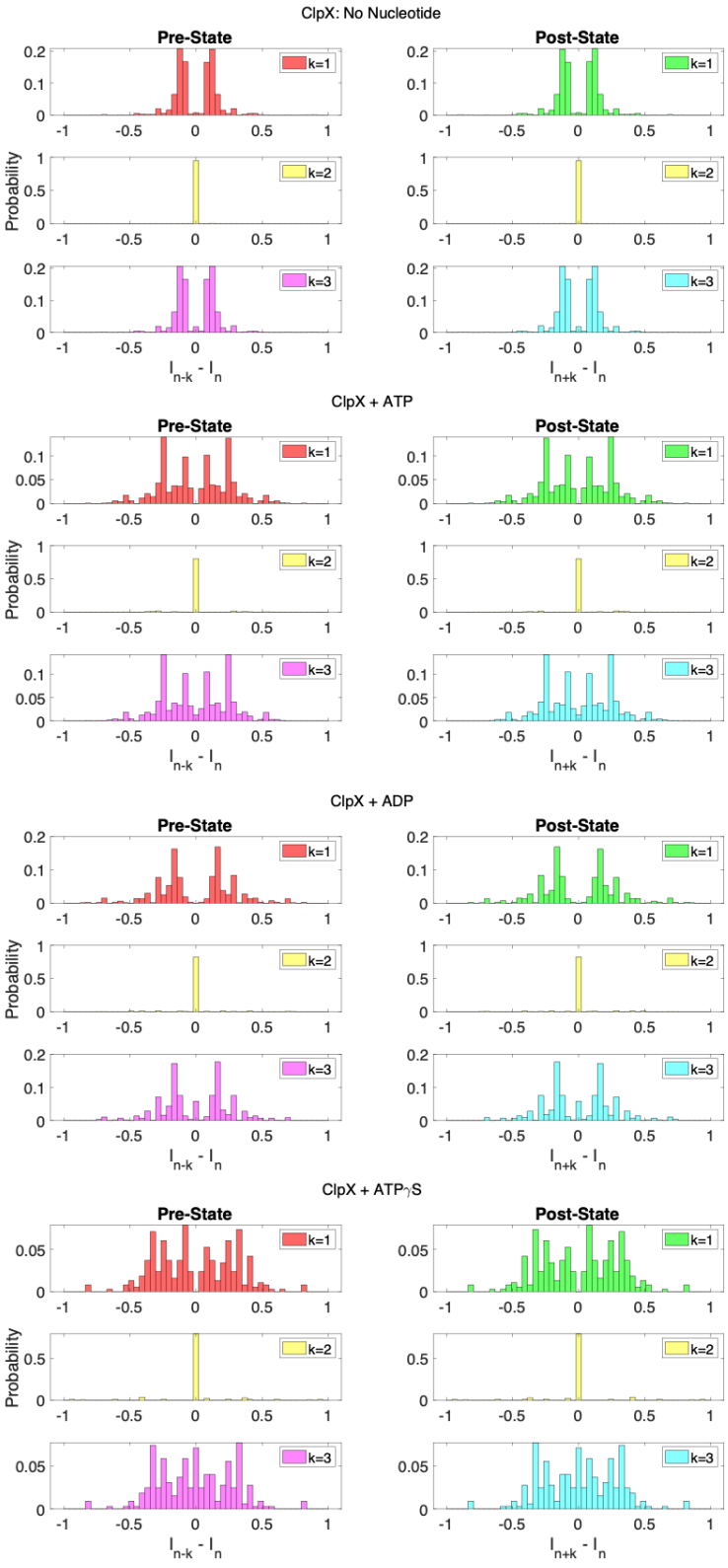
ClpX: No Nucleotide
Pre-State
Post-State
k=1
k=2
k=3
Probability
$I_{n-k} - I_n$
$I_{n+k} - I_n$
ClpX + ATP
ClpX + ADP
ClpX + ATPγS

Figure 2.12:

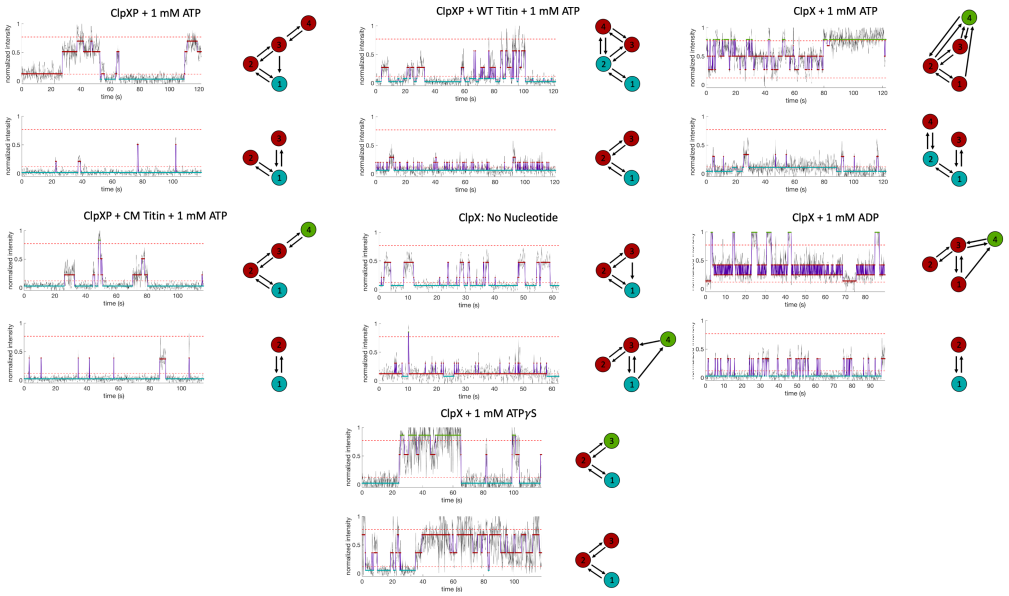
ClpXP + 1 mM ATP
ClpXP + WT Titin + 1 mM ATP
ClpX + 1 mM ATP
ClpXP + CM Titin + 1 mM ATP
ClpX: No Nucleotide
ClpX + 1 mM ADP
ClpX + 1 mM ATPγS
normalized intensity
time (s)

Figure 2.13:

2.6 Materials and Methods

2.6.1 Protein Expression and Purification

ClpX constructs were derived from E. coli ClpXΔN (residues 61-424). The modification C169S was introduced to remove an accessible native cysteine. ClpX hexamers were constructed from a dimer of trimers fused via sortase ligation. Each trimer was purified using Ni-NTA chromatography and digested with TEV protease to cleave the H_6 tagged TEV. Trimer A, which had a Q167C modification (W-W-Q) was labeled with ATTO 550-maleimide and trimer B, which had a K213C modification (K-W-W) was labeled with DabcylPLUS-maleimide. Trimers were reacted with 3-fold excess of the required maleimide-functionalized fluorophore or quencher at room temperature for 30 minutes. The reaction was quenched with 1mM DTT and desalted with Xlink buffer using a PD10 column (GE Healthcare). Trimer B also had a C-terminal biotin acceptor peptide sequence (GLNDIFEAQKIEWHE) that was recognized for biotin conjugation by biotin ligase (BirA) from E. coli. The biotin tags were used to immobilize ClpX constructs on streptavidin coated surfaces for single-molecule measurements.

Trimers A and B contained the appropriate modifications for successful sortase ligation. Trimer A had a C-terminal LPETG sortase recognition tag and Trimer B had an N-terminal poly-glycine motif that was exposed upon digestion with TEV protease. An evolved S. aureus sortase-A enzyme with P94S/D160N/K194T substitutions [26] was used to ligate the trimers. Sortase reaction mixtures consisted of 5 μM trimer A, 5 μM trimer B and 1 μM sortase. The reaction was done at room temperature for 2-4 hours in Xlink buffer supplemented with 5 mM $CaCl_2$ and 1 mM DTT. Titin I27-ssrA substrates and ClpP were expressed and purified as previously outlined [4, 27]. Unfolded titin I27-ssrA substrates were produced by denaturing native substrates in iodoacetic acid, as shown in [4].

2.6.2 Bulk Fluorescence Assay

ClpX ATP hydrolysis rates were measured using an NADH enzyme coupled assay [**?**]. The GFP-ssrA degradation rate was measured using an SF-300X stopped-flow instrument (KinTek). Equal volumes of an ATP solution and premixed ClpX and substrate were quickly combined and the initial fluorescence decrease of the substrate was observed (excitation 480 nm; emission 510 nm). Fluorescence quenching measurements of ClpX were carried out using a PTI QM-20000-4SE spectrofluorimeter (excitation 530, emission 580).

2.6.3 Single Molecule Coverslip Preparation

Glass coverslips (Fisherbrand) were sonicated sequentially in deionized water, methanol and 1M KOH. The etched coverslips were sonicated at 35 °C in a solution with 1% (w/v) of PEG mixture (1% biotin-PEG-silane, MW 5000; 99% mPEG-silane, MW 5000, Laysan Bio) and 0.8 mM trimethylamine in 30 mL of ACS grade toluene (Fisher Scientific). The coverslips were then washed with toluene, copious amounts of deionized water and dried with pressurized air. The PEG-functionalized coverslips were stored at -20 °C in 50 mL Falcon tubes filled with nitrogen until flow cells were assembled.

2.6.4 Single Molecule Fluorescence Assay

Flow cells were constructed by forming a channel between two strips of double-sided tape sandwiched between a glass slide and a PEG coverslip. A 0.1 mg/mL solution of streptavidin in PBS (100 mM phosphate buffer, pH 7.5) was introduced to the flow cell and allowed to incubate for 10 minutes. Unbound streptavidin was washed out with PD (25 mM HEPES pH 7.6, 100 mM KCl, 10 mM MgCl2, 10% glycerol (vol/vol)) and 40 µL of 625 pM ClpXP in PD in the presence of 3 mM ATP was flowed into the flow channel and incubated for 20 minutes. Afterwards, unbound ClpXP was washed out with an ATP solution containing ClpP followed imaging buffer with an oxygen scavenging and triplet-state

quencher (0.8% D(+)-glucose, 16500 units/mL glucose oxidase, 217000 units/mL catalase, and 2 mM Trolox) and the desired nucleotides/substrates and ClpP prior to imaging.

2.6.5 Instrument Setup

Data was collected on a custom-built objective-side total internal fluorescence (TIRF) microscope. The instrumental setup consists of a 100x 1.49 NA objective (Nikon), illumination at ZZ mW from a laser diode (Blue Sky Research) and an EMCCD camera (Andor) for fluorescence imaging. Data was acquired at 8.8 Hz.

2.6.6 Data Analysis

Custom Matlab scripts were used to process and analyze the data. Hidden Markov Modeling (HMM) was used to create idealized traces for identifying conformational states and extracting dwell time kinetics [19, 18]. Only traces showing a single photobleaching step, an emission intensity above 2000 counts/sec and emission lasting longer than 10 seconds were analyzed.

2.7 Acknowledgements

We thank Ben Stinson and Tristan Bell for producing ClpX, ClpP and ssrA-tagged substrates and performing bulk measurements. We thank Robert Sauer and Tania Brady for numerous helpful discussions and thoughtful suggestions. This work was supported by NSF (1330792) and GAANN (P200A090323).

2.8 Bibliography

[1] Phyllis I Hanson and Sidney W Whiteheart. AAA+ proteins: have engine, will work. *Nature reviews. Molecular cell biology*, 6(7):519–29, jul 2005.

[2] T Ogura and a J Wilkinson. AAA+ superfamily ATPases: common structure–diverse function. *Genes to cells : devoted to molecular & cellular mechanisms*, 6(7):575–97, jul 2001.

[3] Tania a Baker and Robert T Sauer. ClpXP, an ATP-powered unfolding and protein-degradation machine. *Biochimica et biophysica acta*, 1823(1):15–28, jan 2012.

[4] Jon a Kenniston, Tania a Baker, Julio M Fernandez, and Robert T Sauer. Linkage between ATP consumption and mechanical unfolding during the protein processing reactions of an AAA+ degradation machine. *Cell*, 114(4):511–20, aug 2003.

[5] Andreas Martin, Tania a Baker, and Robert T Sauer. Rebuilt AAA + motors reveal operating principles for ATP-fuelled machines. *Nature*, 437(7062):1115–20, oct 2005.

[6] Steven E Glynn, Andreas Martin, Andrew R Nager, Tania a Baker, and Robert T Sauer. Structures of asymmetric ClpX hexamers reveal nucleotide-dependent motions in a AAA+ protein-unfolding machine. *Cell*, 139(4):744–56, nov 2009.

[7] Benjamin M. Stinson, Andrew R. Nager, Steven E. Glynn, Karl R. Schmitz, Tania A. Baker, and Robert T. Sauer. Nucleotide Binding and Conformational Switching in the Hexameric Ring of a AAA+ Machine. *Cell*, 153(3):628–639, apr 2013.

[8] Christos Gatsogiannis, Dora Balogh, Felipe Merino, Stephan A. Sieber, and Stefan Raunser. Cryo-EM structure of the ClpXP protein degradation machinery. *Nature Structural and Molecular Biology*, 26(10):946–954, 2019.

[9] Zev Ripstein, Siavash Vahidi, Walid A. Houry, John L. Rubinstein, and Lewis E. Kay.

A processive rotary mechanism couples substrate unfolding and proteolysis in the ClpXP degradation machinery. *bioRxiv*, pages 1–50, 2019.

[10] Benjamin M Stinson, Vladimir Baytshtok, Karl R Schmitz, Tania A Baker, and Robert T Sauer. Subunit asymmetry and roles of conformational switching in the hexameric AAA+ ring of ClpX. *Nature Structural & Molecular Biology*, 22(5):411–416, 2015.

[11] Chirlmin Joo, Hamza Balci, Yuji Ishitsuka, Chittanon Buranachai, and Taekjip Ha. Advances in single-molecule fluorescence methods for molecular biology. *Annual review of biochemistry*, 77:51–76, jan 2008.

[12] Phil Holzmeister, Bettina Wünsch, Andreas Gietl, and Philip Tinnefeld. Single-molecule photophysics of dark quenchers as non-fluorescent FRET acceptors. *Photochemical & photobiological sciences : Official journal of the European Photochemistry Association and the European Society for Photobiology*, 13(6):853–8, 2014.

[13] Ludovic Le Reste, Johannes Hohlbein, Kristofer Gryte, and Achillefs N Kapanidis. Characterization of dark quencher chromophores as nonfluorescent acceptors for single-molecule FRET. *Biophysical journal*, 102(11):2658–68, jun 2012.

[14] Stanislav Kalinin, Thomas Peulen, Simon Sindbert, Paul J Rothwell, Sylvia Berger, Tobias Restle, Roger S Goody, Holger Gohlke, and Claus A M Seidel. A toolkit and benchmark study for FRET-restrained high-precision structural modeling. 9(12), 2012.

[15] Björn Hellenkamp, Sonja Schmid, Olga Doroshenko, Oleg Opanasyuk, Ralf Kühnemuth, Soheila Rezaei Adariani, Benjamin Ambrose, Mikayel Aznauryan, Anders Barth, Victoria Birkedal, Mark E. Bowen, Hongtao Chen, Thorben Cordes, Tobias Eilert, Carel Fijen, Christian Gebhardt, Markus Götz, Giorgos Gouridis, Enrico Gratton, Taekjip Ha, Pengyu Hao, Christian A. Hanke, Andreas Hartmann, Jelle

Hendrix, Lasse L. Hildebrandt, Verena Hirschfeld, Johannes Hohlbein, Boyang Hua, Christian G. Hübner, Eleni Kallis, Achillefs N. Kapanidis, Jae Yeol Kim, Georg Krainer, Don C. Lamb, Nam Ki Lee, Edward A. Lemke, Brié Levesque, Marcia Levitus, James J. McCann, Nikolaus Naredi-Rainer, Daniel Nettels, Thuy Ngo, Ruoyi Qiu, Nicole C. Robb, Carlheinz Röcker, Hugo Sanabria, Michael Schlierf, Tim Schröder, Benjamin Schuler, Henning Seidel, Lisa Streit, Johann Thurn, Philip Tinnefeld, Swati Tyagi, Niels Vandenberk, Andrés Manuel Vera, Keith R. Weninger, Bettina Wünsch, Inna S. Yanez-Orozco, Jens Michaelis, Claus A.M. Seidel, Timothy D. Craggs, and Thorsten Hugel. Precision and accuracy of single-molecule FRET measurements—a multi-laboratory benchmark study. *Nature Methods*, 15(9):669–676, 2018.

[16] Abani K. Bhuyan. On the mechanism of SDS-induced protein denaturation. *Biopolymers*, 93(2):186–199, 2010.

[17] Yongdae Shin, Joseph H Davis, Ricardo R Brau, Andreas Martin, Jon a Kenniston, Tania a Baker, Robert T Sauer, and Matthew J Lang. Single-molecule denaturation and degradation of proteins by the AAA+ ClpXP protease. *Proceedings of the National Academy of Sciences of the United States of America*, 106(46):19340–5, nov 2009.

[18] Jan Willem Van De Meent, Jonathan E. Bronson, Chris H. Wiggins, and Ruben L. Gonzalez. Empirical bayes methods enable advanced population-level analyses of single-molecule FRET experiments. *Biophysical Journal*, 106(6):1327–1337, 2014.

[19] Jonathan E Bronson, Jingyi Fei, Jake M Hofman, Ruben L Gonzalez, and Chris H Wiggins. Learning rates and states from biophysical time series: a Bayesian approach to model selection and single-molecule FRET data. *Biophysical journal*, 97(12):3196–205, dec 2009.

[20] Max Greenfeld, Dmitri S. Pavlichin, Hideo Mabuchi, and Daniel Herschlag. Sin-

gle molecule analysis research tool (SMART): An integrated approach for analyzing single molecule data. *PLoS ONE*, 7(2), 2012.

[21] Sean a McKinney, Chirlmin Joo, and Taekjip Ha. Analysis of single-molecule FRET trajectories using hidden Markov modeling. *Biophysical journal*, 91(5):1941–51, sep 2006.

[22] Larry J. Friedman and Jeff Gelles. Mechanism of transcription initiation at an activator-dependent promoter defined by single-molecule observation. *Cell*, 148(4):679–689, 2012.

[23] Randall E Burton, Tania A Baker, and Robert T Sauer. Energy-dependent degradation: Linkage between ClpX-catalyzed nucleotide hydrolysis and protein-substrate processing. *Protein science : a publication of the Protein Society*, 12(5):893–902, 2003.

[24] Maya Sen, Rodrigo A. Maillard, Kristofor Nyquist, Piere Rodriguez-Aliaga, Steve Pressé, Andreas Martin, and Carlos Bustamante. The ClpXP Protease Unfolds Substrates Using a Constant Rate of Pulling but Different Gears. *Cell*, 155(3):636–646, oct 2013.

[25] Juan Carlos Cordova, Adrian O Olivares, Yongdae Shin, Benjamin M Stinson, Stephane Calmat, Karl R Schmitz, Marie-Eve Aubin-Tam, Tania a Baker, Matthew J Lang, and Robert T Sauer. Stochastic but Highly Coordinated Protein Unfolding and Translocation by the ClpXP Proteolytic Machine. *Cell*, 158(3):647–658, jul 2014.

[26] Irwin Chen, Brent M. Dorr, and David R. Liu. A general strategy for the evolution of bond-forming enzymes using yeast display. *Proceedings of the National Academy of Sciences of the United States of America*, 108(28):11399–11404, 2011.

[27] Yong In Kim, Randall E. Burton, Briana M. Burton, Robert T. Sauer, and Tania A.

Baker. Dynamics of substrate denaturation and translocation by the ClpXP degradation machine. *Molecular Cell*, 5(4):639–648, 2000.

Chapter 3

NUCLEOTIDE BINDING STOICHIOMETRY, TRANSACTION RATES AND SUBUNIT COORDINATION IN ClpX MEASURED WITH SINGLE-MOLECULE FLUORESCENCE QUENCHING

3.1 Summary

The ring-shaped AAA+ enzyme ClpX from Escherichia coli uses the energy of ATP binding and hydrolysis to unfold and translocate target proteins into the proteolytic lumen of ClpP. However, it is still unclear how ClpX subunits interact with nucleotides and coordinate these interactions with other subunits to maintain robust motor function. Here, we have developed a single-molecule fluorescence quenching assay to observe nucleotide transactions in a single ClpX subunit using a novel ATP analog with a dark quencher moiety that we call ATPQ. Fluorescence quenching of a TAMRA labeled ClpX subunit by ATPQ allowed us to observe nucleotide binding/unbinding without being restricted by the concentration barrier imposed by dye-labeled molecules in solution. Our results show that ClpX can bind up to 4-5 nucleotides at saturation, substrate unfolding and translocation increase nucleotide transaction rates of individual subunits and subunits arranged in either the ortho and meta configuration bind nucleotides cooperatively.

3.2 Introduction

AAA+ (ATPases associated with various activities) motors are enzymes that use the energy of ATP binding and hydrolysis to remodel macromolecules in the cell. Enzymes in the AAA+ family play important roles in diverse cellular processes, such as membrane fusion and protein disaggregation and degradation [6, 14, 19]. AAA+ machines typically form multimeric rings and must coordinate nucleotide interactions between ring-members to ensure proper energy transduction and maintain robust machine function. Understanding

how nucleotides interact with individual subunits of these enzymes is key to developing an accurate description of their molecular mechanisms.

The AAA+ enzyme ClpX from Escherichia coli self-assembles into a hexamer and binds to the peptidase ClpP in the presence of ATP to form the protease ClpXP. ClpX, an unfoldase, unravels proteins tagged for degradation and threads the polypeptide through its axial pore to the proteolytic lumen of ClpP. ClpXP mediated mechanical denaturation of a single protein substrate is fueled by numerous ATP binding and hydrolysis events [16]. ATP, ADP and other nucleotides bind to the pocket formed at the hinge between the large and small domain of a ClpX subunit [5, 17]. The six subunits of ClpX are identical polypeptides, but ensemble measurements have shown differences in their binding affinities. Hersch et al. demonstrated that three groups of subunits exist: ones that do not bind nucleotide, slow binders and fast binders [8]. Moreover, this study showed that a ClpX hexamer can bind up to 4 nucleotides at a time. However, these biochemical experiments rely on hydrolytically inactive ClpX hexamers and non-hydrolyzable ATP analogs [8, 11, 17].

What is the overall nucleotide occupancy of a working ClpXP motor? Are there differences in the nucleotide transaction rates of individual ClpX subunits? How do subunits coordinate nucleotide binding with neighboring subunits? To answer these questions, we have developed a single-molecule total internal reflection fluorescence (sm-TIRF) assay that monitors nucleotide binding/unbinding using a novel ATP analog with a dark quencher moiety. Fluorescence quenching allows us to observe molecular interactions without being restricted by the concentration barrier imposed by dye-labeled molecules in solution. Unlike previous studies, this technique was able to measure the binding rates and occupancy of hexamers with six-functional subunits using a hydrolyzable ATP analog. Additionally, we have engineered doubly-labeled hexamers to determine how multiple subunits coordinate nucleotide binding and unbinding.

3.3 Results

3.3.1 ClpX construct and ATP analog used to observe nucleotide binding

To observe nucleotide binding and unbinding events in individual ClpX subunits, we designed a ClpX construct that was fluorescently labeled near the nucleotide binding pocket and an ATP analog with an attached dark-quencher moiety. Residue 330 was chosen for labeling based on its proximity to the nucleotide binding pocket in the L conformation [5, 17]. Labeling of ClpX with TAMRA-maleimide was facilitated through a K330C modification to one subunit in a ClpXδN trimer gene and the removal of all exposed endogenous cysteines through a C169S mutation. Some batches of the modified ClpX trimer had a C-terminal biotin tag for surface immobilization in ClpX-only single-molecule measurements. A covalent ClpX hexamer was formed via sortase ligation of the labeled trimer with another ClpX trimer (labeled or unlabeled subunits).

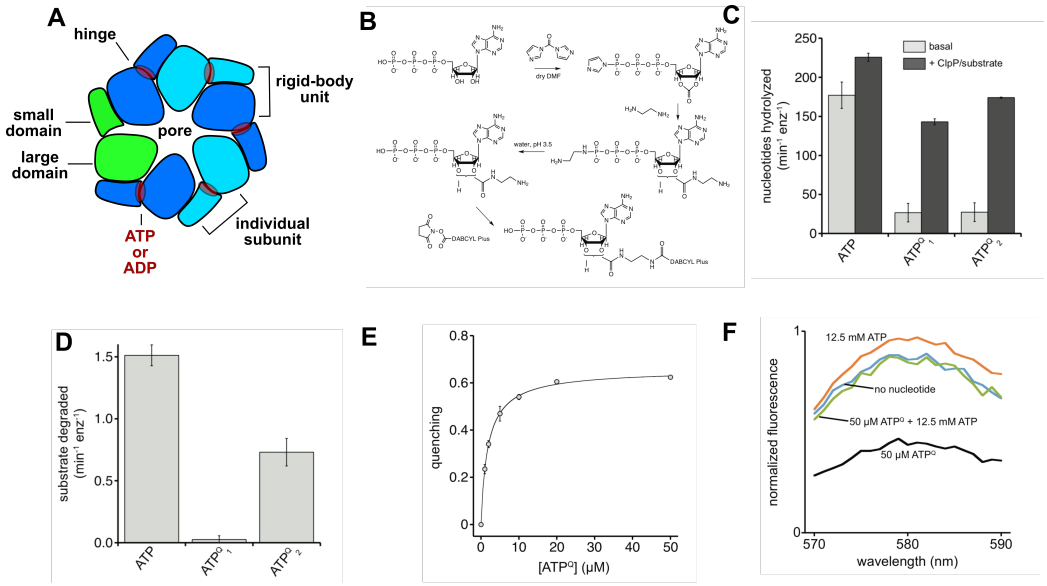

Figure 3.1: **ATPQ is a Fluorescence Quenching ATPQ Analog** (A) Illustration showing structural elements of a ClpX hexameric ring. (B) Reactions scheme for synthesizing ATPQ (C) Hydrolysis rate of ATPQ by ClpX compared to ATP. The presence of ClpP and substrate enhance hydrolysis to near wild type levels. (D) ATPQ2 but not ATPQ1 supports ClpXP mediated substrate degradation. (E) Quenching increases with increasing concentrations of ATPQ. (F) Excess ATP outcompetes ATPQ for ClpX binding sites.

We synthesized an ATP analog with a ribose-linked quencher based on the method presented by Hazlett et al. [7]. The 2 and 3 hydroxyls of ATP were activated by carbonyldiimidazole to form a cyclic carbonate species, then reacted with ethylenediamine to produce ethylenediamine-ATP (eda-ATP). Eda-ATP was reacted with Dabcyl Plus-succinimidyl ester to yield a mixture of 2' and 3' isomers of Dabcyl Plus-eda-ATP, which we call ATPQ. Chromatography of the isomeric mixture on a DEAE-sepharose column produced two peaks (Fig. 3.2a(i)), which contained molecules that migrated at slightly different rates in thin-layer chromatography (Fig. 3.2b-c). The purified isomers were stored at pH 6.0 and –80 °C to inhibit isomerization [15]. The two peaks re-isomerized after multiple days at room temperature ((Fig. 3.2a(ii-iii)).

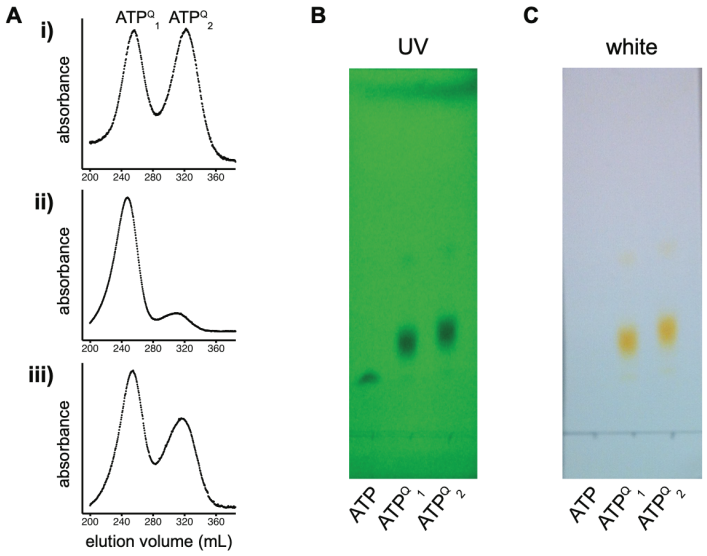

Figure 3.2: **Isomers of ATPQ** (A) 2' and 3' ATPQ isomers were purified by chromatography on a DEAE- Sepharose column and tracked using absorbance at 280 nm. (i) The initial reaction mixture contained two peaks, corresponding to each isomer. (ii) Isolated ATPQ1, chromatagrpahed immediately after thawing. (iii) Isolated ATPQ1 chromatographed after 5 days at room temperature. (B)-(C) ATP and purified ATPQ isomers were both chromatographed on F254 indicator silica gel TLC plates and observed by UV illumination (B) or white light illumination (C).

A suitable ATP analog for our single-molecule binding assay should not only quench fluorescence when bound but also support ClpX nucleotide hydrolysis and substrate degra-

dation activity. Both ATPQ isomers were hydrolyzed by ClpX alone 7 times slower than ATP (Fig. 3.1c). However, the presence of ClpP and an ssrA-tagged protein substrate enhanced ClpX's hydrolysis rate of both isomers up to 60-80% the rate of ATP hydrolysis at the same condition (Fig. 3.1c). Interestingly, the ClpXP substrate degradation rate with ATPQ2 was half the rate of ATP-fueled degradation, but ATPQ1 did not support substrate degradation(Fig. 3.1d). Therefore, we only used ATPQ2 (ATPQ here on) for all other measurements in this study.

We performed ensemble fluorescence experiments to measure ATPQ binding before designing a single-molecule binding assay. We mixed a constant concentration of singly-labeled ClpXTAMRA with increasing concentrations of ATPQ and measured the fluorescence output with a fluorimeter. A fit of the resulting binding curve revealed that ATPQ has an apparent binding affinity (KD) for ClpX of 2 μM and saturates at 65% quenching (Fig. 3.1e). Moreover, ATP competition experiments show a recovery of fluorescence at the same concentration of ATPQ that shows pronounced quenching, demonstrating that ATP displaced ATPQ and that both nucleotides bind to the same sites. Taken together, bulk experiments show that ATPQ supports ClpX catalyzed hydrolysis, ClpXP mediated substrate degradation and reports nucleotide binding.

3.3.2 ATPQ shows robust, specific quenching of a fluorescently labeled ClpX subunit at the single-molecule level

We observed ATPQ binding and unbinding to a single subunit of a ClpX hexamer using single-molecule total internal reflection fluorescence (smTIRF) microscopy. Biotinylated singly-labeled ClpXTAMRA hexamers were immobilized on streptavidin-coated glass surfaces in flow cells. Fluorescent ClpX spots were imaged for 10 s before flowing in a buffer containing ATPQ (Fig. 3.3b, lower panel). In the presence of ATPQ, the fluorescence intensity of individual ClpX spots fluctuated between high and low levels before photobleaching in a single step. When the ATPQ buffer was exchanged for an ATP buffer, the imaged spots

exhibited stable fluorescence intensities (Fig. 3.3c).

We varied the concentration of ATPQ from 1 μM to 200 μM to investigate ClpXP's affinity for the nucleotide at the single-molecule level. The initial 10 s wait time before flowing in ATPQ was used to normalize the subsequent quenching events and generate intensity histograms (Fig. 3.3f). For all concentrations of ATPQ, there were two pronounced peaks in the intensity histograms, one near 0 and the other at 1. With no ATPQ present, only one peak arose at a fluorescence intensity of 1. This result suggests that when ATPQ is bound it quenches almost completely. We then integrated the distributions and found the fraction of the distribution less than 0.5 intensity to determine the amount of quenching at each concentration. This data was fitted to a characteristic ligand binding curve for single-site binding. The apparent KD was 5 μM and saturated at 80% quenching, in agreement with bulk measurements. To ensure that ATPQ was binding specifically to the dye-labeled subunit and not merely interacting with the dye only, we performed measurements using a mixture of ATPQ and excess ATP (Fig. 3.3d, lower panel). ATP outcompeted ATPQ, and the strong zero peak present at an equal concentration of ATPQ only vanishes when excess ATP is added (Fig. 3.4c). This result shows that ATPQ binds to the nucleotide-binding pocket to quench the fluorescence of TAMRA, confirming ensemble results.

3.3.3 ClpPplatform facilitates ClpXP formation for nucleotide binding experiments

How does ClpP affect nucleotide binding at the single-molecule level? To answer this question, we constructed a biotinylated-ClpP variant we call ClpPplatform that can tether non-biotinylated, dye-labeled ClpX hexamers to a streptavidin-coated surface (Fig. 3.4a). Fluorescent spots were virtually absent when ClpPplatform was excluded from this assay. Non-biotinylated ClpXTAMRA bound to ClpPplatfom (ClpXP) exhibited ATPQ concentration-dependent quenching. Additionally, we generated a binding curve for ATPQ binding to ClpXP and determined the Kd to be 5 μM and saturates at 80% binding. Therefore, ClpP-platform supports ClpXP complexation and ATPQ binding can be observed in ClpXP at

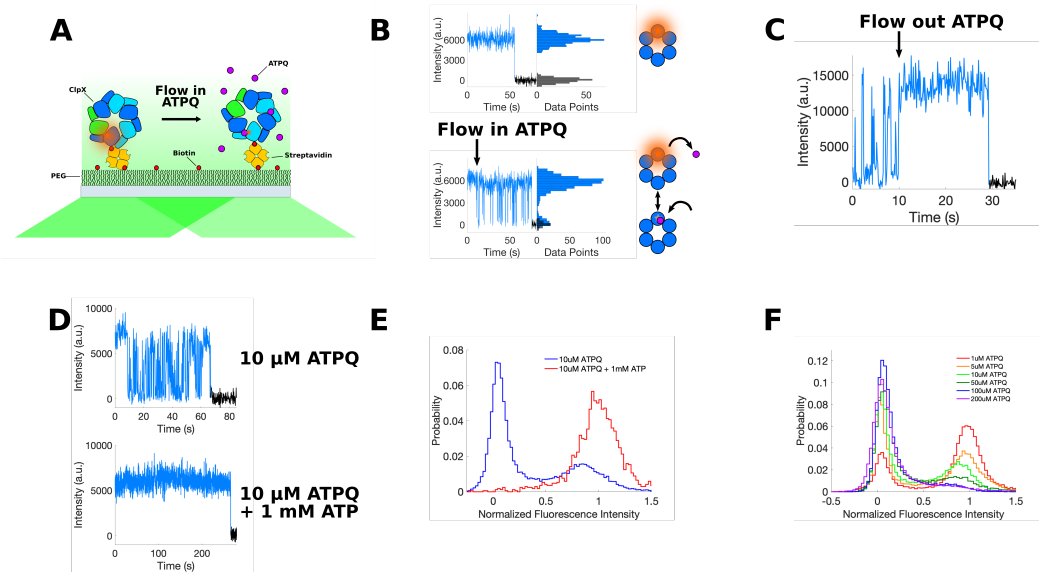

Figure 3.3: **ATPQ Single-Molecule Binding Assay** (A) Schematic showing biotinylated, dye-labeled ClpX hexamers immobilized on a streptavidin-coated glass surface. Our measurements consist of a short period without ATPQ to measure unquenched fluorescence levels followed by ATPQ flowing to monitor binding. (B) Single-molecule trajectories with and without ATPQ. (C) Washing out ATPQ with buffer halts quenching. (D) ATP competition with ATPQ can be observed at the single-molecule level. Quenching stops with excess ATP. (E) Intensity histograms for ATP/ATPQ competition experiment. (F) Intensity histograms for single-molecule ATPQ titration experiments. The quenched peak close to 0 increases while the unquenched peak decreases with increasing concentrations of ATPQ.

the single-molecule level.

3.3.4 Substrate Dependence of ATPQ Binding

We investigated the influence of different substrates on nucleotide binding in ClpXP by flowing in saturating concentrations of these substrates along with ATPQ in our single-molecule assay (Fig. 3.5a). We used a native version of titinI27-ssrA (WT Titin) and a version chemically unfolded by carboxymethylation. These two variants allow us to assess how unfolding and translocation affect nucleotide transaction rates and overall binding stoichiometry. We chose a concentration of 30 µM ATPQ for our substrate experiments because it is well above the Kd for ATPQ binding, which will allow these substrates to

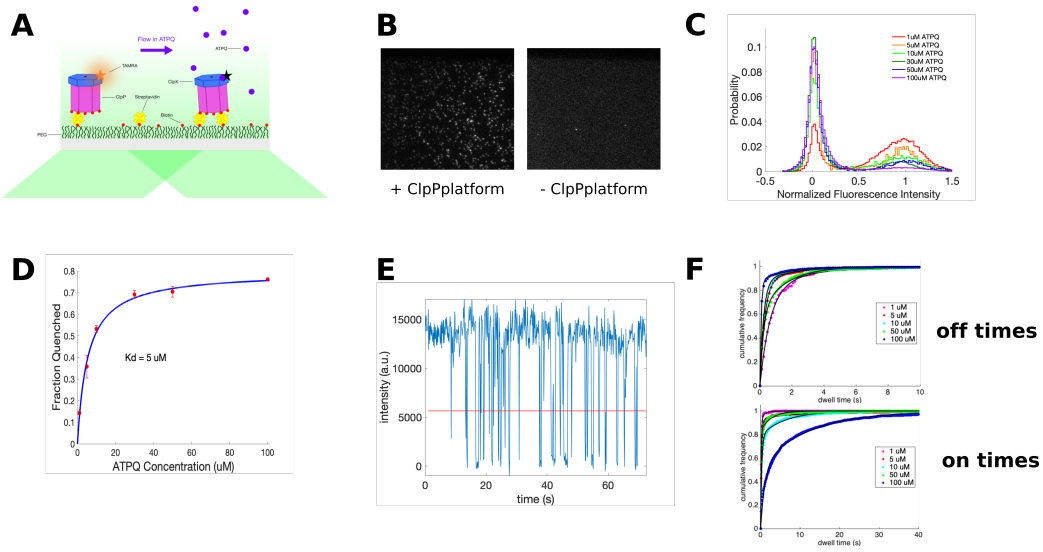

Figure 3.4: **ATPQ Binding to ClpXP** (A) Illustration showing ClpXP bound to a streptavidin-coated surface via ClpPplatform. The experiment is performed as before. (B) Images of slides incubated with non-biotinylated ClpX and ATP with and without pre-bound ClpPplatform. ClpX binding depends on the presence of ClpPplatform. (C) ATPQ titration of ClpXP. A similar trend to ClpX is observed for ClpXP. (D) Binding curve for ClpXP. (E) Example trace with thresholding method for dwell time extraction. Since there are two possible states in the trajectories (low and high intensity) dwell times are extracted using thresholding. An intermediate value between the high and low state is chosen and dwells above and below the threshold are sorted into off and on times, respectively. (F) Dwell-time cumulative frequencies for ClpXP.

interact with our surface-bound ClpXP. ClpXP in the absence of substrate showed the most quenching, followed by CM Titin and WT Titin. This result is further supported by dwell time cumulative frequencies. The no substrate condition had a longer quenched dwell and shorter unquenched dwell than CM Titin and WT Titin. WT Titin spends less time in the quenched dwell and more time in the unquenched dwell than the other two conditions. This result is a clear indication that ClpXP modulates its interactions with nucleotides based on individual stages of protein degradation.

3.3.5 Doubly-Labeled ClpX Hexamers Used to Probe Subunit Coordination

We extended our single-molecule binding assay to observe nucleotide binding in two ClpX subunits simultaneously in ortho, meta and para orientations. Both subunits were

labeled with TAMRA dyes. These experiments were done at 0, 10 and 100 μM ATPQ each to evaluate nucleotide binding over a wide range of concentrations (Data not shown). The amplitude of the unquenched fluorescence peak at a normalized intensity of 1 decreased with increasing concentration of ATPQ for all three doubly-labeled constructs, similar to the singly-labeled ClpX construct. However, the intensity distributions for all three doubly-labeled ClpX constructs had a second quenched intensity peak at 0.5 intensity. Since fluorescence spots in these experiments represent two dyes, an intensity of 1 indicates both dyes are fluorescing. An intensity of 0.5 indicates that one of the two subunits is bound with ATPQ and 0 intensity means that both subunits are bound. Trajectories for 0 and 100 μM ATPQ showed a single pronounced peak at intensities 1 and 0, respectively, for all three conditions. Therefore, we focused on data at 10 μM ATPQ because this concentration led to significant populations in all three binding states of the distributions. The histograms for the ortho, meta and para constructs were fit to a triple Gaussian function (Fig. 3.5d-f). Interestingly, the proportions of unbound, singly-bound and doubly-bound hexamers varied between the three constructs. This implies that certain ClpX subunits can enhance nucleotide binding in other subunits in certain orientations.

3.4 Discussion

We have developed a technique for monitoring nucleotide binding and unbinding in on and two ClpX subunits using fluorescence quenching and smTIRF. Our ATP analog supports hydrolysis, ClpP binding and substrate degradation, allowing us to study a functional ClpX motor. Moreover, since ATPQ is not fluorescent, we can use saturating concentrations of the nucleotide without significantly increasing background noise.

ATPQ binding results in almost total quenching of the TAMRA-labeled subunit. This allowed us to identify distinct quench and unquenched peaks in the intensity histograms and evaluate overall binding stoichiometry in ClpX hexamers. Binding curves generated from single-molecule data show that ClpX and ClpXP saturate at approximately 80% quench-

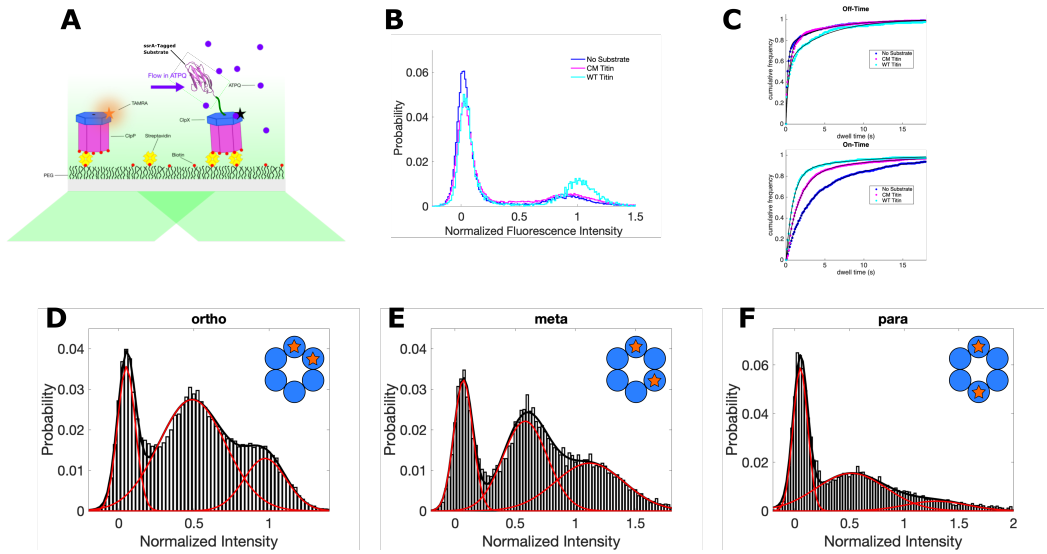

Figure 3.5: **Substrate Dependence and Subunit Coordination** (A) Substrate experiments are performed by adding saturating concentrations of ssrA-tagged substrates to flow-in buffer containing ATPQ. (B) Intensity histograms for ClpXP without substrate and in the presence of saturating CM-Titin and WT-Titin. (C) Dwell time cumulative frequencies for different substrate conditions. (D) Intensity histogram for doubly-labeled "ortho" hexamer. (E) Intensity histogram for doubly-labeled "meta" hexamer. (F) Intensity histogram for doubly-labeled "para" hexamer.

ing. This corresponds to about 5 subunits bound at any given time. Saturation in ensemble experiments occurs at around 65%. This slight discrepancy may be because quenching in all hexamers are averaged together in bulk measurements, whereas we excluded traces that did not show binding before photobleaching. These non-binding trajectories represent functional motors that have an occupied subunit during our observation window because these types of traces are observed when ClpX is bound to ClpPplatform. Since ClpP binding is a functional readout for ClpX, these motors are not likely to be defective. Therefore, 4-5 ClpX subunits are bound with nucleotide at saturation. This binding stoichiometry is higher than what was reported with hydrolysis-defective mutant ClpX hexamers but confirms previous results that some subunits must remain unoccupied in a working ClpX motor [8].

These single-molecule results also show that pronounced changes in overall binding

dwell time kinetics occur in the presence of different substrates. Solution experiments have established that ClpP binding suppresses ATP hydrolysis by ClpX, but translocation of unfolded substrate and unfolding of native substrates significantly enhances hydrolysis [9]. Our single-molecule results show that more quenching occurs in the absence of substrate and quenching decreases with increasing substrate thermodynamic stability (unfolded ¿ folded). This seemingly counterintuitive result can be explained by inspecting the quenched (on) and unquenched (off) dwell times at the different substrate conditions. Our dwell time cumulative frequencies show that the presence of substrates significantly decreases ATPQ on times and marginally increases off times. A decrease in on-time corresponds to a faster ATPQ processing rate because each nucleotide molecule has a shorter residence time at those conditions. Therefore, our assay allows us to extract the underlying molecular mechanisms for ClpX activity.

Our doubly-labeled ClpX hexamers allow us to investigate how subunits coordinate nucleotide binding with other subunits. Positive cooperativity between two subunits would occur if nucleotide binding in one subunit enhances binding in the other subunit. Two subunits would be non-cooperative is they are independent of each other and negative cooperativity occurs if one subunit suppresses binding in another. A non-cooperative arrangement for our doubly-labeled constructs would have a 1:2:1 ratio of areas for the 2-bound, 1-bound and 0-bound populations based on probability. More binding than that would indicate positive cooperativity and less binding represents negative cooperativity. None of the arrangements we constructed had subunits that bind with negative cooperativity. Para and ortho subunits had positive cooperativity and meta subunits were non-cooperative. This result reveals that significant coordination of binding occurs between ortho and para subunits, and suggests a mechanistic model much more complex than concerted and sequential firing of subunits [11]. Additionally, bulk binding assays on these constructs report Hill constants significantly greater than 1 (positive cooperativity) for ortho and para subunits and a Hill constant of 1.1 for meta subunits (non-cooperative) (Data not shown).

Researchers have shown that ClpX hexamers must be loaded with ATP before ClpP binding and substrate degradation can commence [17]. ClpX subunits may be able to enhance the binding affinity of other subunits in the ring to achieve maximum binding and load subunits in particular orientations for proper function. Because this technique uses a single dye, it can be extended to look at multiple dyes at once using alternating excitation (ALEX) smTIRF. Future experiments using this approach will allow researchers to observe the binding order of subunits and monitor 3 or more subunits at once. Previous experiments suggested that ClpX follows a probabilistic mechanism rather than a concerted or sequential model. Detailed single-molecule nucleotide binding experiments will help researchers refine the details of ClpX's complex model.

3.5 Materials and Methods

3.5.1 Protein Expression and Purification (courtesy of B. Stinson)

ClpX constructs used in single-molecule and ensemble ATPQ binding experiments were generated from E. coli ClpXN¬ (residues 61-424). The mutation C169S was made to remove a surface-exposed native cysteine. ClpX pseudo hexamers were assembled from a dimer of trimers fused via sortase ligation. Each trimer was purified using Ni-NTA chromatography and digested with TEV protease to cleave the H_6-tagged TEV. Trimer A, which had a K330C modification (W-W-K) was labeled with Tetramethylrhodamine-maleimide (TAMRA-maleimide) and trimer B, had either no modification for singly-labeled ClpX constructs (W-W-W) or a K330C modification on either the first, second, or third subunit for ortho, meta, or para doubly-labeled constructs, respectively (K-W-W, W-K-W, and W-W-K) was labeled with TAMRA-maleimide. Trimers were reacted with 3-fold excess of the required maleimide-functionalized fluorophore at room temperature for 30 minutes. The reaction was quenched with 1mM DTT and desalted with Xlink buffer using a PD10 column (GE Healthcare). Trimer B for biotinylated ClpX constructs had a C-terminal bi-

otin acceptor peptide sequence (GLNDIFEAQKIEWHE) that was recognized for biotin conjugation by biotin ligase (BirA) from E. coli. The biotin tags were used to immobilize ClpX constructs on streptavidin-coated surfaces for single-molecule measurements. Trimers A and B contained the appropriate modifications for successful sortase ligation. Trimer A had a C-terminal LPETG sortase recognition tag and Trimer B had an N-terminal poly-glycine motif that was exposed upon digestion with TEV protease. An evolved S. aureus sortase-A enzyme with P94S/D160N/K194T substitutions [2] was used to ligate the trimers. Sortase reaction mixtures consisted of 5 μM trimer A, 5 μM trimer B and 1 μM sortase. The reaction was done at room temperature for 2-4 hours in Xlink buffer supplemented with 5 mM $CaCl_2$ and 1 mM DTT. Non-biotinylated ClpX constructs were immobilized on streptavidin-coated coverslips through binding to biotinylated ClpP constructs we call ClpPplatform. ClpPplatform was constructed from one seven-membered ring of wild-type subunits and another ring of seven subunits each with an M5A modification that was biotinylated. ClpP-M5A-His6-biotin and excess parental ClpP were dialyzed against 150 mM ammonium sulfate. The mixture was then dialyzed into a low-salt buffer and ClpPplatform was purified using Ni2+-NTA affinity. Titin I27-ssrA substrates were expressed and purified as previously outlined [9, 10]. Unfolded titin I27-ssrA substrates were produced by denaturing native substrates in iodoacetic acid, as shown in [9].

3.5.2 ATPQ Synthesis (courtesy of B. Stinson)

Our method for synthesizing ATPQ was developed by modifying published techniques [3, 4, 7, 12]. DABCYL PlusTM acid, succinimidyl ester (SE) was purchased from Anaspec; other compounds were purchased from Sigma. A solution of ATP disodium salt (275 mg dissolved in 2 mL water) was passed over a column of Dowex 50W X8 (0.77 g; H+ form) to produce free ATP acid. Ethanol (100 mL) was added and the solvents in the mixture were evaporated by rotary evaporation. The residue was dissolved in methanol (8 mL plus 476 L tributylamine), and that mixture was evaporated to dryness by rotary evaporation. The

resulting ATP tributylammonum salt was dissolved in anhydrous DMF (8 mL) stored over 4 Å molecular sieves and dried by repeated rotary evaporation of dry DMF (3x). Dry DMF (8 mL) was added and the solution was placed under an argon atmosphere and cooled to 4 °C. Carbonyldiimidazole (405 mg) was added, the reaction was stirred at 4 °C for 4 h, and unreacted carbonyldiimidazole was consumed through the addition of methanol (144 L). Ethylenediamine (167 L in 5 mL dry DMF) was added to this solution dropwise at 4 °C. The resulting white precipitate was recovered via centrifugation and washed 3x with anhydrous DMF. The precipitate was dissolved in water (30 mL), adjusted to pH 2.5 with HCl, and stirred at 4 °C overnight to remove the -phophoramidate. The solution was then adjusted to pH 7.0 and chromatographed on a MonoQ column using a gradient of 10 mM to 600 mM triethylammonium bicarbonate buffer (pH 7.8). Fractions containing eda-ATP were identified by TLC, pooled, lyophilized, dissolved in water (2 mL), mixed with DABCYL Plus acid, SE (25 mg dissolved in 1 mL DMSO), and allowed to react at room temperature overnight in the dark. DABCYL Plus-eda-ATP was precipitated by adding 6 volumes of acetone, collected by centrifugation, and washed 3x with acetone to remove unreacted dye. The resulting red-orange precipitate was dissolved in water (2 mL), loaded onto a 100 mL DEAE Sepharose column, and eluted isocratically with 0.6 M ammonium bicarbonate (pH 7.8). Mass spectrometry verified that the major peaks corresponded to isomers of DABCYL Plus-eda-ATP. These peaks were pooled separately, lyophilized, dissolved at a concentration of 20 mM in 50 mM MES (pH 6.0), and stored frozen at –80 °C. Aluminum-backed silica gel 60 F254 TLC plates were used to track reaction progress with a water:ammonia:isopropanol:1,4-dioxane (4:3:2:4) solvent system. RF values: ATP, 0.21; ADP, 0.26; eda-ATP, 0.13; ATPQ1, 0.34; ATPQ2, 0.38; ADPQ1, 0.57; ADPQ2, 0.58.

3.5.3 Bulk Fluorescence Assays (courtesy of B. Stinson)

Fluorescence measurements were acquired with a SpectraMax M5e plate reader (Molecular Devices). ATP hydrolysis was measured by the Enz Chek phosphate assay (Molecular

Probes) and quantified by comparison to an inorganic-phosphate standard curve. Degradation of the cp7-GFP-ssrA protein substrate by ClpXP variants was monitored by changes in fluorescence (excitation 467 nm; emission 511 nm) [13]. Fluorescence quenching of K330C-TAMRA labeled ClpX by ATPQ was monitored by excitation at 540 nm and collecting and averaging the emission spectrum from 570-590 nm. Quenching was defined as 1-F/F0, where F0 is fluorescence intensity in the absence of ATPQ. Bulk quenching values were corrected for the inner-filter effect by subtracting the quenching observed with unreacted TAMRA-maleimide dye and an equivalent concentration of ATPQ.

3.5.4 Single-Molecule Coverslip Preparation

Glass coverslips (Fisherbrand) were sonicated sequentially in deionized water, methanol and 1M KOH. The etched coverslips were sonicated at 35 °C in a solution with 1% (w/v) of PEG mixture (1% biotin-PEG-silane, MW 5000; 99% mPEG-silane, MW 5000, Laysan Bio) and 0.8 mM trimethylamine in 30 mL of ACS grade toluene (Fisher Scientific). The coverslips were then washed with toluene, copious amounts of deionized water and dried with pressurized air. The PEG-functionalized coverslips were stored at -20 °C in 50 mL Falcon tubes filled with nitrogen until flow cells were assembled.

3.5.5 Single-Molecule Fluorescence Assay

To construct our flow cells, two holes were drilled into a microscope slide, the slide was cleaned and etched, then inlet and outlet tubes were created by fusing surgical tubing to the holes in the slide with epoxy. A flow channel between the inlet and outlet tubes by forming a gasket between two strips of double-sided tape sandwiched between the glass slide and a PEG coverslip. Any gaps in the device were sealed with epoxy. The inlet tube was cut down to 2-3 mm so that pipette tips filled with different buffers can be inserted easily. A syringe was attached to the outlet tube to induce a vacuum and create flow. A 0.1 mg/mL solution of streptavidin in PBS (100 mM phosphate buffer, pH 7.5) was introduced to the

flow cell and allowed to incubate for 10 minutes. Unbound streptavidin was washed out with PD (25 mM HEPES pH 7.6, 100 mM KCl, 10 mM MgCl2, 10% glycerol (vol/vol)) and 40 μL of 625 pM ClpX in PD in the presence of 3 mM ATP was flowed into the flow channel and incubated for 20 minutes. Afterward, unbound ClpX was washed out with an ATP solution followed by an imaging buffer with an oxygen scavenging and triplet-state quencher (0.8% D(+)-glucose, 16500 units/mL glucose oxidase, 217000 units/mL catalase, and 2 mM Trolox) and the desired nucleotides/substrates before imaging. For ClpXP measurements, a 20-minute incubation of ClpPplatform with the streptavidin-coated surface preceded incubation of ClpX in the presence of ATP to promote binding. ATPQ binding was observed at the single-molecule level by flowing in the desired concentration of ATPQ along with oxygen scavenger and triplet-state quencher. 25 μM ssrA-tagged substrates were included for substrate measurements.

3.5.6 Instrument Setup

Data collection was done on a custom-built objective-side total internal fluorescence (TIRF) microscope. The instrumental setup consists of a 100x 1.49 NA objective (Nikon), illumination at ZZ mW from a laser diode (Blue Sky Research) and an EMCCD camera (Andor) for fluorescence imaging. Data were acquired at 8.8 Hz.

3.5.7 Data Analysis

Custom Matlab scripts were used to process and analyze the data. Hidden Markov Modeling (HMM) was used to create idealized traces for identifying conformational states and extracting dwell time kinetics [1, 18]. Only traces showing a single photobleaching step, an emission intensity above 2000 counts/sec and emission lasting longer than 10 seconds were analyzed.

3.6 Acknowledgements

We thank Ben Stinson for synthesizing ATPQ, producing ClpX, ClpP and ssrA-tagged substrates and performing bulk measurements. We thank Robert Sauer and Tania Brady for numerous helpful discussions and thoughtful suggestions. This work was supported by NSF (1330792) and GAANN (P200A090323).

3.7 Bibliography

[1] Jonathan E Bronson, Jingyi Fei, Jake M Hofman, Ruben L Gonzalez, and Chris H Wiggins. Learning rates and states from biophysical time series: a Bayesian approach to model selection and single-molecule FRET data. *Biophysical journal*, 97(12):3196–205, dec 2009.

[2] Irwin Chen, Brent M. Dorr, and David R. Liu. A general strategy for the evolution of bond-forming enzymes using yeast display. *Proceedings of the National Academy of Sciences of the United States of America*, 108(28):11399–11404, 2011.

[3] Christine R. Cremo, Joan M. Neuron, and Ralph G. Yount. Interaction of Myosin Subfragment 1 with Fluorescent Ribose-Modified Nucleotides. A Comparison of Vanadate Trapping and SH1-SH2 Cross-Linking. *Biochemistry*, 29(13):3309–3319, 1990.

[4] John F. Eccleston David M. Jameson. Fluorescent Nucleotide Analogs: Synthesis and Applications. In *Methods in enzymology*, volume 278, pages 363–390. 1997.

[5] Steven E Glynn, Andreas Martin, Andrew R Nager, Tania a Baker, and Robert T Sauer. Structures of asymmetric ClpX hexamers reveal nucleotide-dependent motions in a AAA+ protein-unfolding machine. *Cell*, 139(4):744–56, nov 2009.

[6] Phyllis I Hanson and Sidney W Whiteheart. AAA+ proteins: have engine, will work. *Nature reviews. Molecular cell biology*, 6(7):519–29, jul 2005.

[7] Theodore L. Hazlett, Keith J.M. Moore, Peter N. Lowe, David M. Jameson, and John F. Eccleston. Solution Dynamics of p21ras Proteins Bound with Fluorescent Nucleotides: A Time-Resolved Fluorescence Study. *Biochemistry*, 32(49):13575–13583, 1993.

[8] Greg L Hersch, Randall E Burton, Daniel N Bolon, Tania a Baker, and Robert T

Sauer. Asymmetric interactions of ATP with the AAA+ ClpX6 unfoldase: allosteric control of a protein machine. *Cell*, 121(7):1017–27, jul 2005.

[9] Jon a Kenniston, Tania a Baker, Julio M Fernandez, and Robert T Sauer. Linkage between ATP consumption and mechanical unfolding during the protein processing reactions of an AAA+ degradation machine. *Cell*, 114(4):511–20, aug 2003.

[10] Yong In Kim, Randall E. Burton, Briana M. Burton, Robert T. Sauer, and Tania A. Baker. Dynamics of substrate denaturation and translocation by the ClpXP degradation machine. *Molecular Cell*, 5(4):639–648, 2000.

[11] Andreas Martin, Tania a Baker, and Robert T Sauer. Rebuilt AAA + motors reveal operating principles for ATP-fuelled machines. *Nature*, 437(7062):1115–20, oct 2005.

[12] Mitsuaki Maeda, Arvind D. Patel and Alexander Hampton. Formation of ribonucleotide 2',3'-cyclic carbonates during conversion of ribonucleoside 5'-phosphates to diphosphates and triphosphates by the phosphorimidazolidate procedure. 4(8):2843–2853, 1977.

[13] Andrew R Nager, Tania a Baker, and Robert T Sauer. Stepwise unfolding of a β barrel protein by the AAA+ ClpXP protease. *Journal of molecular biology*, 413(1):4–16, oct 2011.

[14] T Ogura and a J Wilkinson. AAA+ superfamily ATPases: common structure–diverse function. *Genes to cells : devoted to molecular & cellular mechanisms*, 6(7):575–97, jul 2001.

[15] Kazuhiro Oiwa, John F. Eccleston, Michael Anson, Mahito Kikumoto, Colin T. Davis, Gordon P. Reid, Michael A. Ferenczi, John E.T. Corrie, Akira Yamada, Haruto Nakayama, and David R. Trentham. Comparative single-molecule and ensemble myosin enzymology: Sulfoindocyanine ATP and ADP derivatives. *Biophysical Journal*, 78(6):3048–3071, 2000.

[16] Adrian O Olivares, Tania A Baker, and Robert T Sauer. Mechanical Protein Unfolding and Degradation. *Annual Review of Physiology*, 80(1):413–429, 2018.

[17] Benjamin M. Stinson, Andrew R. Nager, Steven E. Glynn, Karl R. Schmitz, Tania A. Baker, and Robert T. Sauer. Nucleotide Binding and Conformational Switching in the Hexameric Ring of a AAA+ Machine. *Cell*, 153(3):628–639, apr 2013.

[18] Jan Willem Van De Meent, Jonathan E. Bronson, Chris H. Wiggins, and Ruben L. Gonzalez. Empirical bayes methods enable advanced population-level analyses of single-molecule FRET experiments. *Biophysical Journal*, 106(6):1327–1337, 2014.

[19] Susan Roehl White and Brett Lauring. AAA+ ATPases: achieving diversity of function with conserved machinery. *Traffic (Copenhagen, Denmark)*, 8(12):1657–67, dec 2007.

Chapter 4

COMBINED OPTICAL TRAPPING AND SINGLE-MOLECULE FLUORESCENCE USED TO OBSERVE CONFORMATIONAL MOTIONS AND NUCLEOTIDE BINDING DURING PROTEIN DEGRADATION BY ClpXP

4.1 Summary

The model AAA+ motor ClpX uses ATP-fueled conformational motions to mechanically denature a protein's native structure and thread the unfolded polypeptide to the ClpP degradation chamber. Ensemble measurements have shown that conformational movements and flexibility are necessary to couple ATP hydrolysis to protein degradation. However, the conformational dynamics of subunits in a substrate-engaged ClpX hexamer have never been observed. Here, we have created a combined optical trapping and single-molecule fluorescence quenching assay to simultaneously observe conformational motions and substrate degradation in ClpXP. Our results reveal that ClpX subunits mostly occupy a compact conformation during substrate degradation and that conformational switching occurs at all stages of protein degradation cycle. Surprisingly, large conformational changes coincide with translocation pauses, suggesting that stalled ClpX motors use these transitions to reset mechanical activity.

4.2 Introduction

AAA+ motors are proteins that use conformational motions fueled by ATP binding and hydrolysis to rearrange biomolecules. Enzymes in the AAA+ family typically form ring-shaped hexamers and perform a variety of tasks such as DNA unwinding, protein-oligomer disassembly and protein degradation [1]. Determining which structural changes in AAA+ machines lead to mechanical work is crucial to building a complete mechanism for these motors.

Escherichia Coli ClpX is a hexameric AAA+ protein that uses the energy from ATP binding and hydrolysis to unfold and translocate protein substrates [2]. In the presence of ATP, ClpX binds the barrel-shaped peptidase ClpP to form the protease ClpXP. ClpXP mediated protein degradation occurs when ClpX binds the degradation tag, or degron, of proteins tagged for removal from the cell [3]. ClpX denatures the protein by pulling on the appended degron and spools the unfolded polypeptide to the degradation chamber of ClpP. Crystal structures of ClpX show two distinct conformations: nucleotide loadable, or L, and nucleotide unloadable, or U [4]. However, the U conformation is absent in numerous cryo-EM structures of ClpXP which show a variety of L conformations arranged in a spiral staircase pattern [5, 6, 7]. It is not known whether subunits dynamically switch conformational states or if certain structural transitions coincide with specific events in the mechanochemical cycle of ClpX-mediated protein degradation.

What sort of conformational changes are required to unfold, translocate and exit a translocation pause during protein degradation? Single-molecule techniques have been used in several studies to answer mechanistic questions about ClpX [8, 9, 10, 11, 12, 13, 14**?**]. However, individual single-molecule techniques are insufficient for monitoring the conformational changes that occur during specific steps in ClpXP's mechanochemical cycle. Combined force-fluorescence measurements have been widely used to concurrently measure structural and mechanical activities of biomolecules [15, 16, 17]. Additionally, fluorescence quenching allows us to observe smaller intra- and intermolecular distance changes than traditional FRET [18, 19, 20].

Here, we have developed a combined single-molecule fluorescence quenching and optical tweezers assay to simultaneously observe conformational switching in a single ClpX subunit while monitoring substrate unfolding and translocation by ClpXP. This assay allowed us to observe that large conformational changes are required to exit a translocation pause and that nucleotide analogs such as ATPQ can induce these pauses.

4.3 Results

We designed single-chain ClpXN hexamers with an ATTO 550 fluorophore covalently linked to the large domain of a ClpX subunit and a DabcylPLUS dark quencher attached to the large domain of clockwise neighboring subunit. These labeling sites were chosen because small domains and large domains of clockwise neighboring subunits form rigid bodies (Fig. 4.1a) [4, 21]. Relative rotations of the large and small domain of the fluorescent subunit about the connecting hinge domain would be reported as changes in fluorescence intensity due to the quenching of ATTO 550 by DabyclPLUS. This modification was achieved by producing single-chain trimers, one with a Q167C point mutation for labeling maleimide-functionalized ATTO 550 and the other with a K213C modification for attaching maleimide-functionalized DabyclPLUS. Each trimer was reacted with their respective dye and fused via sortase ligation. We called the resulting single-chain ClpX hexamer QA5. Unlike the ClpX construct engineered in Chapter 2 (QA5B), this construct lacks a biotin label. This biotin-free ClpX construct can be immobilized to a streptavidin-coated coverslip surface via a biotinylated ClpP construct, ClpPplatform (Chapter 3).

We verified surface-immobilization of ClpX through binding to ClpPplatform with a ClpX construct with the same modifications as QA5 except for DabcylPlus labeling (A5) (Fig. 4.1d). In the absence of ClpP platform, virtually no A5 spots were imaged on a coverslip surface. Previous optical tweezer nanometry studies have shown that processive protein unfolding and translocation by ClpX requires binding of ClpP [8]. Our surface attachment strategy ensures that surface-bound ClpX molecules are bound to ClpP and that ClpXP is oriented upright to facilitate active substrate tether formation using a substrate-coated optically trapped bead.

Similar to the biotinylated constructs introduced in chapter 2, our ClpX construct showed large fluctuations in fluorescence intensity that we attribute to conformational motions of the labeled subunit (Fig. 4.1b). Additionally, the bulk ATP hydrolysis rate of QA5 was similar to wild type ClpX with and without ClpP present (Fig. 4.2a). Bulk fluorescence

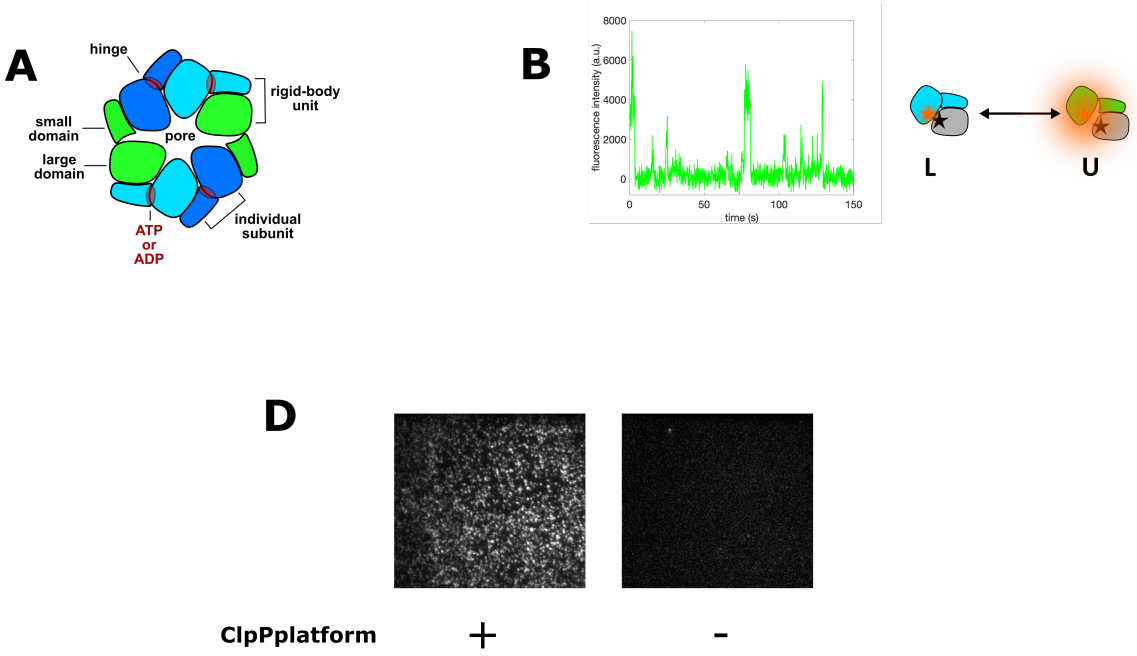

Figure 4.1: **ClpX construct for monitoring conformational motions.** (A) Schematic of ClpX hexamer. (B) Example trace of QA5. (C) A5 incubated with ATP in the presence (left) and absence (right) of ClpPplatform.

measurements show that both QA5 and QA5B exhibit a similar increase in fluorescence quenching as the concentration of ATP increases (Fig. 4.2b). These results show that our modifications do not affect ClpX activity and report the conformational state of the labeled subunit.

Our results from chapter 2 show that the presence of ClpP and ssrA-tagged protein substrates affect the ratio of subunit classes and the rate of conformational switching. To directly visualize the conformational dynamics of a ClpX subunit in a ClpXP motor actively degrading a protein substrate, we need to simultaneously measure fluorescence quenching of QA5 and record the mechanical activity of ClpXP using an optically trapped tethered substrate bead. We accomplished this by coating an anti-digoxigenin functionalized polystyrene bead with a multimeric protein substrate appended with the ssrA degradation tag recognized by ClpX. The protein substrate was attached to the anti-digoxigenin bead using a 100 bp dsDNA tether that had a digoxigenin moiety on one end and a HaloTag ligand on the other. Our protein substrate had a HaloTag protein fused to the N-terminus

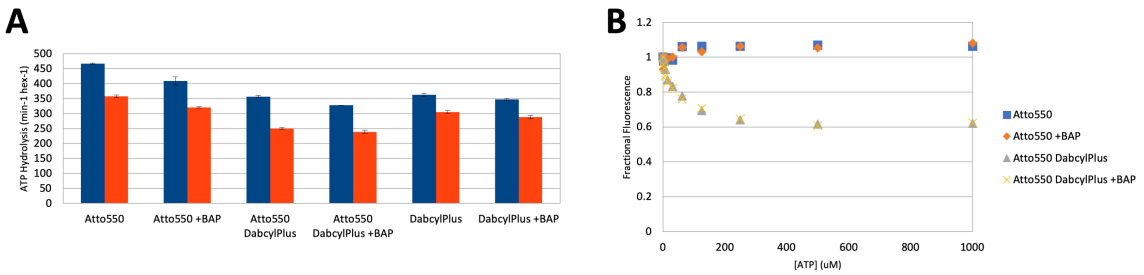

Figure 4.2: **QA5 hydrolyzes ATP and quenches fluorescence.** (A) Ensemble ATP hydrolysis rates for different fluorescently labeled constructs including QA5. (B) Fluorescence quenching for QA5 and QA5B increase with increasing concentrations of ATP.

which covalently binds to the HaloTag ligand (Halo citation). This allows us to form stable substrate-coated beads for single-trap optical trapping measurements.

We used a custom-built combined optical trapping and single-molecule Total Internal Fluorescence (TIRF) instrument to perform our force-fluorescence experiments on ClpXP [15]. This apparatus uses a two-channel function generator to alternate the intensity of the fluorescence and trapping lasers at 50 kHz. This method, called Interlaced Optical Force-Fluorescence (IOFF) avoids prematurely photobleaching our fluorophore, ATTO 550, through simultaneously exposure to an excitation and trapping laser [22, 17, 23].

Our assay is built on a coverslip surface of a flow cell passivated with polyethylene glycol (PEG) which occludes nonspecific binding of biomolecules. Approximately 1-5% of PEG molecules on the surface had a terminal biotin group to facilitate attachment of streptavidin. After sequentially adding each component to produce surface-bound ClpXP complexes, substrate-coated polystyrene beads were added to the flow cell with ATP and the flow cell was loaded on the microscope. ClpXP-substrate tethers were actively assem-

bled by first trapping a substrate bead and moving it close to the coverslip surface. Once the trapped bead was near with the flow cell surface, a piezo stage was used to slowly move the stage beneath the bead in 50 nm increments until an immobilized ClpXP molecule engaged an ssrA-tagged substrate on the bead. Once a tether was formed, the fluorescence shutter was opened and concurrent measurements of bead position and fluorescence intensity were acquired until the tether ruptured.

Previous optical tweezer nanometry experiments show that ClpXP mechanical activity during substrate degradation using a trapped bead is characterized by a rapid decrease of in bead displacement from the trap center during protein unfolding and a gradual increase in bead displacement during protein translocation [8, 10, 11, 9, 12, 13, 14]. Although these studies employed a two-bead, dual trap assay geometry, the same signature features can be observed in our surface-based single-trap assay. Various types of protein substrates were used to perform these experiments. Carboxymethylated ssrA-TitinI27 (CM Titin) was used to observe translocation only, an ssrA-TitinI27 substrate with the ssrA degron attached to the N-terminus instead of the C-terminus (N-titin) was used to increase the rate of substrate unfolding, and an ssrA-TitinI27 with a V13P mutation was used to observe conformational changes during pre-unfolding dwells along with protein unfolding and translocation.

Our single-molecule trajectories show that large conformational changes can occur during pre-unfolding dwells and translocation steps (Fig. 4.3). Interestingly, large conformational changes were not observed at the exact moment of protein unfolding, suggesting that a large conformational change is not required to achieve cooperative unfolding of a protein substrate.

Researchers have shown that translocation pauses occasionally occur while ClpXP processes protein substrates during optical trapping experiments [10, 9, 12, 14]. These events are characterized by dwells in substrate translocations that last longer than 2.5 s. Using different ssrA-tagged substrates, our combined force-fluorescence assay has shown that large conformational changes occur during a translocation pause (Fig. 4.4). After a pause be-

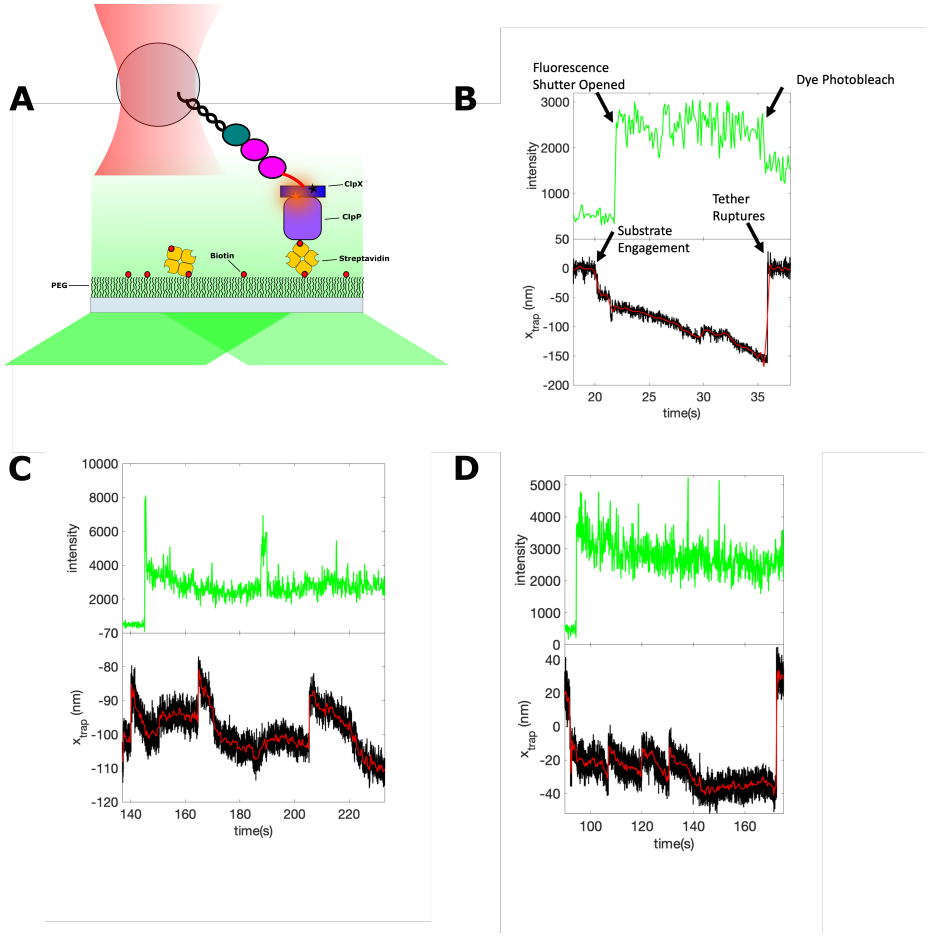

Figure 4.3: **Combined optical trapping and single-molecule fluorescence assay.** (A) Schematic showing geometry of the combined force-fluorescence assay. Not drawn to scale. (B) Example trace of ClpXP (QA5-ClpPplatform) translocating CM Titin. (C) ClpXP degrading V13P. (D) ClpXP degrading N-Titin.

gins, the labeled subunit of QA5 increases its fluorescence intensity indicating a transition to a more extended conformation. Upon resumption of translocation stepping, the tagged subunit decreases its fluorescence intensity which represents a return to a more compact conformation. Sen et al. demonstrated that increasing concentrations of ATPS cause an increase in the occurrence of pauses [14]. This phenomenon is likely due to the fact that ATPS is hydrolyzed much more slowly than ATP and may stall the motor as it remains bound without being hydrolyzed. Our results suggest that exiting a translocation pause requires subunit extension followed by constriction. This mechanism may be a way for ClpXP to eject nucleotides that are not hydrolyzing fast enough and rebind new nucleotide molecules to resume translocation.

4.4 Discussion

The model AAA+ machine ClpX has been thoroughly studied using biochemical and single-molecule techniques [10**?** , 24, 25]). However, direct observation of conformational motions during the mechanochemical cycle of ClpXP has eluded researchers. Here, we present the first demonstration of conformational state and protein degradation being monitored simultaneously., We observed that ClpXP spends most of its time in a quenched, L-like conformation and briefly visits more extended conformations during all stages of protein degradation. This result agrees with our fluorescence-only results (Chapter 2).

For our fluorescence-only single-molecule quenching assay for ClpX, we were able to normalize our quenched fluorescence intensity by flowing in SDS to chemically denature our ClpX construct and separate the attached probes to unquench ATTO 550. This approach could not be incorporated into our combined force-fluorescence assay because optical trapping measurements are taken one molecule at a time and chemically unfolding ClpX after each measurement would drastically decrease the efficiency of this assay. Furthermore, performing a buffer exchange during a force measurement would add unwanted noise to the force/displacement data. Because of this, we were unable to calibrate the quenched

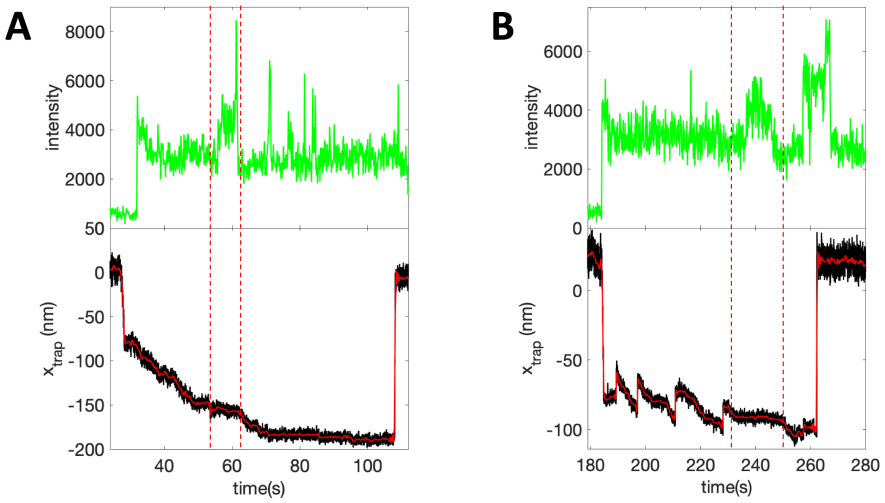

Figure 4.4: **Conformational changes during translocation pauses.** (A) Example trace showing a conformational transition during translocation of CM Titin. (B) (A) Example trace showing a conformational transition during translocation of N-Titin.

intensity levels of QA5 and definitively ascribe different intensity levels to certain conformation. Nevertheless, our assay does allow us to qualitatively describe our real-time structural data and identify large structural transitions that coincide with mechanical events during ClpX-mediated protein degradation.

Surprisingly, the most striking events happened during translocation pauses. Both large conformational changes and binding/unbinding of a bulky ATP analog occur during translocation pauses (Figure 4). ATPS, which is hydrolyzed by ClpXP at a much slower rate than ATP also induces pauses in translocation [14]. Therefore, a translocation pause may represent the moment a ClpX subunit cannot properly hydrolyze a nucleotide and must wait until the nucleotide is released before it can resume translocation. Our results suggest that this release may be coupled with an opening up of ClpX subunits as the ring resets and rebinds nucleotides. By adapting our ATPQ binding assay (Chapter 3) to our combined force-fluorescence strategy, we may be able to recapitulate Sen et al.'s result of increased pausing in the presence of an ATP analog and directly see the moment ATPQ binds and

unbinds during a pause.

These preliminary results set the stage for a more in-depth mechanistic study of ClpXP using our combined optical trapping and single-molecule fluorescence setup. However, quantitative analysis of conformational dynamics requires a method to normalize the quenched intensity of QA5 to the average unquenched intensity of ATTO 550. Because fluorescence from the ClpXP molecule of interest is focused through a pinhole onto a photon-counting silicon avalanche photodiode (SAPD), illumination by the excitation laser is always the same. Therefore, we could image multiple molecules of A5 and normalize the signal from QA5 to the average intensity of A5 fluorescence collected with our SAPD. We could also calibrate our fluorescence signal with a series of standards that contain ATTO 550 and DabcylPLUS at varying distances from one another. After normalizing and calibrating the fluorescence signal, Hidden Markov Modeling (HMM) can be used to identify states and extract dwell times from noisy trajectories [26]. Once these advancements are implemented, this assay has the potential to reveal many more important details in the overall mechanism of ClpXP.

4.5 Materials and Methods

4.5.1 Protein Expression and Purification

(courtesy of B. Stinson) ClpX constructs were derived from E. coli ClpXΔN (residues 61-424). The modification C169S was introduced to remove an accessible native cysteine. ClpX hexamers were constructed from a dimer of trimers fused via sortase ligation. Each trimer was purified using Ni-NTA chromatography and digested with TEV protease to cleave the H_6-tagged TEV. Trimer A had a Q167C modification (W-W-Q) and was labeled with ATTO 550-maleimide and trimer B had a K213C modification (K-W-W) and was labeled with DabcylPLUS-maleimide. Trimers were reacted with 3-fold excess of the required maleimide-functionalized fluorophore or quencher at room temperature for 30

minutes. The reaction was quenched with 1mM DTT and desalted with Xlink buffer using a PD10 column (GE Healthcare).

Trimers A and B contained the appropriate modifications for successful sortase ligation. Trimer A had a C-terminal LPETG sortase recognition tag and Trimer B had an N-terminal poly-glycine motif that was exposed upon digestion with TEV protease. An evolved S. aureus sortase-A enzyme with P94S/D160N/K194T substitutions [**?**] was used to ligate the trimers. Sortase reaction mixtures consisted of 5 μM trimer A, 5 μM trimer B and 1 μM sortase. The reaction was done at room temperature for 2-4 hours in Xlink buffer supplemented with 5 mM $CaCl_2$ and 1 mM DTT. These non-biotinylated ClpX constructs were immobilized on streptavidin-coated coverslips through binding to biotinylated ClpP constructs we call ClpPplatform. ClpPplatform was constructed from one seven-membered ring of wild-type subunits and another ring of seven subunits each with an M5A modification that was biotinylated. ClpP-M5A-His6-biotin and excess parental ClpP were dialyzed against 150 mM ammonium sulfate. The mixture was then dialyzed into a low-salt buffer and ClpPplatform was purified using $Ni2^{+}$-NTA affinity. Titin I27-ssrA substrates were expressed and purified as previously outlined [27, 28].. Unfolded titin I27-ssrA substrates were produced by denaturing native substrates in iodoacetic acid, as shown in [27].

4.5.2 ATPQ Synthesis

(courtesy of B. Stinson) Our method for synthesizing ATPQ was developed by modifying published techniques [29**?** , 30, 31]. DABCYL PlusTM acid, succinimidyl ester (SE) was purchased from Anaspec; other compounds were purchased from Sigma. A solution of ATP disodium salt (275 mg dissolved in 2 mL water) was passed over a column of Dowex 50W X8 (0.77 g; H+ form) to produce free ATP acid. Ethanol (100 mL) was added and the solvents in the mixture were evaporated by rotary evaporation. The residue was dissolved in methanol (8 mL plus 476 L tributylamine), and that mixture was evaporated to dryness by rotary evaporation. The resulting ATP tributylammonium salt was dissolved in anhydrous

DMF (8 mL) stored over 4 Å molecular sieves and dried by repeated rotary evaporation of dry DMF (3x). Dry DMF (8 mL) was added and the solution was placed under an argon atmosphere and cooled to 4 °C. Carbonyldiimidazole (405 mg) was added, the reaction was stirred at 4 °C for 4 h, and unreacted carbonyldiimidazole was consumed through the addition of methanol (144 L). Ethylenediamine (167 L in 5 mL dry DMF) was added to this solution dropwise at 4 °C. The resulting white precipitate was recovered via centrifugation and washed 3x with anhydrous DMF. The precipitate was dissolved in water (30 mL), adjusted to pH 2.5 with HCl, and stirred at 4 °C overnight to remove the -phophoramidate. The solution was then adjusted to pH 7.0 and chromatographed on a MonoQ column using a gradient of 10 mM to 600 mM triethylammonium bicarbonate buffer (pH 7.8). Fractions containing eda- ATP were identified by TLC, pooled, lyophilized, dissolved in water (2 mL), mixed with DABCYL Plus acid, SE (25 mg dissolved in 1 mL DMSO), and allowed to react at room temperature overnight in the dark. DABCYL Plus-eda-ATP was precipitated by adding 6 volumes of acetone, collected by centrifugation, and washed 3x with acetone to remove unreacted dye. The resulting red-orange precipitate was dissolved in water (2 mL), loaded onto a 100 mL DEAE Sepharose column, and eluted isocratically with 0.6 M ammonium bicarbonate (pH 7.8). Mass spectrometry verified that the major peaks corresponded to isomers of DABCYL Plus-eda-ATP. These peaks were pooled separately, lyophilized, dissolved at a concentration of 20 mM in 50 mM MES (pH 6.0), and stored frozen at –80 °C. Aluminum-backed silica gel 60 F254 TLC plates were used to track reaction progress with a water:ammonia:isopropanol:1,4-dioxane (4:3:2:4) solvent system. RF values: ATP, 0.21; ADP, 0.26; eda-ATP, 0.13; ATPQ1, 0.34; ATPQ2, 0.38; ADPQ1, 0.57; ADPQ2, 0.58.

4.5.3 Single-Molecule Coverslip Preparation

Glass coverslips (Fisherbrand) were sonicated sequentially in deionized water, methanol and 1M KOH. The etched coverslips were sonicated at 35 °C in a solution with 1% (w/v)

of PEG mixture (1% biotin-PEG-silane, MW 5000; 99% mPEG-silane, MW 5000, Laysan Bio) and 0.8 mM trimethylamine in 30 mL of ACS grade toluene (Fisher Scientific). The coverslips were then washed with toluene, copious amounts of deionized water and dried with pressurized air. The PEG-functionalized coverslips were stored at -20 °C in 50 mL Falcon tubes filled with nitrogen until flow cells were assembled.

4.5.4 Combined Force-Fluorescence Assay

Flow cells were created by forming a channel using two strips of double-sided tape on a microscope slide and sealing a PEGylated coverslip on top of the flow channel. A 0.1 mg/mL solution of streptavidin in PBS (100 mM phosphate buffer, pH 7.5) was introduced to the flow cell and allowed to incubate for 10 minutes. Unbound streptavidin was washed out with PD (25 mM HEPES pH 7.6, 100 mM KCl, 10 mM MgCl2, 10% glycerol (vol/vol)) and 10 µL of ClpPplatform (biotinylated ClpP construct) was incubated with the streptavidin-coated surface for 10 minutes. Unbound ClpPplatform was washed out with PD and 40 µL of 625 pM ClpX in PD in the presence of 3 mM ATP was flowed into the flow channel and incubated for 15 minutes. Afterward, unbound ClpX was washed out with an ATP solution followed by an imaging buffer with an oxygen scavenging and triplet-state quencher (0.8% D(+)-glucose, 16500 units/mL glucose oxidase, 217000 units/mL catalase, and 2 mM Trolox), the desired nucleotides and substrate-coated beads before beginning the experiment.

Substrate-coated beads were prepared by either crosslinking Anti-Digoxigenin antibody (Roche) with Protein-G coated beads (0.78 µm in diameter, Spherotech, Inc.) using the BS3 crosslinker (Thermo Scientific) or with carboxylate functionalized beads (1.09 µm, Spherotech, Inc) using the EDC crosslinker. SsrA-tagged protein substrates with a HaloTag domain (Promega), were incubated overnight with a 100bp dsDNA spacer modified with a HaloTag Ligand (Promega) on one end and a Digoxigenin tag on the opposite end. The covalently linked DNA-Substrate tethers were then incubated with Anti-Digoxigenin beads

for at least 30 minutes before being introduced to the flow cell. To assemble tethers, beads in solution were trapped by our optical tweezers and brought in close proximity to the coverslip surface. A piezo-stage (Physik Instrumente) was used to incrementally move the coverslip surface below the trapped bead until a surface-immobilized ClpXP motor engaged a DNA-substrate tether, which can be identified by tracking the bead displacement from the trap center. Upon substrate engagement, fluorescence illumination was turned on using a computer-controlled shutter. Bead displacement and fluorescence data was acquired at 90 Hz using a custom written LabView (National Instruments, Inc.) program. After the tether ruptures and the fluorophore photobleachs, position and stiffness calibrations of the optical tweezers were carried out as previously described [32]. The stiffness of the optical trap was maintained at 0.10 pN/nm. The interlaced optical force-fluorescence (IOFF) instrument used here is a modified version of an instrument previously described. [15]. Briefly, optical trapping (1064 nm, Coherent, Inc.) and fluorescence (532 nm, World Star Tech) lasers were interlaced out-of-phase at 50 kHz using a two-function generator (Sony, Inc.) to send modulating input signals into separate Acousto-Optic Deflectors (IntraAction). A low-power detection laser (975 nm, Corning Lasertron) was kept on continuously during our experiments to track displacement of the trapped bead. A set of computer automated shutters were used to control light exposure onto a photon-counting silicon avalanche photodiode (PerkinElmer) to acquire focused photons filtered by a pinhole (Thorlabs). The pinhole was aligned at a conjugate plane to the coverslip surface, and centered at the position that overlapped with the trapping and detection lasers.

4.5.5 Data Analysis

Custom Matlab scripts were used to process and analyze the data. Hidden Markov Modeling (HMM) was used to create idealized traces for identifying conformational states and extracting dwell time kinetics [33, 26]. Only traces showing a single photobleaching step, an emission intensity above 2000 counts/sec and emission lasting longer than 10

seconds were analyzed.

4.6 Acknowledgements

We thank Ben Stinson and Tristan Bell for producing ClpX, ClpP and ssrA-tagged substrates and performing bulk measurements. We thank Juan Carlos Cordova for contributing to the design of the assay, data collection and analysis. We thank Robert Sauer and Tania Brady for numerous helpful discussions and thoughtful suggestions. This work was supported by NSF (1330792) and GAANN (P200A090323).

4.7 Bibliography

[1] Phyllis I Hanson and Sidney W Whiteheart. AAA+ proteins: have engine, will work. *Nature reviews. Molecular cell biology*, 6(7):519–29, jul 2005.

[2] Tania a Baker and Robert T Sauer. ClpXP, an ATP-powered unfolding and protein-degradation machine. *Biochimica et biophysica acta*, 1823(1):15–28, jan 2012.

[3] Robert T Sauer and Tania a Baker. AAA+ proteases: ATP-fueled machines of protein destruction. *Annual review of biochemistry*, 80:587–612, jun 2011.

[4] Steven E Glynn, Andreas Martin, Andrew R Nager, Tania a Baker, and Robert T Sauer. Structures of asymmetric ClpX hexamers reveal nucleotide-dependent motions in a AAA+ protein-unfolding machine. *Cell*, 139(4):744–56, nov 2009.

[5] Xue Fei, Tristan A Bell, Simon Jenni, Benjamin M Stinson, Tania A Baker, Stephen C Harrison, and Robert T Sauer. Structures of the ATP-fueled ClpXP proteolytic machine bound to protein substrate. *bioRxiv*, page 704999, 2019.

[6] Christos Gatsogiannis, Dora Balogh, Felipe Merino, Stephan A. Sieber, and Stefan Raunser. Cryo-EM structure of the ClpXP protein degradation machinery. *Nature Structural and Molecular Biology*, 26(10):946–954, 2019.

[7] Zev Ripstein, Siavash Vahidi, Walid A. Houry, John L. Rubinstein, and Lewis E. Kay. A processive rotary mechanism couples substrate unfolding and proteolysis in the ClpXP degradation machinery. *bioRxiv*, pages 1–50, 2019.

[8] Marie-Eve Aubin-Tam, Adrian O Olivares, Robert T Sauer, Tania a Baker, and Matthew J Lang. Single-molecule protein unfolding and translocation by an ATP-fueled proteolytic machine. *Cell*, 145(2):257–67, apr 2011.

[9] Adrian O Olivares, Andrew R Nager, Ohad Iosefson, Robert T Sauer, and Tania A

Baker. Mechanochemical basis of protein degradation by a double-ring AAA+ machine. *Nature Structural & Molecular Biology*, 21(10):871–875, 2014.

[10] Juan Carlos Cordova, Adrian O Olivares, Yongdae Shin, Benjamin M Stinson, Stephane Calmat, Karl R Schmitz, Marie-Eve Aubin-Tam, Tania a Baker, Matthew J Lang, and Robert T Sauer. Stochastic but Highly Coordinated Protein Unfolding and Translocation by the ClpXP Proteolytic Machine. *Cell*, 158(3):647–658, jul 2014.

[11] Rodrigo a Maillard, Gheorghe Chistol, Maya Sen, Maurizio Righini, Jiongyi Tan, Christian M Kaiser, Courtney Hodges, Andreas Martin, and Carlos Bustamante. ClpX(P) generates mechanical force to unfold and translocate its protein substrates. *Cell*, 145(3):459–69, apr 2011.

[12] Adrian O. Olivares, Hema Chandra Kotamarthi, Benjamin J. Stein, Robert T. Sauer, and Tania A. Baker. Effect of directional pulling on mechanical protein degradation by ATP-dependent proteolytic machines. *Proceedings of the National Academy of Sciences*, page 201707794, 2017.

[13] Piere Rodriguez-Aliaga, Luis Ramirez, Frank Kim, Carlos Bustamante, and Andreas Martin. Substrate-translocating loops regulate mechanochemical coupling and power production in AAA+ protease ClpXP. *Nature Structural & Molecular Biology*, 2016(October), 2016.

[14] Maya Sen, Rodrigo A. Maillard, Kristofor Nyquist, Piere Rodriguez-Aliaga, Steve Pressé, Andreas Martin, and Carlos Bustamante. The ClpXP Protease Unfolds Substrates Using a Constant Rate of Pulling but Different Gears. *Cell*, 155(3):636–646, oct 2013.

[15] Ricardo R Brau, Peter B Tarsa, Jorge M Ferrer, Peter Lee, and Matthew J Lang. Interlaced optical force-fluorescence measurements for single molecule biophysics. *Biophysical journal*, 91(3):1069–77, aug 2006.

[16] Matthew J. Comstock, Taekjip Ha, and Yann R. Chemla. Ultrahigh-resolution optical trap with single-fluorophore sensitivity. *Nature Methods*, 8(4):335–340, 2011.

[17] MJ Lang, PM Fordyce, AM Engh, and KC Neuman. Simultaneous, coincident optical trapping and single-molecule fluorescence. *Nature methods*, 1(2):1–7, 2004.

[18] Phil Holzmeister, Bettina Wünsch, Andreas Gietl, and Philip Tinnefeld. Single-molecule photophysics of dark quenchers as non-fluorescent FRET acceptors. *Photochemical & photobiological sciences : Official journal of the European Photochemistry Association and the European Society for Photobiology*, 13(6):853–8, 2014.

[19] Ludovic Le Reste, Johannes Hohlbein, Kristofer Gryte, and Achillefs N Kapanidis. Characterization of dark quencher chromophores as nonfluorescent acceptors for single-molecule FRET. *Biophysical journal*, 102(11):2658–68, jun 2012.

[20] Ruobo Zhou, Simone Kunzelmann, Martin R Webb, and Taekjip Ha. Detecting Intramolecular Conformational Dynamics of Single molecules in short distance range with subnanomolar sensitivity. *Nano*, pages 5482–5488, 2011.

[21] Steven E Glynn, Andrew R Nager, Tania a Baker, and Robert T Sauer. Dynamic and static components power unfolding in topologically closed rings of a AAA+ proteolytic machine. *Nature structural & molecular biology*, 19(6), may 2012.

[22] J. Ferrer, D. Fangyuan, R. Brau, P. Tarsa, and M. Lang. IOFF Generally Extends Fluorophore Longevity in the Presence of an Optical Trap. *Current Pharmaceutical Biotechnology*, 10(5):502–507, 2009.

[23] Meindert A. Van Dijk, Lukas C. Kapitein, Joost Van Mameren, Christoph F. Schmidt, and Erwin J.G. Peterman. Combining optical trapping and single-molecule fluorescence spectroscopy: Enhanced photobleaching of fluorophores. *Journal of Physical Chemistry B*, 108(20):6479–6484, 2004.

[24] Benjamin M. Stinson, Andrew R. Nager, Steven E. Glynn, Karl R. Schmitz, Tania A. Baker, and Robert T. Sauer. Nucleotide Binding and Conformational Switching in the Hexameric Ring of a AAA+ Machine. *Cell*, 153(3):628–639, apr 2013.

[25] Benjamin M Stinson, Vladimir Baytshtok, Karl R Schmitz, Tania A Baker, and Robert T Sauer. Subunit asymmetry and roles of conformational switching in the hexameric AAA+ ring of ClpX. *Nature Structural & Molecular Biology*, 22(5):411–416, 2015.

[26] Jan Willem Van De Meent, Jonathan E. Bronson, Chris H. Wiggins, and Ruben L. Gonzalez. Empirical bayes methods enable advanced population-level analyses of single-molecule FRET experiments. *Biophysical Journal*, 106(6):1327–1337, 2014.

[27] Jon a Kenniston, Tania a Baker, Julio M Fernandez, and Robert T Sauer. Linkage between ATP consumption and mechanical unfolding during the protein processing reactions of an AAA+ degradation machine. *Cell*, 114(4):511–20, aug 2003.

[28] Yong In Kim, Randall E. Burton, Briana M. Burton, Robert T. Sauer, and Tania A. Baker. Dynamics of substrate denaturation and translocation by the ClpXP degradation machine. *Molecular Cell*, 5(4):639–648, 2000.

[29] Christine R. Cremo, Joan M. Neuron, and Ralph G. Yount. Interaction of Myosin Subfragment 1 with Fluorescent Ribose-Modified Nucleotides. A Comparison of Vanadate Trapping and SH1-SH2 Cross-Linking. *Biochemistry*, 29(13):3309–3319, 1990.

[30] Theodore L. Hazlett, Keith J.M. Moore, Peter N. Lowe, David M. Jameson, and John F. Eccleston. Solution Dynamics of p21ras Proteins Bound with Fluorescent Nucleotides: A Time-Resolved Fluorescence Study. *Biochemistry*, 32(49):13575–13583, 1993.

[31] Mitsuaki Maeda, Arvind D. Patel and Alexander Hampton. Formation of ribonucleotide 2',3'-cyclic carbonates during conversion of ribonucleoside 5'-phosphates to

diphosphates and triphosphates by the phosphorimidazolidate procedure. 4(8):2843–2853, 1977.

[32] Lang MJ, Asbury CL, Shaevitz JW, and Block SM. An automated two-dimensional optical force clamp for single molecule studies. *Biophysical journal*, 83(1):491–501, 2002.

[33] Jonathan E Bronson, Jingyi Fei, Jake M Hofman, Ruben L Gonzalez, and Chris H Wiggins. Learning rates and states from biophysical time series: a Bayesian approach to model selection and single-molecule FRET data. *Biophysical journal*, 97(12):3196–205, dec 2009.

Chapter 5

CONCLUSIONS AND FUTURE WORK

AAA+ enzymes are an essential class of molecular motors that orchestrate a vast array of cellular processes in all forms of life. ClpXP is a model AAA+ motor that has been characterized at the bulk and single-molecule level. The work presented in this dissertation is a significant advancement in the understanding of the molecular mechanisms of ClpXP. Shin et al. designed the first single-molecule fluorescence assay for ClpXP and we have used their methods to create novel single-molecule assays[**?**]. We have developed the first single-molecule assays to observe conformational switching and nucleotide binding in a single subunit of ClpX. These techniques can be applied to myriad molecular motors to unravel their underlying mechanisms.

For our nucleotide binding fluorescence quenching assay, we designed and synthesized an ATP analog, ATPQ, that was hydrolytically active and supported ClpXP-mediated substrate degradation. Additionally, our ClpX construct did not require mutations that affect ATPase activity to detect binding events. Using this assay, we were able to quantitatively describe the binding stoichiometry and kinetics of a single ClpX subunit. We also measured the effects of ClpP and ssrA-tagged substrates on ATPQ binding and monitored binding in two ClpX subunits simultaneously. Most ligand binding single-molecule fluorescence assays rely on imaging fluorescently-labeled ligands [2]. This strategy limits accessible ligand concentrations to 1 nM to maintain single-molecule detection [4]. Our approach avoids increasing the fluorescence background in sm-TIRF binding experiments by labeling a dark quencher to our ligand, ATP. We were able to measure nucleotide binding at a saturating concentration of 200 μM. This method will allow other researchers to observe ligand binding at physiologically relevant concentrations without significantly increasing background fluorescence. Dark quencher-ligand binding experiments can be enhanced by

using zero-mode waveguides to image at concentrations above 200 μM [3]. Future advancements in the assay should include the use of fluorophores of different colors to track the order of binding in multiple subunits. This extension of the assay we designed here will add finer detail to our current model of subunit coordination in ClpX.

We have engineered the first assay of conformational switching in a ClpX subunit. Our data show that several conformational classes of ClpX subunits with different switching kinetics exist, and their proportions and switching kinetics depend on nucleotide identity and the presence of ClpP and substrates. Moreover, we enhanced our assay by calibrating fluorescence quenching of our fluorophore (ATTO 550) by our dark quencher (Dabcyl Plus) to distance using a novel single-molecule DNA annealing assay. This allowed us to correlate normalized fluorescence intensity in ClpX to conformations seen in crystal and cryo-EM structures. Conventional single-molecule FRET (smFRET) experiments depend on FRET pairs with a typical Förster radius of 5 nm. This characteristic distance means that conventional smFRET is most sensitive to distance changes between 4-6 nm. Using out DNA annealing assay, we have measured the Föster radius of our fluorophore-quencher pair to be 2.96 nm. Additionally, our calibration curve for our probes show that they are sensitive to distance changes between 1-4 nm. This distance range is perfectly suited for conformational changes in individual ClpX subunits that would be invisible to traditional smFRET. Additionally, our use of SDS to unquench the fluorophore allowed us to convert fluorescence quenching into a ratiometric measurement similar to FRET. Moreover, our calibration of the probes with our DNA annealing assay made this a quantitative method to measure intramolecular distances. This technique can be applied to a wide range of molecular motors that have eluded smFRET experiments. This assay can be advanced through the use of multiple fluorophores of various colors to examine how different subunits coordinate their movements. Also, further development of our combined optical trapping and fluorescence quenching assay of the ClpX construct that reports conformational motions will help us correlate conformational switching with specific events in the mechanochemical cycle

of protein degradation by ClpXP.

The Lang lab has developed a technique to simultaneous measure force and fluorescence from a single molecule called interlaced optical force-fluorescence (IOFF) [1]. We have implemented this technique to watch conformational switching and ClpXP catalyzed substrate unfolding and translocation concurrently. Preliminary data show that large conformational switching events coincide exiting pauses in translocation. However, protein unfolding did not result in a concomitant conformational change. One limitation of this combined fluorescence quenching-optical trapping assay is that SDS cannot be used to unquench ATTO 550. This is because flowing in SDS will cause ClpX to dissociate from ClpPplatform, thereby breaking its connection to the glass surface. Also, all experiments end after SDS flow in so this assay would only be able to produce data for one molecule per slide because optical tweezers measure one molecule at a time. A ClpX construct that is not labeled with a Dabcyl Plus quencher can be used as an alternative to SDS for normalization. IOFF uses a pinhole to image fluorescence from spots co-aligned with the trapping laser, so all fluorescence collected using IOFF comes from the same illumination area in the field-of-view of the microscope. This technique would help us determine the true conformational state of the labeled subunit from its normalized intensity and permit the measurement of multiple ClpX molecules per sample slide.

The techniques developed and advanced here can be applied to a wide range of molecular motors. Researchers in other labs can apply our techniques to different AAA+ motors to learn if other members of this enzyme family have similar mechanisms to ClpX. We anticipate multi-color fluorescence quenching and combined fluorescence quenching and optical tweezer will be used soon to probe deeper questions about ClpXP's overall mechanism.

5.1 Bibliography

[1] Ricardo R Brau, Peter B Tarsa, Jorge M Ferrer, Peter Lee, and Matthew J Lang. Interlaced optical force-fluorescence measurements for single molecule biophysics. *Biophysical journal*, 91(3):1069–77, aug 2006.

[2] Takashl Funatsu, Yoshie Harada, Maklo Tokunaga, Kiwamu Salto, and Toshio Yanagida. Imaging of single fluorescent molecules and individual ATP turnovers by single myosin molecules in aqueous solution. *Nature*, 374:555–559, 1995.

[3] H. J. Levene, J. Korlach, S. W. Turner, M. Foquet, H. G. Craighead, and W. W. Webb. Zero-mode waveguides for single-molecule analysis at high concentrations. *Science*, 299(5607):682–686, 2003.

[4] Anna B Loveland, Satoshi Habuchi, Johannes C Walter, and Antoine M Van Oijen. A general approach to break the concentration barrier in single-molecule imaging. 9(10):987–995, 2012.

Appendix A

PROTOCOLS

A.1 **Buffer Recipes**

1. 1x PBS (pH 7.4)

   Materials:
   800 mg NaCl (137 mM)
   20 mg KCl (2.7 mM)
   144 mg Na_2HPO_4 (10 mM)
   24 mg KH_2PO_4 (1.8 mM)
   80 ml H_20

   (a) Combine all materials
   (b) Adjust pH to 7.4
   (c) Adjust volume to 100 mL with H_2O
   (d) Filter using a 0.2 μm filter

2. 1x PBST (pH 7.4)

   Materials:
   800 mg NaCl
   20 mg KCl
   144 mg Na_2HPO_4
   24 mg KH_2PO_4
   80 ml H_20
   10 μl Tween-20

   (a) Combine all materials
   (b) Adjust pH to 7.4
   (c) Adjust volume to 100 mL with H_2O
   (d) Filter using a 0.2 μm filter

3. 1xPD (protein degradation buffer for ClpX, 25 mM, pH 7.6)

Materials:
0.59575 g HEPES (25 mM)
0.7455 g KCl (100 mM)
0.2033 g $MgCl_2$ (10 mM)
90 mL ddH_2O
10 mL glycerol (10%)
0.2 m filter

(a) Combine all materials
(b) Adjust pH to 7.6
(c) Adjust volume to 100 mL with H_2O
(d) Filter using a 0.2 μm filter

4. 1xPD with Tween (protein degradation buffer for ClpX, 25 mM, pH 7.6)

Materials:
0.59575 g HEPES (25 mM)
0.7455 g KCl (100 mM)
0.2033 g $MgCl_2$ (10 mM)
90 mL ddH_2O
10 mL glycerol (10%)
0.2 m filter
10 μl Tween-20

(a) Combine all materials
(b) Adjust pH to 7.6
(c) Adjust volume to 100 mL with H_2O
(d) Filter using a 0.2 μm filter

5. T-50 Buffer (pH 8)

Materials:
157.6 mg Tris-HCl (10 mM) 292.2 mg NaCl (50 mM)

(a) Combine all materials
(b) Adjust pH to 8
(c) Adjust volume to 100 mL with H_2O
(d) Filter using a 0.2 μm filter

6. 100x Gloxy (16 500 U/mL Glucose Oxidase, 217 000 U/mL Catalase)

Materials:
X mg Glucose Oxidase (X = 16 500 U/mL * 0.2 mL * (1/(GO U/g))*(1000 mg/1 g))
Y µL Catalase (Y = 217 000 U/mL * 0.2 mL * (1/Cat U/mg) * (1/Cat mg/mL))
Z = 200 – Y µL T-50

(a) Weigh X mg of Glucose Oxidase in a centrifuge tube
(b) Add Z L of T-50 Buffer
(c) Add Y L of Catalase
(d) Centrifuge for 2 mins @ 4 °C and 13,000g (cfi)
(e) Remove supernatant and filter with a 0.22 m filter

7. 2 mM Trolox (pH 8)

Materials:
5 mg of 6-hydroxy-2,5,7,8-tetramethylchroman-2-carboxylic acid
1.66 mL of PD

(a) Dissolve 5 mg of Trolox in 1.66 mL of PD of your choice
(b) Vortex for 2 mins
(c) Filter with a 0.2 m filter
(d) Add 1M KOH until the pH is 8.0

8. 0.1 M MES buffer with 0.01% tween-20 (pH 4.5)

Materials:
MES
Tween-20

(a) Prepare 100 mL of buffer by mixing the following:
    - 1.95 mg MES
    - 10 L Tween-20
    - deionized water up to 100 mL total volume
(b) Adjust the solution to a pH of 4.5.

9. 0.1 M borate buffer (pH 8.5)

Materials:
Boric Acid
Deionized water

(a) Prepare 100 mL of buffer by mixing the following:
    - 0.618 g boric acid
    - deionized water up to 100 mL total volume

(b) Adjust the solution to a pH of 8.5 using NaOH.

A.2 **Glass Surface Passivation with PEG-Silane**

This protocol produces (poly)ethylene glycol (PEG) polymer brushes on the surfaces of glass coverslips. 1% of the PEG molecules on the surface have Biotin covalently linked to the end of the chain.

Materials:
mPEG-Silane, MW 5000 (Laysan Bio)
Biotin-PEG-Silane MW 5000 (Laysan Bio)
Triethylamine (Cat 90335 Sigma)
Toluene (Cat 244511 Sigma)
Methanol (Cat 179337 Sigma)
Potassium Hydroxide pellets (Cat 221473 Sigma)

1. Remove triethylamine from the 4 °C refrigerator and the PEG-silane jar (contains mPEG-SIL and Bio-PEG-SIL) from the -20 °C freezer. Wrap the bottle of triethylamine and the jar of PEG in aluminum foil and allow them to thaw for at least an hour. These reagents are moisture sensitive and must equilibrate to room temperature before use.

2. Rinse the glass-staining jar (reaction container) with DI water. Sonicate for 10 minutes with DI water. Repeat the process with methanol.

3. Place glass coverslips in the glass staining jar. Rinse twice and sonicate for 10 minutes with DI water. Repeat the process with methanol.

4. Sonicate the coverslips in 1M KOH for 20 minutes then rinse them with DI water.

5. While the coverslips are sonicating in KOH, remove mPEG-SIL and Bio-PEG-SIL from the PEG jar. Weigh the microcentrifuge tube (eppendorf tube). Place approximately 297 mg of mPEG and 3 mg of Bio-PEG-SIL (1%) in the eppendorf tube. Reweigh the eppendorf tube to ensure that 300 mg of PEG has been placed in the tube.

6. Rinse the KOH-etched coverslips twice with toluene. Pour 30 mL of toluene into a small beaker. Add 3.38 µL of triethylamine and empty the eppendorf tube of PEG into the beaker of toluene. Mix thoroughly and pour into the glass-staining jar of etched coverslips.

7. Sonicate the reaction mixture for 30 minutes at 35 °C.

8. Wash twice with toluene, then multiple times with DI water until coverslips are clean.

9. Dry the coverslips with nitrogen, place in a sealed dessicator and store at -20 °C. PEG coverslips are best if used within 2 weeks.

A.3 **Flow Cells for Fluorescence Flow Experiments**

Materials:
Dremmel Drill
Drill Bit
Microscope Glass Slide (Fischer)
Tygon Tubing
Epoxy
PEG coverslip
Double-sided tape
Syringe adapter (McMaster Carr)
1 mL Syringe

1. Drill 2 mm holes 30 mm apart on a microscope slide. Make sure both holes are equal distances from the closest edge of the slide.
2. Clean the slides by first sonicating them in water for 10 minutes then methanol for 10 minutes.
3. Rinse the slides 3 times with water and dry them with pressurized air.
4. Cut a 9-inch segment of Tygon tubing and trim the ends at a diagonal.
5. Insert each end into the two holes in the slide from one side. Pull both ends of the tubing 2 cm through the other side of the slide.
6. Mix a dollop of epoxy on a sheet of aluminum foil and apply it to where the tubing and slide holes meet on the side where the tubing connects both holes.
7. Allow the epoxy to cure for 30 minutes.
8. Remove a Falcon tube containing a PEG coverslip from the -20 ºC Freezer and allow it to thaw to room temperature.
9. Once the epoxy has cured, cut one end of the loop close to the slide. Use a razor blade to trim the ends of tubing hanging off the bottom of the slide.
10. Place two strips of double sided tape on either side of the holes along the long edges of the bottom of the slide.
11. Put the PEG coverslip on top of the double-sided tape. Remove the over-hanging pieces of tape with a razor blade. Seal the tape by rubbing the coverslip against the tape with a 0.65 µL Eppendorf tube.
12. Apply drops from a freshly mixed dollop of epoxy to the two openings to the flow channel close to the holes on the bottom of the slide. Flip the slide over and allow the epoxy to cure for 30 minutes.

13. Attach a syringe adapter to the open end of the tubing and connect a 1 mL syringe to the adapter.

A.4 smTIRF Assay for Observing Conformational Motions in ClpX

Materials:
PBS
PD
Flow cell with tygon tubing
Streptavidin (1 mg/mL in PBS, Sigma)
ClpX labeled with ATTO 550 and DABCYL Plus (100 nM)
ClpP (1 μM)
ssrA-tagged protein substrate (250 μM)
ATP or nucleotide of your choice (50 mM)
ATP regeneration system (20x)
Gloxy (100x)
Trolox (2 mM)
Glucose solution (10% w/v)
SDS (2%)

1. Assemble a flow cell with tygon tubing according to protocol A.3.
2. Dilute streptavidin to 0.1 mg/mL in PBS with a final volume of 40 μL. Carefully remove pipette tip, insert it into the inlet of the flow cell and gently pull on the syringe plunger to flow the solution into the flow channel (Follow this procedure for all flow-ins). Inspect the flow channel for bubbles and incubate for 10 minutes.
3. For ClpX only experiments, dilute ClpX to 187.5 pM in PD with a final volume of 80 μL.
4. For ClpXP experiments, mix 2 μL ClpX, 1 μL ClpP, 1.2 μL ATP, 1 μL ATP regeneration system and 14.8 μL PD. Cover centrifuge tube with aluminum foil and incubate for 5 minutes. Mix 2 μL of this mixture with 1 μL ClpP, 3 μL ATP, 2.5 μL ATP regeneration and 71.5 μL PD.
5. Wash out unbound streptavidin with 100 μL PD.
6. Flow in 50 μL of mixture from either step 3 or 4 into the flow cell and incubate for 10 minutes.
7. Turn on 532 nm laser and start EMCCD software (Andor).
8. For ClpX only experiments, wash out unbound ClpX with 100 μL PD.
9. For ClpXP experiments, wash out unbound ClpXP with 100 μL of ATP solution (92 μL PD, 3 μL ATP and 5 μL ATP regeneration system).
10. Make imaging solution by mixing 5 μL ATP regeneration system, 6 μL ATP, 1 μL gloxy, 28 μL Trolox, 8 μL glucose solution and the balance of PD. For ClpXP experiments add 1 μL ClpP. For substrate experiments add 10 μL of substrate.

11. Flow in 100 μL of imaging solution.
12. Load flow cell on microscope stage.
13. Tape syringe to eyepiece of microscope.
14. Prepare imaging solution with 50 μL SDS. Remove syringe tip and insert it into the flow cell inlet. Do not flow in buffer.
15. Set timer for at least 1 minute.
16. Turn off light, open dark box shutter and start imaging flow cell.
17. Start acquisition and the timer.
18. Once timer goes off, slowly flow buffer containing SDS into the flow cell.
19. Once recording ends, close dark box shutter and save data.

A.5 **SDS-PAGE**

Materials:
NuPAGE 10% Bis-Tris Gel, 1.0 mm mini gel (cabinet, Bio Core or Thermo)
MES SDS Running Buffer 20x (chemical shelf, Bio Core or Thermo)
SeeBlue Plus2 Pre-stained Protein Standard (top shelf of 4 ºC, Themo)
NuPAGE LDS Sample Buffer 4x (top shelf of 4 ºC, Thermo)
SimplyBlue Safe Stain (chemical shelf, Thermo)

1. Add 50 mL of MES SDS Running Buffer 20x to 950 mL of DI water.
2. Turn on heating block and allow it to warm up to 70 ºC.
3. Remove gel from pouch.
4. Rinse gel cassette with DI water.
5. Peel off tape.
6. Gently pull out comb.
7. Rinse the wells 3 times with 1 mL of 1x running buffer.
8. Orient the cassette so that notched wells face inward towards the inner chamber and close it with the clamp.
9. Fill the inner chamber with buffer to test the seal.
10. Fill the entire container with buffer.
11. Remove bubbles with a 1 mL pipette or Kim wipes.
12. If the heating block has reached 70 °C, add 5 µL of protein to an Eppendorf tube and allow it to denature on the heating block for 10 minutes.
    (a) Do not exceed 10 minutes. The sample will evaporate.
13. Prepare your samples for the gel as follows:
    (a) Undiluted protein
        i. 1 µL protein
        ii. 2.5 µL sample buffer
        iii. 6.5 µL DI water
        iv. 10 µL total volume
    (b) 10 times diluted protein
        i. 2 µL protein
        ii. 2.5 µL sample buffer

iii. 5.5 µL DI water
iv. 10 µL total volume

(c) Control

i. 2.5 µL sample buffer
ii. 7.5 DI water

(d) Protein Ladder

i. 10 µL undiluted

14. Carefully add samples to the wells.
15. Ladder/Control/Sample 1/Sample 2/etc.
16. Close the lid and connect the cables (red to red, black to black).
17. Run at 200 V for 35 – 45 minutes (check on it regularly).
18. When finished, turn off voltage and remove the gel cassette.
19. Rinse the gel cassette with DI water.
20. Carefully pry open cassette with gel knife.
21. Carefully cut around the edges to loosen the gel.
22. Put gel in a container for staining and washing.
23. Follow directions on SimplyBlue SafeStain:
    (a) Rinse the gel 3 times with DI water for 5 minutes each (on gel rotator)
    (b) Add enough stain to cover the gel and let it rotate for at least 1 hour
    (c) Remove stain, add DI water and allow it to rotate for 1 hour
    (d) Remove water, add fresh water and allow it to rotate for 1 hour

A.6 **Labeling Amine-DNA Oligo with Dabcyl Plus Succinimidyl Ester**

Materials:
DNA-amine (15 bp)
PBS pH 7.4 or Tetraborate Buffer pH 8.5
DMSO
Dabcyl Plus Succinimidyl Ester
1 M Tris pH 8.3
Illustra Microspin G-25 Columns

1. Dissolve DNA in PBS (I used 400 μM DNA, but higher is better). The ideal buffer is tetraborate at pH 8.5. If it is available, use tetraborate instead of PBS. **Do not use buffers that contain primary amines such as Tris.**

2. Prepare 100 mM Dabcyl Plus SE in DMSO.

3. Add sufficient Dabcyl Plus SE for a 12.5x molar excess. Wrap with aluminum foil and react at room temperature overnight.

4. Quench reaction with 10x molar excess of Tris to Dabcyl Plus SE.

5. Purify labeled DNA with G-25 columns using PBS.

A.7 **Labeling Thiol-DNA Oligo with ATTO 550 Maleimide**

Materials:
DNA-thiol (15 bp)
PBS
DMSO
DTT
ATTO 550 maleimide
2-mercaptoethanol
Illustra Microspin G-25 Columns

1. Dissolve DNA in PBS at pH 7 – 7.5 (I used 60 µM DNA, but higher is better). At this pH range, the thiol group is sufficiently nucleophilic. The ideal pH for the maleimide reaction is pH 7.

2. Reduce the protective disulfide group on the DNA with 10-fold molar excess DTT. Incubate for 20 minutes.

3. Remove excess DTT with buffer exchange on G-25 column using degassed PBS.

4. Prepare 200-fold molar excess ATTO 550 maleimide in DMSO.

5. Add enough stock ATTO 550 maleimide solution for a 20-fold molar excess of maleimide to DNA. Wrap with aluminum foil and react for 2 hours at room temperature or overnight at 4° C.

6. Quench reaction with 10-fold molar excess 2-mercaptoethanol to maleimide.

7. Purify labeled DNA with G-25 columns using PBS.

A.8 **Making Accessible Volume Clouds with FPS Software**

1. Use Avogadro software to create 3D model for dsDNA used in experiment based on the sequence.
2. Remove hydrogens from DNA model. Export model as pdb.
3. Draw the structure of the fluorophore attached to its linker molecule in ChemDraw. Open structure up in Chem3DDraw.
4. Measure linker length and three radii for the fluorophore in Chem3DDraw. Use these parameters for AV simulation in FPS.
5. Upload pdb file of DNA in FPS. Enter in the fluorophore parameters, attachment point atom in the DNA molecule and choose three radii simulation and either donor or acceptor.
6. Run calculation and save AV simulation. Repeat steps 3-5 for other fluorophores/quenchers used in the experiment.
7. Calculate inter-dye distance by choosing inter-dye distance and uploading donor and acceptor AVs.

A.9 **PCR amplification of dsDNA for ClpXP assays**

To amplify dsDNA of different predetermined lengths from the plasmid M13mp18, use the same reverse primer and change the forward primer to yield the desired length of the dsDNA.

The Primers used here are:
Reverse Primer:
5'- Amino - TTG AAA TAC CGA CCG TGT GA - 3'

5'- Dithiol - TTG AAA TAC CGA CCG TGT GA - 3'

Forward Primers:
For 100bp DNA: 5' - Dig - TGT ATA ACG CAT ATG ATA CT - 3'

For 1010bp DNA: 5' - Dig - TAT TGC GTT TCC TCG GTT TC - 3'

For 3500bp DNA: 5'- Biotin - AAT CCG CTT TGC TTC TGA CT- 3'

Materials:
Flat cap PCR tubes (Thermo Sci. catAB-0620)
Forward Primer (IDT, custom oligo)
Reverse Primer (IDT, custom oligo)
dNTP solution (New England Biolabs catN04475)
m13mp18 plasmid (Bayou Biolabs catP-105)
Phusion DNA Polymerase (New England Biolabs catM0530S)
TE buffer (Ambion catAM9849)
UltraPure water (Invitrogen cat10977-015)
QIAquick PCR purification kit (Qiagen cat 28106)
UV-Vis spectrophotometer (Thermo Sci. NanoDrop 2000)

1. Remove all materials form the freezer and allow any frozen solutions to thaw at room temperature. Upon thawing, immediately place them on ice.
2. To prepare 1mL of PCR reaction mixture, mix the following in a 1.7mL microtube:
    - 715 µL U.P. water
    - 25 µL of 20 µM forward primer in TE buffer
    - 25 µL of 20 µM reverse primer in TE buffer
    - 20 µL of 10 mM dNTPs mixture
    - 5 µL of 50ng/ µL m13mp18 plasmid in TE buffer
    - 200 µL of 5X GC buffer
    - 10 µL Phusion polymerase

3. Mix thoroughly by gently pipetting the solution up and down.

4. Add 100 µL of PCR reaction mixture to 10 flat-cap PCR tubes.

5. Immediately transfer tubes to PCR machine and run the "PHUSION" program/routine (outlined below).

   PHUSION PCR program:

   1 98 °C during 30sec

   2 98 °C during 10sec

   3 49 °C during 30sec

   4 72 °C during 90sec

   5 repeat steps 2-3-4 for a total of 35X

   6 72 °C during 10 min

   7 keep at 4 °C

6. Upon completion of the PCR program, purify the DNA using the Qiaquick purification kit (protocol for purification is included in the kit). For the last step in the purification protocol resuspend using **30 µL of PBS** instead of elution buffer included in the kit.

7. Measure the nucleic acid concentration of the purified DNA using the NanoDrop. Normal yields for this protocol are 200ng/ µL (100 nM for 3500bp dsDNA).

A.10 **DNA Gel Electrophoresis**

Use this DNA-agarose gel to ensure that the PCR amplification reaction and DNA purification yields the desired length and quality of DNA.

Materials:
10 mM TE buffer pH 7.5
5X TBE buffer (Invitrogen 955155301)
6X gel loading buffer (Sigma G7654)
1kb dsDNA ladder mixture (Bayou biolabs L-201)
Agarose (VWR EM-2120)
SybrGreen 10,000X (Molecular Probes S7563)
GelRed Nucleic Acid Gel Stain 10,000X (Biotium 41003)
Gel Electrophoresis system (e.g. Owl EasyCast B1 Mini Gel Electrophoresis System)
UV Lamp

1. Combine 60 ml 5X TBE with 540 mL of DI H2O to make 1X TBE In a 250 ml Erlenmeyer flask combine 0.8 g Agarose with 100 ml 1X TBE and microwave for 2 minutes on HI. Watch the flask and stop heating if solution begins to boil over, after a few seconds resume heating (repeat as necessary, but ensure the full 2min of heating are completed otherwise, agarose won't fully dissolve and this procedure won't work correctly)
2. Allow agarose solution to cool for 4 minutes
3. Add 8 µl of SybrGreen or 10 µl of GelRed
4. Prepare electrophoresis chamber for gel pouring and align comb
5. Pour the agarose solution in the chamber and allow 30 minutes to cool
6. Rotate the chamber so that the combs are proximal to the cathode (black terminal)
7. Fill the electrophoresis apparatus with the remainder of the 1X TBE buffer (500 ml).
8. Remove the comb and inspect the well walls
9. For each PCR sample combine the following:
   (a) 1.8 µl PCR product(*)
   (b) 16.2 µl TE buffer
   (c) 3 µl 6X gel loading buffer
10. Add 6 µl of the DNA ladder mixture to a well
11. Place 16 µl of the PCR sample/loading buffer into a well, repeat for each sample to be run

12. Replace the gel box cover and begin run at 110V
13. Run until the marker lines (blue and yellow) near the anode side of the gel (between 1.5 and 2.5 hours)
14. View bands on a gel imaging system (e.g. Alpha Innotech FluorChem 8900) or using a hand-held Ultraviolet Lamp.
15. Dispose of the gel in the appropriate Biohazardous container

(*) If the band is not clear (e.g. squiggly/smeared) the concentration of DNA in the well may be too high. Dilute the DNA to get better band resolution.

A.11 **DNA-Halotag Ligand Conjugation**

Materials:
NH2-DNA @ 200ng/μL in PBS (see protocol on PCR amplification)
HaloTag Succinimidyl Ester (O4) ligand (Promega P6751)
DMSO (Sigma)
1 M Tris, pH 8.3
QIAquick PCR purification kit (Qiagen cat 28106)
Bio-Rad Micro Bio-Spin 6 columns (BioRad cat 732-6221)
PBS buffer, pH 7.4

1. Add 5 μL 0.1 M HaloTag SE ligand in DMSO to 200 μL of dsDNA with a terminal amine group (final concentration is 2.5 mM) Aliquot the remaining solution of 0.1 M HaloTag SE ligand and store at -80 ºC.

2. Cover the reaction tube with aluminum foil and let it sit @ RT 4 hours.

3. Add 5 μL of 1 M Tris pH 8.3 (final concentration is 25 mM) to quench the reaction. Store the tube of DNA @ -20°C until the next step.

4. Purify the HT ligand functionalized DNA using 2 QIAquick columns (use PCR purification protocol). Add 1 mL PB buffer to reaction and elute with 50 μL of PBS for each column. Incubate for 1 minute before spinning down using the centrifuge.

5. Do another purification step using 2 MBS6 columns. Prepare six MBS6 columns by exchanging the buffer to PBS as described below (*). Add 50 μL of DNA to each column and spin down at 1000 g for 4 minutes.

6. Aliquot and store @ -20 °C.

A.12 **Anti-Digoxigenin Functionalized Beads**

This protocol is a modified version of a protocol developed by Marie Eve Aubin-Tam, a former post-doctoral researcher in the Lang lab.
Materials:
MES buffer
Borate buffer
PBS (pH 7.4)
Carboxy polystyrene beads (1.09 m)
anti-Digoxigenin antibody
Bovine Serum Albumin (BSA)
Ethanolamine
Cup sonicator
Tube Rotator
Microcentrifuge

1. Make MES (0.1 M with 0.01% tween-20, pH 4.5), borate (0.1 M, pH 8.5), and PBS (pH 7.4) buffers according to the recipes in section A.1.
2. Mix 100 L of 1 m carboxy polystyrene beads with 100 L of MES buffer.
3. Spin down (9000 rpm for 4 minutes) and resuspend in 200 L MES buffer (repeat 5x).
4. Sonicate using a cup sonicator for 2 minutes at 40%.
5. Add 200 L of freshly made EDC solution 2% w/v (corresponds to 10 mg EDC in 500 L MES buffer).
6. Incubate the bead mixture for 3 hours at room temperature on a rotator.
7. Spin down (9000 rpm for 4 minutes) and resuspend the bead mixture in 1 mL of borate buffer.
8. Spin down (9000 rpm for 4 minutes) and resuspend the bead mixture in 400 L of borate buffer.
9. Sonicate using a cup sonicator for 2 minutes at 40%.
10. Add 80 L of 200 g mL1 anti-DIG and 24 L of 5 mg mL1 BSA in borate buffer (filtered).
11. Incubate the bead mixture on a rotator for 1 hour at room temperature and then overnight at 4 °C.
12. Stop the reaction by adding 10 L of 0.25 M ethanolamine (0.25 M solution of ethanolamine corresponds to 10 L ethanolamine + 650 L borate buffer).

A.13 Combined Optical Trapping and Fluorescence Assay for monitoring U-L transitions with Fluorescence Quenching

Materials:
PEG coverslips
Anti-Dig coated beads
ClpX labeled with fluorophore and quencher
ClpP(platform)
ATP Regeneration System (ARS):Creatine Kinase and Creatine Phosphate
Oxygen Scavenger System: Gloxy and Glucose
Trolox
PD buffer
PBS buffer

1. Mix 15uL of dig-100bp-HaloTag ligand (@ 50 ng/ul) with 3 µL of Halotag-titin substrate @ 20 µM.
2. Rotate overnight at 4 ºC.
3. Remove a PEG-coverslip from the – 20 ºC freezer and allow it to equilibrate to room temperature 30 minutes before assembling the flow cell.
4. Turn on the lasers to the correct settings for the IOFF configuration*.
5. Clean beads by adding 20uL of anti-dig bead stock (¡1month old) to a 0.7mL microtube and spin them down for 2 minutes @ 10k rpm in 4 ºC microcentrifuge.
6. Remove supernatant and resuspend the pellet in 10 µL of filtered PD buffer.
7. Sonicate the 2min @ 35% in cold water. Do not add ice.
8. Add 2 µL of anti-dig beads to full DNA-substrate aliquot made in step1 and incubate until the last step (30-60 minutes).
9. Degas trolox and OSS tubes under vacuum using bench top desiccator.
10. Dilute 5 µL of streptavidin @1mg/mL to 0.1mg/ml in PBS and add 10 µL to a PEG coverslip flow cell.
11. Incubate for 10 minutes.
12. Flow out unbound streptavidin with 100 µL of PD and flow in 12 µL of 500 nM ClpP(platform).
13. Incubate for 10 minutes.
14. Flow out unbound ClpP(platform) with 100 µL of PD and flow in 1 nM** ClpX(ATTO 550/DABCYL Plus) by mixing:

- 5 µL ClpX(A/D) @ 10 nM
- 2.5 µL ARS
- 3 µL ATP
- 39.5 µL of PD

15. Incubate 15min***
16. Wash with 89 µL PD + 5 µL ARS + 6 µL ATP
17. Spin down substrate coated anti-dig beads from step 3 in 4 ºC centrifuge @ 10k rpm for 2 minutes. The pellet will be very small but visible. Resuspend beads in 12 µL of BSA @ 1 mg/mL. Add beads to flow cell reservoir. Do this before adding streptavidin.
18. Make imaging solution by mixing the following components:
    - 26 µL PD
    - 2.5 µL ARS
    - 3 µL ATP
    - 0.5 µL gloxy
    - 14 µL Trolox
    - 4 µL glucose
19. Remove supernatant and resuspend beads in 12 µL of imaging solution. Alternatively, seal the bead reservoir and add imaging solution to the main flow channel.
20. Flow in bead solution.
21. Seal slide with vacuum grease.
22. Set timer for 1 hour.
23. Load the slide on microscope stage.

*To switch trapping and fluorescence lasers to IOFF configuration, turn on the function generator and set both channels to the pulse function at 50 kHz. The duty cycles are 50% for trapping and 30% for fluorescence. Use the oscilloscope to visualize the signal. Adjust the phase for one of the channels until the two signals are completely out of phase. Disconnect the oscilloscope and reconnect the original BNC cables. Those BNC cables are already connected to signal mixers. Next, connect the trapping and fluorescence AODs to their respective mixers and close the loop back to the AODs.

**This will change depending on how much biotin-peg was used for making that particular batch of PEG slides (I always aim for 1% bPEG, but sometimes use as much as 5%

depending how efficiently I weighed the PEG in that batch).

***During this incubation time, make sure the instrument is in IOFF configuration, the Andor EMCCD has cooled and lasers have stabilized to the following laser powers:
Trapping Laser: 10.75A
Detection Lasers: 70 mA
Fluorescence Laser: 2 mW